

Alma Mater Studiorum – Università di Bologna

**DOTTORATO DI RICERCA IN
SCIENZE FARMACEUTICHE**

Ciclo XXV

Settore Concorsuale di afferenza: 03/D1

Settore Scientifico disciplinare: CHIM/08

Titolo tesi

**Innovative Strategies for the Synthesis of Biologically
Active Small Molecules**

Presentata da: *Elisa Giacomini*

Coordinatore Dottorato

Relatore

Prof. Maurizio Recanatini

Prof.ssa Marinella Roberti

Esame finale anno 2013

Outlines of the thesis

Chapter 1. Introduction.

An overview of new strategies in drug discovery: from a target-based, to a multiple ligand strategy; chemical genetics as a research method for drug discovery; role of organic chemistry for the efficient synthesis of biologically active small molecules and diversity oriented synthesis (DOS).

Cancer as a multifactorial disease; a brief description of the main biological aspects involved in neoplastic disorder: cell cycle, apoptosis and epigenetic.

Chapter 2. Aim of the work and synthetic strategies.

Design and synthesis of chimeric compounds able to interact with different pathways involved in cancer cells.

Design and synthesis of a DOS library of macrocyclic peptidomimetics.

Chapter 3. Biological results.

Preliminary biological evaluation of the synthesized chimeric compounds for their antiproliferative activity on Bcr-abl expressing K562 cell lines.

Preliminary biological results of chimeric compounds as histone deacetylases (HDACs) inhibitors.

Chapter 4. Conclusions.

Concluding remarks.

Chapter 5. Experimental procedures.

Synthetic procedures, physical and spectroscopic characterization for intermediates and final compounds.

Biological methods.

Chapter 6. Galloflavin.

Design and synthesis of Galloflavin, a novel inhibitor of lactate dehydrogenase (LDH).

Table of Contents

<i>Abstract</i>	4
1. Introduction	5
1.1 New strategies in drug discovery	6
1.1.1 Target-based drug discovery	6
1.1.2 Multiple ligand strategy in drug discovery.....	8
1.1.2.1 A representative example: multiple ligands strategy in anticancer drug discovery	10
1.1.3 From targets to pathways: new insights in drug discovery	12
1.1.3.1 Chemical Genetics: a research method for drug discovery	14
1.1.4 Biologically active small molecules: role of synthetic organic chemistry in drug discovery	17
1.1.4.1 Target-oriented synthesis (TOS)	18
1.1.4.2 Targeted Library Synthesis.....	19
1.1.4.3 Diversity-oriented synthesis (DOS)	20
1.2. Cancer as multifactorial disease	24
1.2.1 Cell cycle	24
1.2.1.1 Intracellular Control of Cell-Cycle.....	25
1.2.2 Apoptosis	26
1.2.2.1 Morphological Features of Apoptosis	27
1.2.2.2 Molecular mechanisms of apoptosis signalling pathways.....	28
1.2.3 Epigenetic mechanisms	30
1.2.3.1 Histone deacetylases (HDACs)	31
1.2.3.2 HDACs inhibitors.....	32
2. Aim of the work and synthetic strategies	35
2.1. Design and synthesis of chimeric compounds.....	36
2.2 DOS Library of Macrocyclic Peptidomimetics.....	50

3. Biological evaluation	67
3.1. Preliminary biological results of the antiproliferative activity of chimeric compounds on Bcr-Abl expressing K562 cells.....	69
3.2 Preliminary biological results of chimeric compounds as HDAC inhibitors	75
4. Conclusions	78
5. Experimental procedures.....	81
5.1 Experimental procedures of chimeric compounds	82
5.2 Experimental procedures of DOS library	98
5.3 Detailed biological methods	117
6. Galloflavin.....	119
7. Bibliographic References	123

Abstract

The post genomic era, set the challenge to develop drugs that target an ever-growing list of proteins associated with diseases. However, an increase in the number of drugs approved every year is nowadays still not observed. To overcome this gap, innovative approaches should be applied in drug discovery for target validation, and at the same time organic synthetic chemistry has to find new fruitful strategies to obtain biologically active small molecules not only as therapeutic agents, but also as diagnostic tools to identify possible cellular targets.

In this context, in view of the multifactorial mechanistic nature of cancer, new chimeric molecules, which can be either antitumor lead candidates, or valuable chemical tools to study molecular pathways in cancer cells, were developed using a multitarget-directed drug design strategy. According to this approach, the desired hybrid compounds were obtained by combining in a single chemical entity SAHA analogues, targeting histone deacetylases (HDACs), with substituted stilbene or terphenyl derivatives able to block cell cycle, to induce apoptosis and cell differentiation and with Sorafenib derivative, a multikinase inhibitor. The distinct synthons were separately synthesized then linked via amide bond.

The new chimeric derivatives were characterized with respect to their cytotoxic activity and their effects on cell cycle progression on leukemia Bcr-Abl-expressing K562 cell lines, as well as their HDACs inhibition. Preliminary results confirmed that one of the hybrid compounds has the desired chimeric profile.

A distinct project was developed in the laboratory of Dr Spring, regarding the synthesis of a diversity-oriented synthesis (DOS) library of macrocyclic peptidomimetics. From a biological point of view, this class of molecules is extremely interesting but underrepresented in drug discovery due to the poor synthetic accessibility. Therefore it represents a valid challenge for DOS to take on. A build/couple/pair (B/C/P) approach provided, in an efficient manner and in few steps, the structural diversity and complexity required for such compounds. Since a DOS library aims to explore known bioactive chemical space as well as “untapped” regions which may lead to molecules endowed with new biological properties, biological screening of the library against a wide range of biological targets is currently ongoing.

1. Introduction

1.1 New strategies in drug discovery

Over the last fifteen years, the number of new molecular entities (NME) approved by the US Food and Drug Administration (FDA) is constantly around twenty-thirty per year, despite the increased investment in drug research and development. Moreover, just a few of these drugs act on new targets, although the Human Genome Project identified a large number of potential drug targets. One of the major reason lies in target validation: indeed, in a classical drug discovery timeline (Figure 1) this phase lasts about one year, whereas Fishman and Porter pointed out that several years of steady work in both academia and industry are rather required.¹ Hence new and innovative approaches have to be applied to maintain a healthy pipeline of novel validated targets for drug discovery,² as it has been argued that “for many diseases, the most obvious approaches to cures have been tried and have often failed. The challenge now is for scientists to attack major diseases with fresh ingenuity.”³

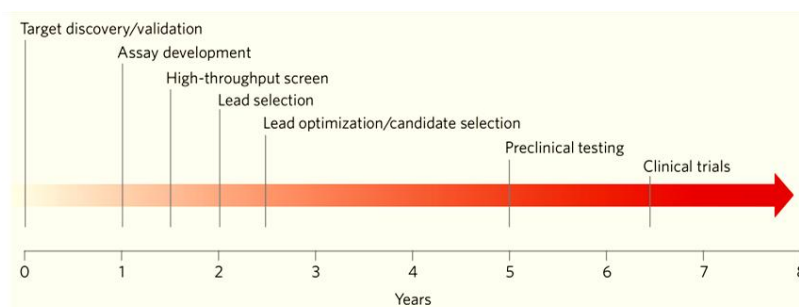


Figure 1. Drug discovery timeline (taken from Fisherman and Porter¹).

1.1.1 Target-based drug discovery

Historically, an entirely human-phenotype approach was the main solution adopted in drug discovery: until the past centuries, drugs extracted from nature were discovered through the observation of their beneficial effects in people with diseases. Obviously nowadays things are completely changed, and our knowledge in this field has enormously grown in the past centuries. Progress in biology and generally in life sciences made the trend in drug discovery to shift from a traditional physiology-based approach to the current reductionist approach focused on single molecular targets.⁴ The so-called “one target-one disease”,

whose main aim is to design ligands able to modulate selectively a single disease target, thus became the dominant paradigm in drug discovery. This concept was highlighted in the “magic bullets postulate”, by Paul Ehrlich, the founder of chemotherapy, who received the Nobel Prize for Physiology or Medicine in 1908:⁵ targeted drugs should go straight to their intended cell-structural targets, pathogens or cancer cell, without interaction in healthy tissue. In cancer therapy, the idea of a compound able to targets a single crucial oncoprotein in an exclusive and highly specific way led up to many targeted drugs. Among the successful case histories, Imatinib **1** (Glivec) (Figure 2) was found to be a potent inhibitor of the BCR–ABL kinase, a fusion protein resulting from a chromosomal translocation known to be the principal cause of cellular proliferation in chronic myeloid leukemia (CML).⁶ Even though Imatinib is considered as a milestone in molecular targeted therapies, it emerged that this drug is actually not entirely specific, but targets tyrosine kinases other than ABL and many growth factor receptors, obtaining a synergistic effect on different pathways involved in the neoplastic development. This lack of specificity has been exploited in the clinic, and Glivec has also been approved for the treatment of chronic eosinophilic leukemia (CEL), and for gastrointestinal stromal tumors (GISTs).⁷

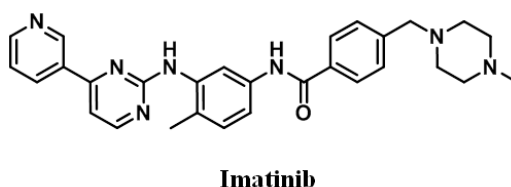


Figure 2. Imatinib (Glivec).

Compounds that modulate not only one, but multiple targets (which are frequently the case) can be advantageous for the treatment of diseases with complex etiologies such as cancer or neurodegenerative diseases. This, together with progress in systems biology, brought up a new appreciation of the role of polypharmacology, since “exquisitely selective compounds, compared with multitarget drugs, may exhibit lower than desired clinical efficacy”.⁸ Moreover, integrating network biology and polypharmacology offers the opportunity to investigate novel and druggable targets.⁸

1.1.2 Multiple ligand strategy in drug discovery

As described above, in recent years the reductionist “one target-one disease” approach has showed not to be satisfactory, and polypharmacology started to take place. This concept is actually well known, since the “drugs-cocktail” was widely used to treat unresponsive patients in many therapeutic areas, as cancer or HIV. The benefits of this approach were compromised by the poor compliance, hence pharmaceutical industry tried to sort this problem out towards “multicomponent drugs” whereby two or more compounds are co-formulated in a single tablet. However, in this case, there were complications due to high cost formulations as well as potential drug-drug interaction. Therefore, an alternative and more secure strategy is provided by a single chemical entity able to modulate biological targets simultaneously,^{9,10} overcoming problems related to the use of “multicomponent drugs” like different bioavailabilities or pharmacokinetics. In this way a drug could address different targets involved in the cascade of pathological events resulting highly effective for treating multifactorial diseases. Obviously, the design and optimization of such multiple ligand (ML) drug is challenging and may not be easy because it could also bind targets not involved with the disease eventually leading (although not necessarily) to side effects (Figure 3).⁴

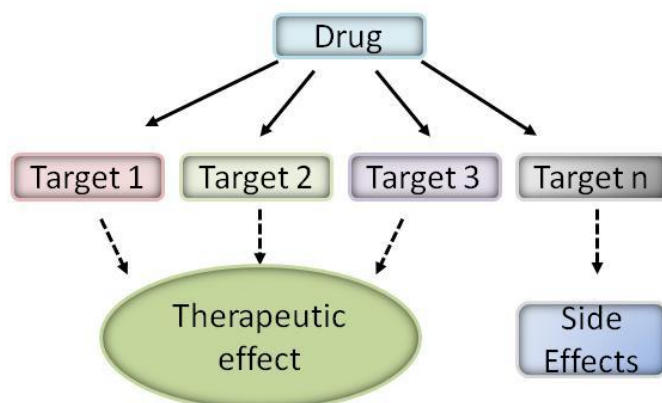


Figure 3. MLs approach to drug discovery (adapted from Cavalli *et al.*⁴).

A rational design of MLs is becoming a new trend, although many drugs have a multi-target profile not purposely designed but rather serendipitously discovered afterwards (like the Imatinib case highlighted before). Two different methods for the generation of ML lead compounds have been reported:^{9,11}

1. *Screening-based approach* (Figure 4).

In this method, classes of compounds known to be active against one of the two targets of interest are cross-screened against the other one. Molecules showing at least a minimal activity on each target undergo through an optimization phase in order to balance the desired profile or to “design out” a third undesired activity.

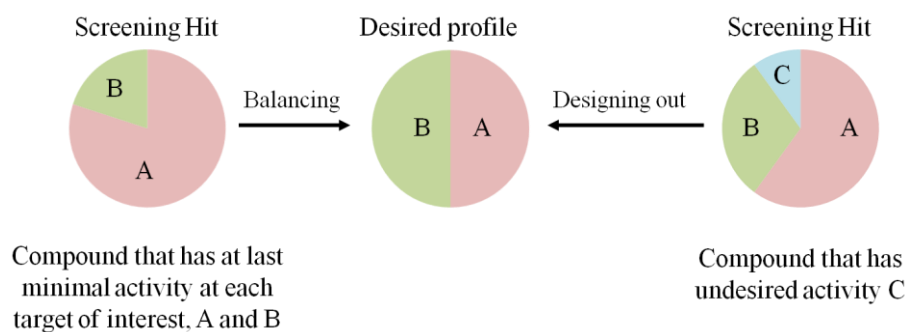


Figure 4. Screening based approach (adapted from Morphy & Rankovic⁹).

2. *Knowledge-based approach (framework combination)* (Figure 5).

Here two different molecules, each selective for different targets, are combined in a single molecular entity to “design in” both activities. The two compounds can be connected via a linker (which sometimes can be cleaved *in vivo*), or their frameworks can be attached together in the fused MLs. Eventually, in the merged MLs, the two frameworks are integrated and overlapped in a common structure: this last approach is the more suitable for medicinal chemists because it allows a multi target profile in a small and simple molecule, hopefully with favourable physicochemical properties.

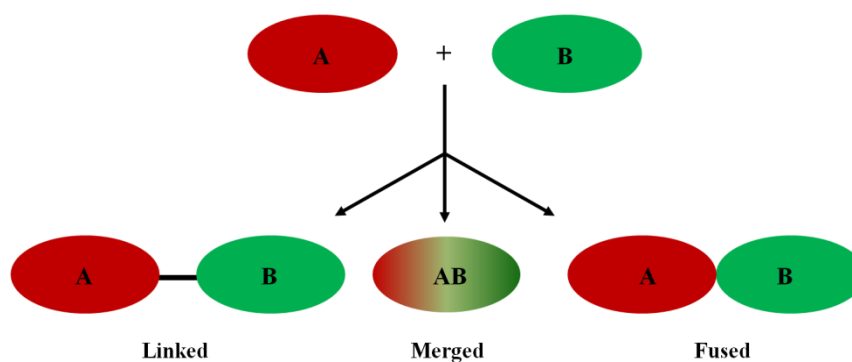


Figure 5. Knowledge based approach (adapted from Morphy & Rankovic⁹).

1.1.2.1 A representative example: multiple ligands strategy in anticancer drug discovery

Hanahan and Weinberg outlined the hallmarks of cancer¹² in six essential alterations acquired during tumor development in cell physiology: self-sufficiency in growth signals and insensitivity to antigrowth signals, evasion of apoptosis, dysregulated cell proliferation, sustained angiogenesis, tissue invasion and metastasis (Figure 6).

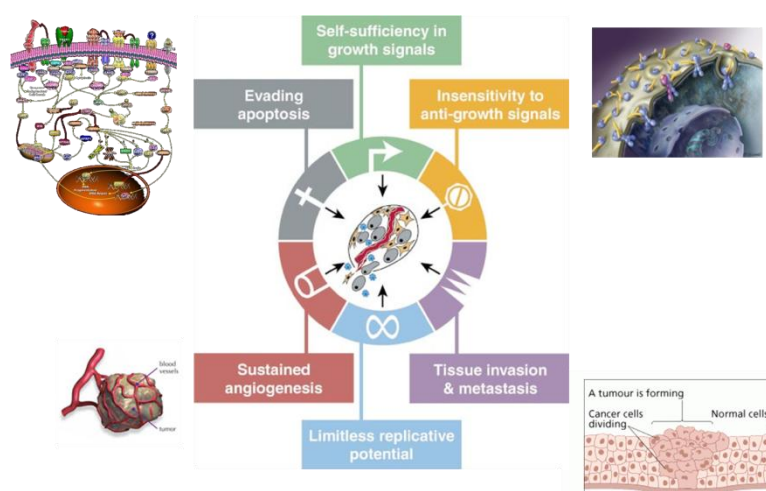


Figure 6. The hallmarks of cancer (adapted from Hanahan *et al.*¹²).

All of these phases are regulated by an interconnecting network of cellular signaling pathways in turn modulated by different elements such as epigenetic changes, oncogenic mutations, molecular chaperones, and ubiquitin proteasome pathways. Among the components of these complicated processes, many new cancer target were identified, thus suggesting new agents to be developed, possibly able to interact with more than one pathway, and to inhibit several proteins, both in tumor cells and in the microenvironment.¹³ In addition, a multi-target strategy might be a new key to overcome problems like drug resistance raised from a “one drug-one target” approach.

MLs design relies on molecular and cellular investigation methods, high throughput screenings (HTS), and on the knowledge of small organic molecules able to bind oncogenic targets. However, this strategy is not so frequently used in

cancer field yet, even though it has been applied for a number of years, and novel antineoplastic drugs have proven to show a multi-target activity. Some representative examples of designed ML as antitumoral agents are reported in this section.

Basing on a knowledge approach, Chen *et al.*¹⁴ obtained dual enzyme inhibitors by combining the structure of mycophenolic acid (MPA) and Merimepodib, inosine monophosphate dehydrogenase (IMPDH) inhibitors, with suberoylanilide hydroxamic acid (SAHA), a potent differentiation agent acting through inhibition of histone deacetylases (HDAC). Because of the synergism showed in combinations of new generation anti-CML drugs with SAHA, the novel hybrids **2** and **3** (Figure 7) were found to be more potent than parent compounds as antiproliferative agents and as differentiation inducers.

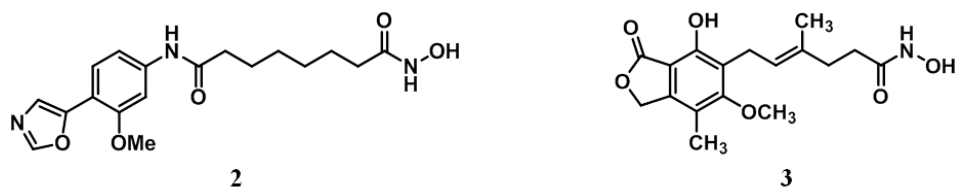


Figure 7. Hybrid compounds targeting IMPDH and HDAC.

Following the same approach, and taking advantage of the synergism already described, Mahboobi *et al.*^{15,16} designed chimeric compounds by merging functional group essential for HDAC inhibitory activity in the kinase inhibitory scaffold of imatinib and lapatinib. The new hybrid compounds **4** and **5** (Figure 8) showed potency comparable to that of parent HDAC inhibitors, whereas the selectivity profile differed from the parents kinase inhibitors.

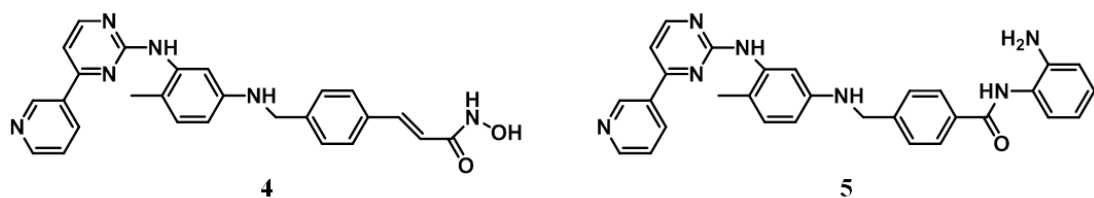


Figure 8. Hybrid HDAC-kinase inhibitory compounds.

In the last example, Gediya *et al.*¹⁷ synthesized hybrid compounds as mutual prodrugs (MPs) connecting all-trans-retinoic acid (ATRA) and histone deacetylase inhibitors via a cleavable linker. The design relies on the observation of the synergistic inhibition of growth in hormone insensitive breast and prostate cancer cell lines, by combination of retinoids with some HDAC inhibitors. Some of these hybrid molecules **6** and **7**, shown in Figure 9, displayed a better activity than the simultaneous administration of their parent components.

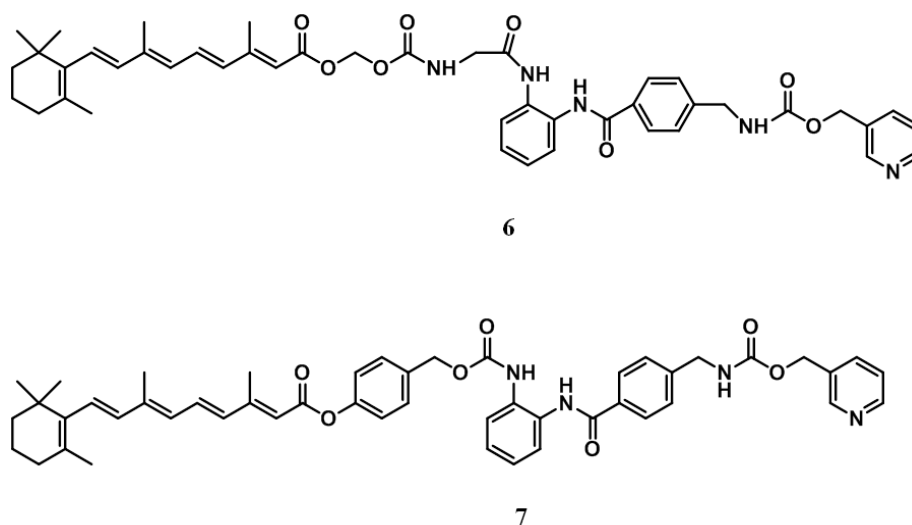


Figure 9. Mutual prodrugs.

The multi-target approach to the discovery of novel drug candidates has entered the drug discovery arena in an explicit way only recently. Nowadays, the paradigm shift ongoing in drug research from a target-based to a system-based⁸ view seems to delineate the most appropriate environment to support the MLs strategy, that is gaining a growing acceptance both in industry and academia.¹⁸

1.1.3 From targets to pathways: new insights in drug discovery

The opportunity presented by the concept of polypharmacology suggested that drug design should be taken on the broader perspective of multiple interactions between ligands and proteins, expanding to a network-wide level.¹⁹ The starting point for this requirement is to investigate the role of molecular pathways in complex diseases by defining the “systems biology” of their signaling networks, including specific cell type activities, dynamic feedback mechanisms and inter-

pathways connectivity. To integrate network biology and chemistry enhances the understanding of biological processes and can provide a suitable “grammar”¹ applicable in drug discovery.

In this context, chemical biology^{20,21} has emerged as an interdisciplinary field that combines chemistry, biology and related disciplines in order to better understand and manipulate biological systems with synthetic small organic molecules. The latter are key elements of a range of topics at the heart of the life sciences, including memory and cognition, sensing and signaling, understanding cell circuitry, and treating disease. For their crucial role in biological systems, small molecules were considered from chemical biologists as the missing link in the “Central Dogma” of biology, and therefore they were included in it (Figure 10). Many connections between small molecules and the three family (DNA, RNA and proteins) of macromolecules occur: small molecules can bind and modulate DNA, RNA or proteins functions, while these macromolecules have been used as templates for design and synthesis of small molecules.²¹

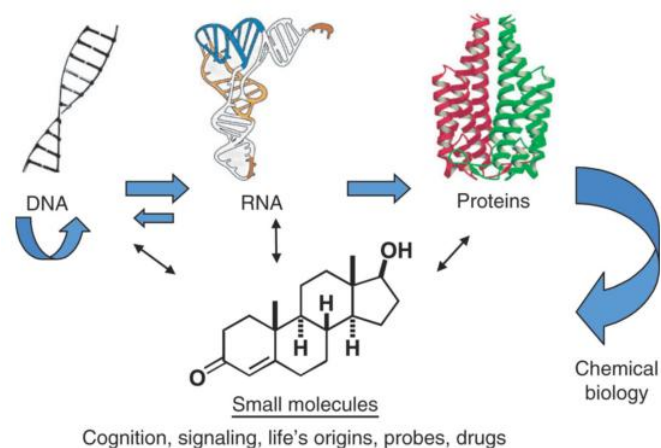


Figure 10. “The missing link in the Central Dogma.”²¹

This macromolecule-perturbing role is important not only in the search of potential lead in drug discovery field, but over the past years small organic molecules have proven to be also valuable tools for investigating biological systems.²²

1.1.3.1 Chemical Genetics: a research method for drug discovery

Chemical Genetics^{2,23,24} is a relatively new field at the interface between cell biology and synthetic organic chemistry that uses small molecules as tools to alter the functions of proteins in a biological system. Its main goals are to identify which proteins regulate different biological processes, to understand in molecular detail how proteins perform their biological functions, and to identify small molecules that may be of therapeutic value in drug discovery and development.

The term Chemical Genetics highlights the similarity of this strategy to the Genetic approach that has been the traditional tool for discovering novel drug targets. Both strategies perturbate the biological systems but the approach is different: genetically a gene function is modulated through a mutation and then the phenotype (physiological effect) is observed, while in Chemical Genetics small organic molecules are used as means to modulate protein function.²⁵

Genetics²⁶ can be divided into two approaches (Figure 11a):

- *Forward genetics* entails introducing random mutations into cells, screening mutant cells for a phenotype of interest and identifying mutated genes in affected cell. A classical forward genetic analysis starts from a phenotype and ends with the identification of the gene that is responsible for that effect (genotype).
- *Reverse genetics* entails introducing a mutation into a specific gene of interest and studying the phenotypic consequences of the mutation in a cellular context or in an organism. In classical reverse genetics, the direction moves from genotype to phenotype.

Although it represents a powerful set of tools for dissecting and understanding biological systems, Genetics has limitations, since not all cell lines are genetically tractable and most gene mutations are usually constitutive so they cannot be turned on or off at will.

Similarly, Chemical Genetics can be divided in two approaches (Figure 11b):

- *Forward chemical genetics* involves the use of exogenous ligands to screen for the phenotype of interest on the biological system under investigation. When the suitable ligand has been identified, the targeted protein must be identified as well. In this case, the “forward” direction is from phenotype to protein.

- *Reverse chemical genetics* entails overexpressing a protein of interest then screening for the right ligand; once it has been chosen, it is used to determine the phenotypic consequences of altering the function of this protein in a cellular context. The “reverse” direction shifts now from protein to phenotype.

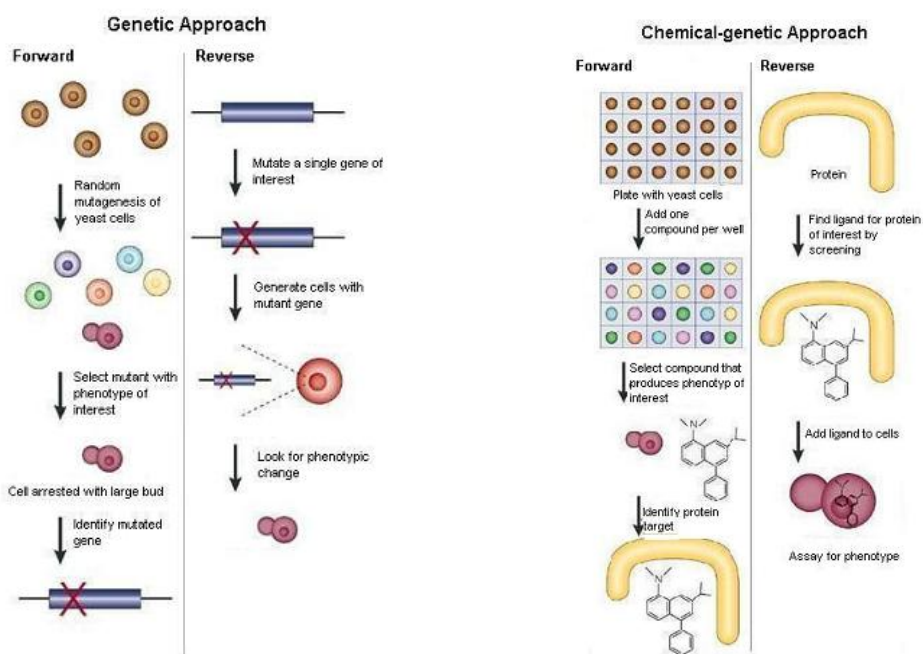


Figure 11. a) Genetics approach. b) Chemical-Genetics approach (taken from Stockwell²⁶).

Chemical Genetics has several advantages over the classic genetics approach. The biological effects are often reversible, due to metabolism or clearing, in contrast to gene mutations and usually rapid (so immediate/early effects can be characterized); all small molecules can be added or removed at anytime point in the experiment (temporal control), while with a genetic knockout steady-state effects are observed. Moreover it is possible to use small molecules in several types of cells which are not genetically tractable. On the other hand, the main disadvantage is the limited application: a small molecule ligand is needed for every gene product, while Genetics can manipulate any gene.

New insights coming from the systematic probing of biological pathways can be used in drug discovery process to develop new pharmacological agents for promoting and restoring health (Figure 12).

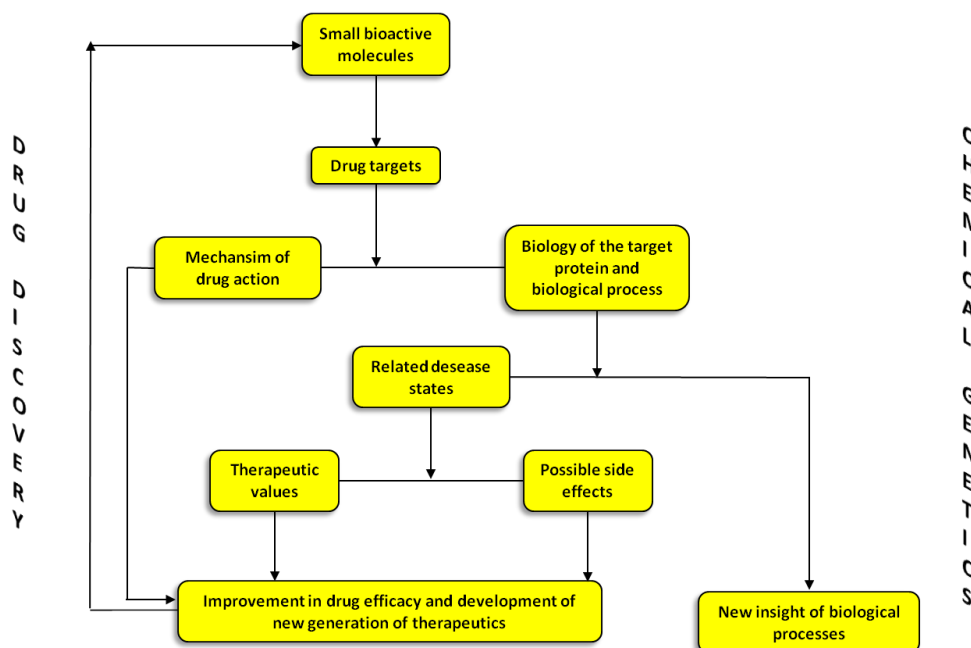


Figure 12. Interconnections between Drug Discovery and Chemical Genetics.

Rather than finding drugs for targets, Chemical Genetics generates targets that are inevitably druggable,²⁷ thus leading to a significant change in the classic process of drug discovery. As shown in Figure 13, the innovative concept of Chemical Genetics-based drug discovery is to start from a biological effect and then to identify a bioactive small molecule responsible for it. At this stage of the process it is possible to assess structure-activity relationships.

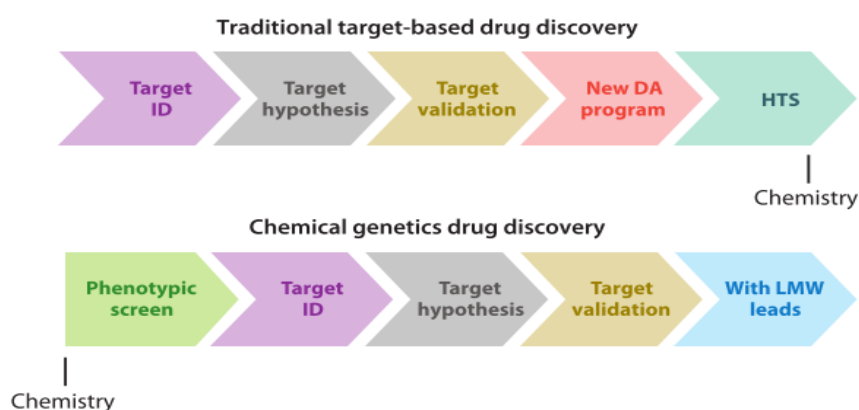


Figure 13. Target-based drug discovery vs chemical genetics drug discovery approach (taken from Cong *et al.*²).

The potency and physical properties of a given compound are then optimized, and eventually a chemical probe is used to identify possible cellular targets that are validated through additional genetic manipulations.

In conclusion, this approach provides opportunities to discover novel mechanisms or targets that are otherwise unobvious.²

1.1.4 Biologically active small molecules: role of synthetic organic chemistry in drug discovery

Synthetic organic chemistry plays a central role in the discovery and development of biologically active small molecules as therapeutic agents and diagnostic tools. Moreover, the “post-genome” era challenged organic chemists to develop drugs that target an ever-growing list of new proteins associated with disease. The prerequisite of biological relevance to be achieved by small organic molecules is found to be provided by natural product-derived compound.²⁸ So two fruitful strategies for discovering probes and drugs have been investigated:²⁹ the first approach is inspired by naturally occurring small molecules often referred to as natural products, while the second approach looks into the entire ensemble of natural products rather than specific ones, paying attention to the their structural complexity and diversity.

At this point, the problem is represented by the vast number of possible small molecules that could be created. Screenings of millions of compounds have been performed by researchers and pharmaceutical companies (typically containing approximately 10^6 compounds), but they present only a cursory examination of all the possible organic compounds comprised in the “chemical space” (Figure 14). Generally, chemical or biological space is defined as a virtual n-dimensional space where dimensions become descriptors of structural, physiochemical or even biological properties. Chemical space can be viewed “as being analogous to the cosmological universe in its vastness, with chemical compounds populating space instead of stars”.³⁰

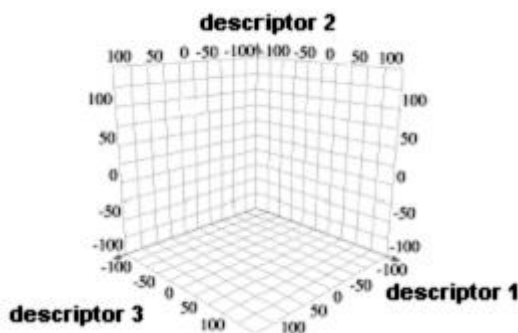


Figure 14. Chemical space.

Synthetic organic chemists aim to gain access to small biologically active molecules using three general approaches:³¹

1. Target-oriented synthesis (TOS);
2. Targeted Library Synthesis;
3. Diversity-oriented synthesis (DOS).

1.1.4.1 Target-oriented synthesis (TOS)

TOS^{31,32} is a practical application of the natural products-inspired approach described above. Once natural compounds of interest are identified, isolated and structurally characterized, they can become target molecule of value for chemical synthesis. Targets can also be represented by drugs or libraries of drug candidates (especially in pharmaceutical companies).

In this strategy, the target molecule is the final reaction product that opportune substrate and proper reaction conditions are required for. E. J. Corey developed a systematic method to plan syntheses of target molecules, receiving for this reason the Nobel Prize in 1990. Corey defined retrosynthesis as the approach in which “target structure is subjected to a deconstruction process which corresponds to the reverse of a synthetic reaction, so as to convert that target structure to simpler precursor structures, without any assumptions with regard to starting materials. Each of the precursors so generated is then examined in the same way, and the process is repeated until simple or commercially available structures result.”³³ Complexity-generating reactions and the so-called “fragment coupling reactions” are the most preferred and therefore widely used in TOS. In terms of chemical space, target molecules address to a precise region of chemical space, most often

defined by a complex natural product known to have a useful biological function (Figure 15).

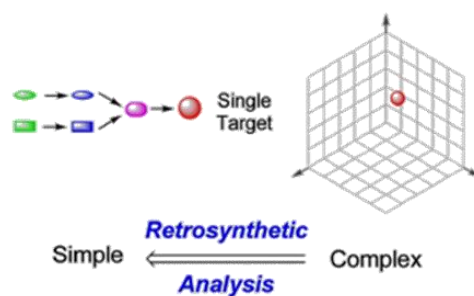


Figure 15. Targeted oriented synthesis (adapted from Galloway *et al.*³⁴).

1.1.4.2 Targeted Library Synthesis

This approach takes advantage of either medicinal or combinatorial chemistry and aims to explore a dense region of chemical space known to have the desired properties to achieve (Figure 16). A targeted library synthesis aims to obtain collections of compounds analog to an identified lead, which can be a specific molecular scaffold or set of scaffolds from a bioactive natural product, a known drug or a rationally designed molecule. These libraries can be designed also as a follow-up to a random library screening in which “hits” have been identified. As for TOS, again in this case a retrosynthetic analysis provides the planning strategy for those collections of compounds.

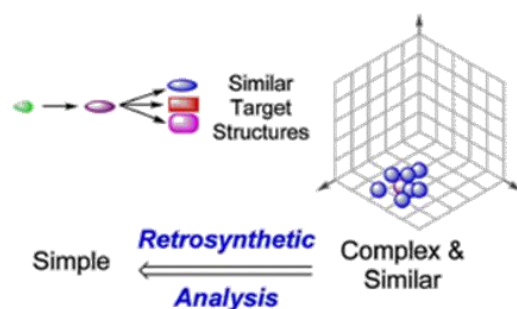


Figure 16. Targetd library synthesis (adapted from Galloway *et al.*³⁴).

1.1.4.3 Diversity-oriented synthesis (DOS)

The previously described approach was found not to improve drug discovery successes as it was expected. One of the main reasons lies in the concept itself, since compound collections obtained through this strategy are comprised of large numbers of structurally similar compounds and aim to explore only regions of chemical space defined by natural products or known drugs. Even the size of the library is not so important, while library diversity, in terms of molecular structure and thus function, is a crucial point.³⁴ Moreover, it can be argued that these regions of chemical space may not be the most fruitful to discover small-molecules that modulate macromolecular function in useful ways: diversity-oriented synthesis (DOS)^{31,32,34} aims to answer this questions.³¹

DOS is a synthetic approach for the efficient generation of chemical libraries containing structurally diverse and complex small organic molecules. As biological activity of any molecule intrinsically depends on its structure, the overall functional and thus structural diversity of a small-molecule library is proportionally correlated with the amount of chemical space occupied. DOS libraries broadly populate known bioactive chemical space (Figure 17), as well as “untapped” regions which may contain molecules with exciting and unusual biological properties. In principle, a “primary screening” of such libraries should provide hits against a wide range of biological targets including the more challenging.

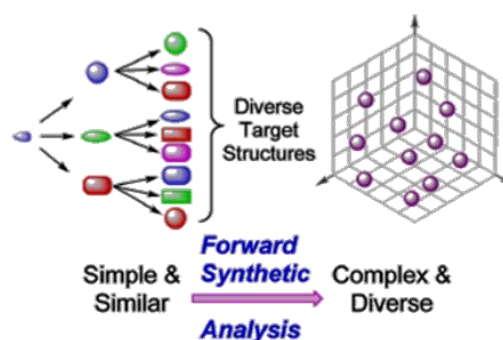


Figure 17. Diversity oriented synthesis (adapted from Galloway *et al.*³⁴).

Retrosynthetic analysis does not suite DOS, since the target is not known; therefore a forward synthetic analysis can be applied. Synthetic pathways are no

longer linear and convergent as in TOS, but they are rather branched and divergent, and the direction has been switched from simple and similar starting materials to complex and diverse final products, usually in no more than five synthetic steps. Hence, from a synthetic point of view, desirable features in DOS small molecules libraries are *structural diversity and complexity*.

Structural Complexity

Low-complexity compounds have a higher probability of weakly binding a target (while they have higher probability of binding too many targets).³⁵ In addition, structural features of natural products suggest that a complex structure is more likely to interact with a biological macromolecule in a selective and specific manner and to modulate protein-protein interaction. Structural complexity is related to the character and number of functional groups within the compound, with particular attention to the combination of rigidifying elements (covalent bonds, noncovalent bonds, and nonbonding interactions) that define its overall three-dimensional shape.

To this purpose, complexity-generating reactions and multi-component reactions are most valuable for accessing complexity in an efficient manner.

Moreover, the identification of pairwise relationships, where the product of one complexity-generating reaction is the substrate for a second one, can lead to high levels of complexity in a very efficient manner.

Structural diversity

An efficient DOS synthesis, must reach the four principal components of structural diversity:

- *Appendage diversity* that consists in variation of structural moieties around a common skeleton. It represents the simplest diversity-generating process and it is adopted by combinatorial chemistry as well. This kind of diversity can be reached either by attaching different appendages to a common scaffold, or by varying the building blocks at different steps of the synthesis. Eventually, this process can be useful to optimize the activity of an identified hit after a random library screening.

- *Functional group diversity* that is represented by the variation in the functional groups present.

- *Stereochemical diversity* that is represented by variation of key elements in term of potential macromolecule-interacting. This diversity leads stereoisomers to interact with chiral macromolecules in distinct ways thus obtaining different biological effects. Stereospecific reactions that proceed with enantio- or diastereo selectivity or synthesis based on enantiomerically pure building blocks of which both enantiomers can be readily available, are exploited to achieve stereochemical diversity.

- *Skeletal (scaffold) diversity* requires the presence of many distinct molecular skeletons. To incorporate such diversity into a library is the most challenging goal of DOS, since to increase the overall structural diversity of compounds collections more likely addresses a broad range of biological targets.³⁴

Two principal approaches are reported for planning DOS pathways that generate skeletal diversity.

The first one is a *reagent-based approach* that involves the use of a common starting material with different reagents to produce a collection of products with distinct molecular skeletons (Figure 18). Diversity can be achieved through two different methods, both involving steps of branching, divergent and complexity-generating reactions: by using a densely functionalized starting materials in which different functionalities in the same molecule are transformed by different reagents, or by exposing a pluripotent functional group in a given molecule to different reagents, resulting in different reactions occurring only with that functional group of the molecule.

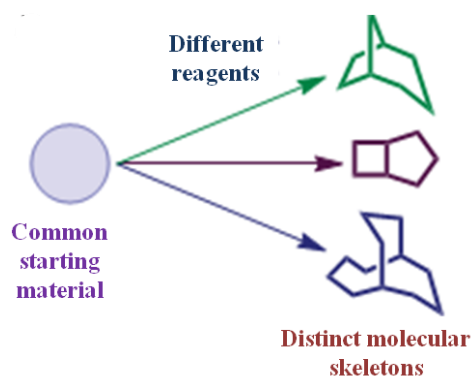


Figure 18. Reagent-based approach (adapted from Galloway *et al.*³⁴).

The second strategy is instead a *substrate-based approach*, based on different starting materials with common reaction conditions (Figure 19). In this case a collection of substrates having different appendages with suitable “pre-encoded” skeletal information (called σ elements) is transformed into the desired collection of products using folding-type reactions like intramolecular reactions that “pair” strategically positioned functional groups in the substrates forming compounds with different skeletons.

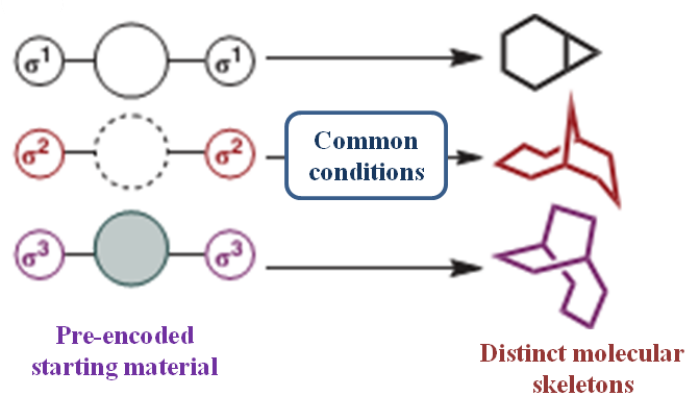


Figure 19. Substrate-based approach (adapted from Galloway *et al.*³⁴).

DOS is a field in continuous evolution that so far has provided a significant advancement, offering a potentially powerful tool for the identification of novel molecules with exciting biological properties in chemical biology and in drug discovery, and for developing innovative synthetic methodologies with broad applications in organic chemistry.

1.2. Cancer as multifactorial disease

Cancer is a multifactorial disease, arising from a complicated network of interdependent biological changes occurring in a single cell. In particular, dysregulation of cell progression, evasion of apoptosis and epigenetic mechanisms contributed at neoplastic progression in every kind of tumor.

Since during my PhD I have been involved in projects aimed at identifying novel biologically active small molecules, which can be either antitumor lead candidates, or valuable chemical tools to study molecular pathways in cancer cells, a brief description of the main biological aspects involved in neoplastic disorder is reported in the following.

1.2.1 Cell cycle

Cell cycle is the consecutive and ordered set of events that regulate eukaryotic cell's growth and division. It consists of four distinct phases (Figure 20): the S phase, in which DNA replication occurs, and the M phase when mitosis and cytokinesis division occur; these phases are interchanged respectively with G1 phase (preparation to replication) and G2 phase (interphase or preparation to mitosis).

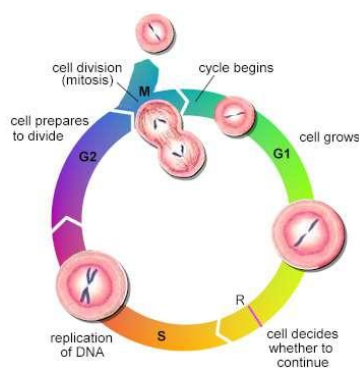


Figure 20. Cell cycle.

In the G0 phase a cell exits from cell cycle, becoming quiescent and thus “resting” for long time (possibly indefinitely as in the case of neurons). Cell cycle progression is tightly coordinated between the different phases by a series of checkpoints that control if the cell enters correctly in the cycle, and prevent entry into the next phase until the events of the preceding phase have been completed.

Several cell cycle checkpoints work in concert to ensure that incomplete or damaged chromosomes are not replicated. When a damage is found, cycle progression is stopped until repairs are made: if it's possible to fix up, the process restarts, otherwise cells undergo through apoptosis. If a checkpoint stops working, mutations occur that can lead to cancerogenesis.

1.2.1.1 Intracellular Control of Cell-Cycle

Cyclin-dependent kinases (CDKs) and cyclins regulate the progression through the cell cycle. CDKs bind cyclins in order to form cyclin-CDK complex, which has an increased kinase activity. CDKs level is usual constant, while cyclin's level oscillates and can become high on demand; these complex are known to phosphorylate hundreds of proteins and by doing so orchestrate many aspects of the cell cycle.

It has been reported that cells possess a unique regulatory mechanism to shift them between proliferative and quiescent states; the restriction point (R) control³⁶ defines the specific time in the cell cycle when the critical decision about growth versus quiescence is made. This checkpoint is in the end of G1 phase: if the cell goes through this point, enters in phase S and grows, otherwise it goes backwards in G0 phase. A major controller of R is the retinoblastoma protein (pRB), a tumor suppressor protein. The hypophosphorylated form of pRb binds E2F and other transcription factors, blocking transition in R. Under conditions favouring proliferation,³⁷ pRb is phosphorylated and “opens” the gate to permit the cell to proceed into late G1³⁸ (Figure 21). Loss of pRB function deprives the cell of an important mechanism for braking cell proliferation. As a matter of fact, dysregulation in R point is found in every malignant cell.

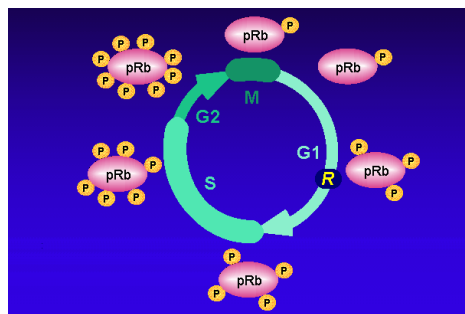


Figure 21. Retinoblastoma protein.

Cell cycle control mechanism is sensitive to extracellular as well as intracellular signal from its genome, and progression through the cycle is possible only with a favourable environment. Genome can be easily altered from a wide range of physical and chemical mutagens, and if a serious damage happens, cell death is desirable as best solution. The p53 tumor suppressor protein plays a central role to preserve genomic integrity and has been described as “the guardian of genome”. p53 maintains cellular homeostasis by preventing possible mutations and it is involved in many cellular pathways; in response to various stress signals, it becomes activated and in this way it can promote a transient cell cycle arrest, apoptosis or permanent cell cycle arrest (senescence) by regulating the transcription of genes involved in these crucial events (Figure 22).³⁹ Given that, it’s evident the important role of p53 in suppressing tumorigenesis: indeed most human cancers have either mutations in p53 or defects in the pathway.⁴⁰

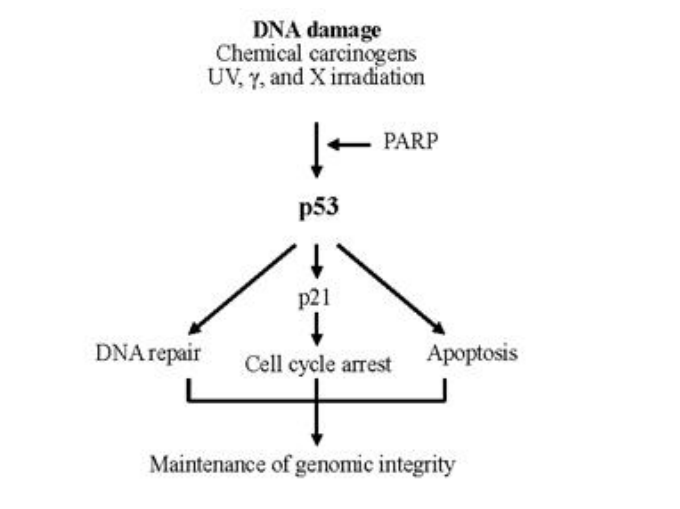


Figure 22. p53 pathway.

1.2.2 Apoptosis

Apoptosis or programmed cell death is a physiological process, necessary for the destruction of cells considered a threat such as cells infected with viruses, cells with DNA damage, cancerous cells, and cells of the immune system after they have fulfilled their functions.⁴¹

The apoptotic mechanism plays an essential role during development of multicellular organism, allowing them to get rid of rogue or harmful cells which threaten the animal's survival. Moreover, it is involved in many cell differentiation processes considering for instance the differentiation of fingers and toes in a human embryo due to apoptosis of interdigit mesenchymal tissue.

Apoptosis is also in equilibrium with cell proliferation for regulation and maintenance of the homeostasis in adult cell population. If the delicate balance between this two mechanisms changes, severe pathological consequences occur: suppression of apoptotic machinery causes autoimmune diseases and it is a hallmark of cancer, while abnormal upregulation of apoptosis contributes to neurological disorders, such as Alzheimer's and Parkinson's diseases.⁴²

Moreover, apoptosis represents a cut-and-dry switch: it is either on or off.⁴³

1.2.2.1 Morphological Features of Apoptosis

Figure 23 reported the stereotypical morphological changes features of an apoptotic cell:⁴⁴ at the beginning, after cytoplasmic condensation, the cell shrinks, shows deformation and loses contact to its neighbouring cells. Aggregates of condensed chromatin granules marginate at the nuclear membrane. The plasma membrane is blebbing and finally the cell is fragmented into compact membrane-enclosed structures, called 'apoptotic bodies' which contain cytosol, the condensed chromatin, and organelles. The apoptotic bodies are engulfed by macrophages and thus are removed from the tissue without causing an inflammatory response. Phagocytosis takes only few minutes; afterwards lysosomal degradation and cellular digestion will occur.

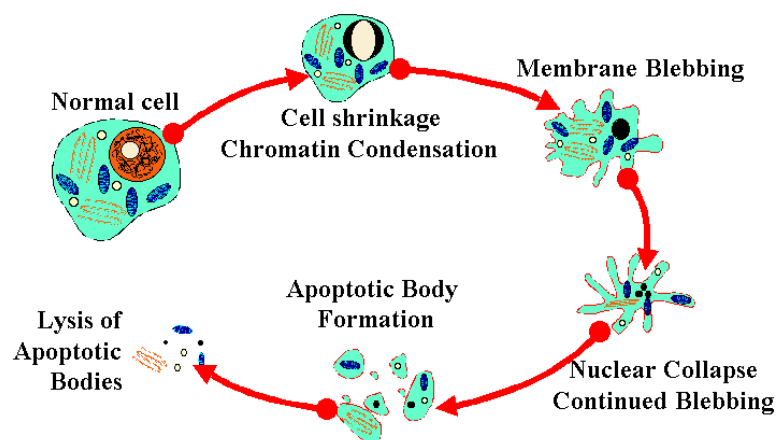


Figure 23. Morphology of apoptosis.

Apoptosis is in contrast to necrosis: while the former is a physiological mechanism, the latter is pathological, and leads to death of cells or tissues following injury. In the necrotic mode of cell death, cells suffer a major insult resulting in a loss of membrane integrity, swelling and disruption of the cells. During necrosis, cellular contents are released uncontrolled into the cell's environment which results in damage of surrounding cells and a strong inflammatory response in the corresponding tissue. The necrotic tissue morphology is, in large part, due to post-mortem events.⁴⁵

1.2.2.2 Molecular mechanisms of apoptosis signalling pathways

Apoptosis is a tightly regulated and highly efficient cell death program; its molecular machinery involves a cascade of complex events, from the delivery of external signals through defined receptor complexes, to the well-regulated expression of a number of genes and the execution of apoptosis by proteases and endonucleases.⁴³ Apoptosis can be triggered by various stimuli from outside or inside the cell that, even though from diverse origin activate a common cell death machinery leading to the characteristic features of apoptotic cell death.

Caspases⁴² constitute a highly conserved family of cysteine proteases, and can be considered the central executioners of apoptosis because they are responsible for the most of morphological changes associated with this process. Their activity is due to a cysteine residue in the active site that cleaves substrates at position next to aspartic acid residues. Fourteen different species of caspases are identified; the ones involved in apoptosis are generally divided into two categories: apoptotic initiators, or ICH-1/Nedd-2 subfamily (caspases -2, -8, -9, -10), and apoptotic effectors, or Ced-3/ CPP-32, (caspases -3, -6, -7). As for most of the proteases, all caspases are produced in cells as catalytically inactive zymogens, named procaspases, and must undergo proteolytic activation during apoptosis. These inert enzymes are composed of three domains: a large subunit (20KDa), which has the cysteine residue, a small subunit (10KDa) and an N-terminal prodomain which is removed during activation. In all the cases examined so far, the mature active form of caspases is a heterotetramer containing two p20/p10 heterodimers each of which contributes aminoacids to the two active sites that appear to work

independently. The activation of an effector caspase is executed by an initiator caspase, through proteolytic cleavage after a specific internal Asp residue to separate the large and small subunits of the mature caspase. Once activated, the effector caspases act on a broad spectrum of cellular targets leading to cell death.⁴⁶

Once induced, cell death can follow several different pathways that can be subdivided into two main categories: extrinsic pathways, in which death receptors are involved, or intrinsic or mitochondrial pathways. The involvement of caspases as final executioners of cell death is the common point in both mechanisms. As shown in Figure 24, the extrinsic pathway is initiated by ligand-induced activation of the death receptors at the plasma membrane, ultimately resulting in the activation of caspase-8 or caspase-10. The intrinsic cell death pathway is triggered by cellular stress signals such as DNA damage, culminating in the activation of caspase-9. Caspase-8 and caspase-9 are the initiator caspases that activate the effector caspases, such as caspase-3 and caspase-7.

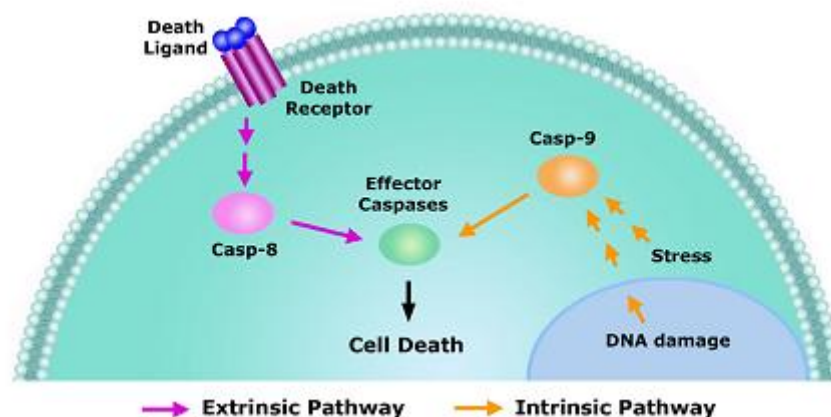


Figure 24. Apoptotic pathways.

Components of the apoptotic signalling network are genetically encoded and ready for action in most cell types; they are kept in an inactive state and are turned on in a response to a death stimulus. When caspases become enzymatically active, apoptosis reaches the “point of no return”. Hence this mechanism must be strictly controlled by numerous genes and proteins, categorized by their activities as inhibitors or initiators of apoptosis. Key regulators are represented by Bcl-2-family proteins that regulate caspase activation either negatively or positively. An

aberrant expression of members of this family has been associated with several tumors. Other apoptosis modulators activate cascades which are in turn subject to regulation by downstream factors such as Bcl-2. Among the upstream modulators are oncogenes such as c-myc, which activates apoptosis, but its function can be blocked by overexpression of Bcl-2 and so expansion of tumors can occur. Ultimately, tumor suppressor p53 induces apoptosis under certain conditions, thereby accounting for at least a portion of its tumor suppressive activity.^{43,47}

1.2.3 Epigenetic mechanisms

Epigenetic is the study of the alteration in gene expression (function) without changing the nucleotide sequence; it refers to all heritable changes in gene expression and chromatin organization that are independent from DNA sequence itself.⁴⁸

The two main epigenetic mechanisms in gene regulation are represented by modification of the chromatin folding: indeed the most important role in such regulations is played by the enzyme that modulate all the proteins involved with DNA in the formation of chromatin, and those proteins themselves. Chromatin is a dynamic complex of nucleic acids (DNA or RNA) and proteins (histones); it represents the “higher-order structure” of DNA, and “packages” the entire cell genome into a smaller volume to fit in the nucleus.

Nucleosomes are the basic structural units of chromatin, and comprise DNA wrapped around a histone octamer formed by four histone partners: a H3-H4 tetramer and two H2A-H2B dimers.⁴⁹ Histones are small basic proteins highly conserved through evolution consisting of a globular domain and a more flexible and charged N-terminal tail that protrudes from the nucleosome.⁵⁰ Dynamic higher order structure of nucleosomes can bring to different levels of chromatin organization, and consequently to a different gene activity: a condensed, transcriptionally silent form named heterochromatin and a less condensed form term euchromatin, which contains most actively transcribed genes (Figure 25).

The different structural conformations adopted by chromatin are dependent on the epigenetic modifications that occur in the DNA and in the histone tails.

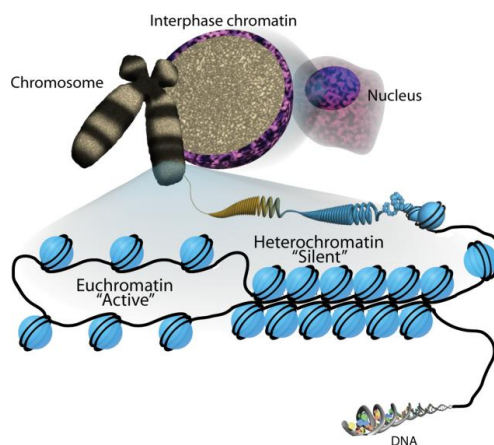


Figure 25. Chromatin organization.

1.2.3.1 Histone deacetylases (HDACs)

Histone post-translational modifications^{51,52} constitute the “histone code”, which is interpreted by additional proteins in order to regulate gene expression. These modifications include acetylation, phosphorylation, methylation, ubiquitination and ADP-ribosylation and take place on the tail domains of histone. The amino terminal tail is lysine rich and contains about half of the positively charged residues. Among these modifications, histone acetylation of the ϵ -amino group of lysine residues was found to play an important role in gene expression, and is correlated with gene activation because neutralizes the positive charge of the histone lysine residues, relaxing the chromatin conformation thus facilitating the binding of transcription factors and subsequently gene transcription.⁵³ Lysine acetylation is a reversible modification affected by a highly balanced system of two classes of enzyme, histone acetylases (HATs) and histone deacetylases (HDACs). HATs catalyze the transfer of acetyl groups from acetyl CoA to the lysine residue. HDACs promote deacetylation of acetylated residue resulting in a closed chromatin structure and in the inhibition of gene transcription (Figure 26).

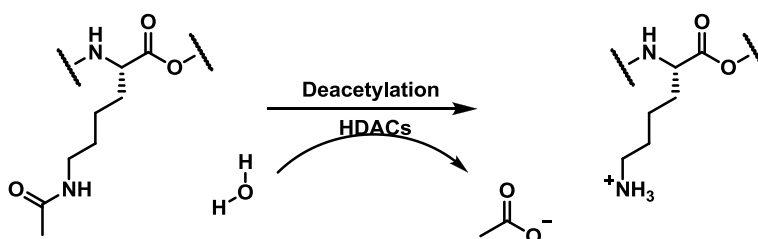


Figure 26. Lysine deacetylation by HDACs

Altered activity of both HATs and HDACs has been identified in several types of cancer.

To date, eighteen human HDACs have been identified and grouped into four classes:⁵³ class I comprises HDACs1, 2, 3 and 8 which are located inside the nucleus; class II comprises HDACs4, 5, 6, 7, 9 and 10 which are located in both the cytoplasm and the nucleus, and are further divided into class IIa (HDAC4, 5, 7, 9) and class IIb (HDAC6 and 10); in class III HDACs are homologous with Sir2, and ultimately class IV comprises HDAC11, homologous with class I and II enzymes. Classes I, II and IV require Zn^{2+} as cofactor for their deacetylase activity, and they are called “conventional HDACs”, whereas sirtuins are NAD^+ dependent.

HDACs have targets other than histones, including transcription factors, such as p53 and c-Myc, and other non-histonic proteins involved in regulation of cell cycle progression and apoptosis.

1.2.3.2 HDACs inhibitors

One of the most interesting features of epigenetics is the reactivation of genes using small molecules able to successfully reverse some epigenetic changes. This potential reversibility of epigenetic aberrations has become tempting targets for cancer treatment with modulators that demethylate DNA or inhibit histone deacetylases, leading to the reactivation of silenced genes.

HDAC inhibitors have emerged as a new class of promising cancer therapeutic agents and have been shown to induce differentiation, apoptosis and to inhibit migration, invasion, and angiogenesis in many cancer cell lines. In October 2006 the FDA approved the first HDAC inhibitor Vorinostat **8** (Zolinza, Suberoylanilide hydroxamic acid, formerly known as SAHA, Merck & co) (Figure 27) to treat the rare cancer cutaneous T-cell lymphoma (CTCL). At least twelve different HDACs are currently in some phase of clinical trials as monotherapy or in combination chemotherapy or radiation therapy in patients with hematologic and solid tumors.⁵⁴

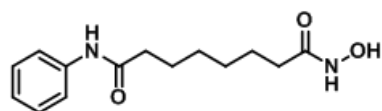


Figure 27. Vorinostat (SAHA).

HDACs inhibitors have been purified from natural sources, or have been synthesized, and they can be structurally grouped into four classes:⁵⁵ hydroxamates, cyclic peptides, aliphatic acid and benzamides as shown in Figure 28. Thricostatin A (TSA) was the first natural hydroxamate found with HDAC inhibitory activity, and is a pan-inhibitors as well as SAHA. Romidepsin, which was approved by the FDA in 2009 for treatment of CTCL, is the most important member in the class of cyclic peptides. It acts as prodrug, converting intracellularly by reducing the disulfide bond to a sulfhydryl group able to interact in the active site pocket of class I HDAC.

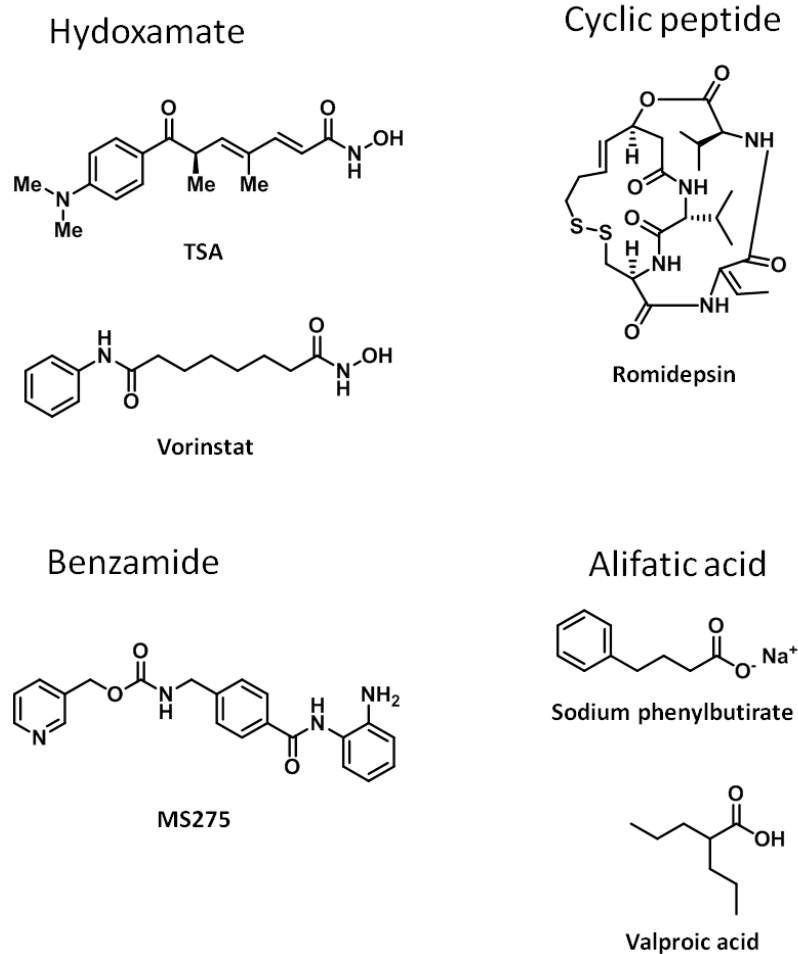


Figura 28. HDAC inhibitors.

Classic pharmacophore of HDAC inhibitors consists of three distinct functional groups, each of which interacts with a specific region of the HDAC active site.^{56,57} These groups include a capping group, which interacts with amino acids near the entrance of the active site; a zinc-binding motif, which resides in the protein interior and complexes the metal ion involved in catalysis; a hydrophobic cavity-binding linker to appropriately arrange the capping and metal binding groups. A representative example is shown in Figure 29.⁵⁷

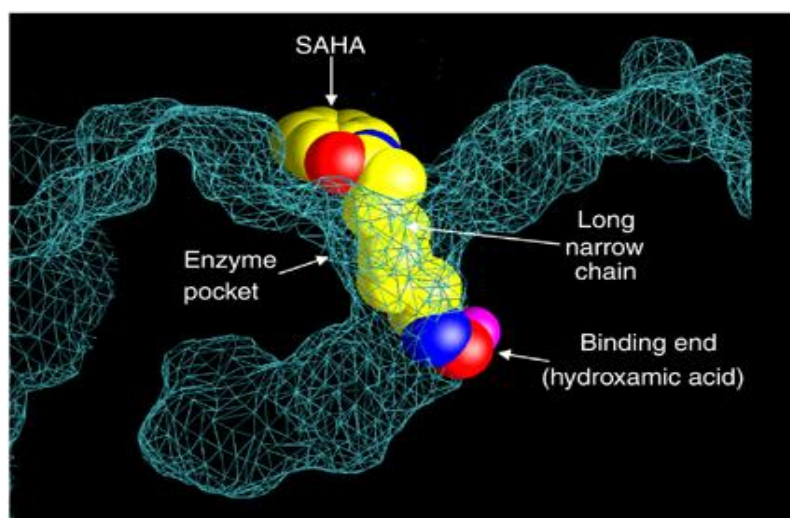


Figure 29. Structure of SAHA bound to an HDAC-like protein (taken from Marks⁵⁷).

To date, clinical trials of HDAC inhibitors have been focused on cancer treatment, but there is growing evidence about their potential therapeutic effects against neurodegenerative disease and many other nonmalignant diseases as diabetes, inflammation and arthritis.

2. Aim of the work and synthetic strategies

2.1. Design and synthesis of chimeric compounds

One of the strategies for the development of novel anticancer treatment aims to affect mechanisms that regulate important cell functions with small molecules. As a matter of fact, neoplastic diseases are characterized by multiple genetic and epigenetic alterations of critical regulatory proteins leading them to mutated form associated with deregulated cell proliferation, suppression of apoptosis and aberrant epigenetic changes. The identification and understanding of the numerous molecular and cellular mechanisms underlying these critical processes can help to elucidate the molecular biology essential for their functioning and can offer valuable insights toward the development of innovative anticancer drugs.

A multiple-target drug design could fulfill the complex nature of cancer, by addressing more than a single pathway and avoiding resistance problems.

Over the past years, the research group in which I worked during my PhD has been engaged in a project aimed at identifying novel biologically active small molecules, which can be either antitumor lead candidates, or valuable chemical tools to study molecular pathways in cancer cells. From a chemical point of view, the main interest was focused to privileged structures or molecular scaffold suitable to the rapid parallel synthesis of natural-like derivatives. For this purpose, a novel class of *cis*- and *trans*-stilbene-compounds⁵⁸ (Figure 30) structurally related to resveratrol **9**, a natural compound widely investigated for its chemopreventive and chemotherapeutic properties, was synthesized with the aim of discovering new lead compounds with pro-apoptotic activity.

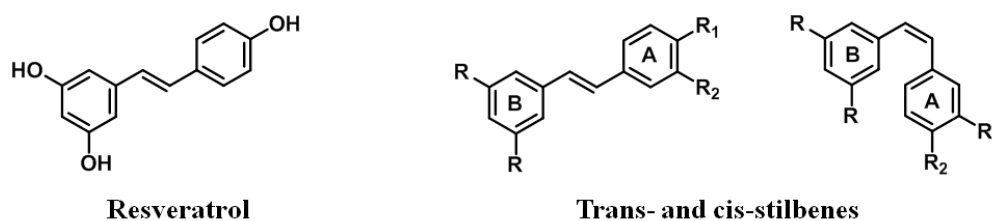


Figure 30. Stilbene-derivatives library.

Many derivatives were found to be active as apoptosis-inducing agents in HL60 leukemia cell lines, and some of them showed to be active even toward

resistant HL60R cell lines. This study confirmed the stilbene architecture as privileged scaffold.

These interesting results prompted to further investigate this structure; therefore a phenyl ring was incorporated as a bioisosteric substitution of the stilbene alkenyl bridge in order to increase the chemical diversity. Thus, a second library of terphenyl and biphenyl derivatives has been synthesized^{59,60} (Figure 31).

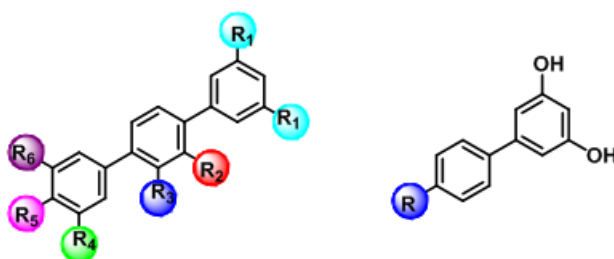


Figure 31. Terphenyl and biphenyl library.

Among these derivatives, trihydroxylated terphenyl **10** showed to be able to block cell cycle in G0-G1 phase (Figure 32) in Bcr-Abl-expressing K562 cell lines and to induce functional and morphological differentiation (Figure 33) in sensitive acute myelogenous leukemia HL60 cell lines.⁶⁰

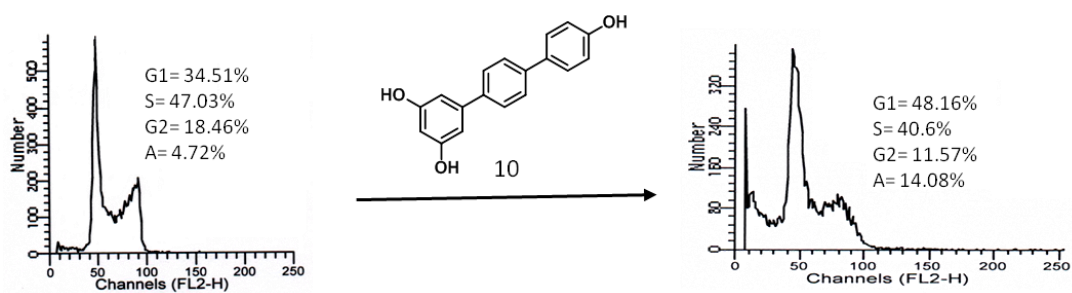


Figure 32. Cell cycle distribution of K562 cell exposed for 48 h to 50 μM of **10**.

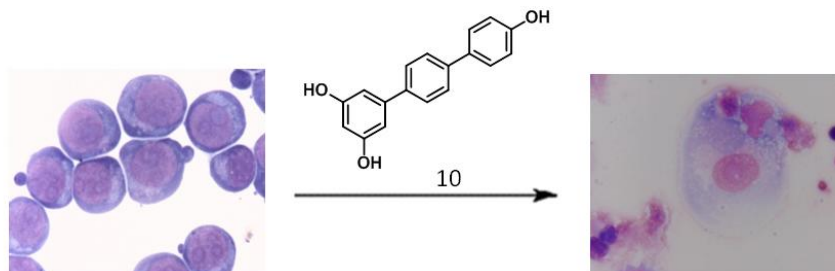


Figure 33. Morphologic changes in HL60 cells after 96 h exposure to **10** (10 μM).

A further development of this project aimed to increase the biological profile by enhancing the structural complexity and diversity of these compounds. Therefore, a new collection of molecules comprising of a natural-like scaffold as complexity-bearing core and bi- or terphenyl as privileged fragments was obtained (Figure 34).^{61,62} A class of natural terphenyl derivatives with the spiro ring motif (spiromentins) is also present in nature.⁶³

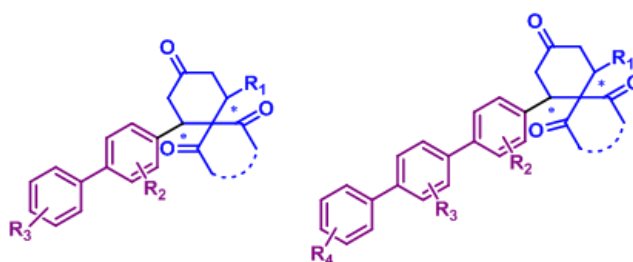


Figure 34. Library of hybrids of spirocyclic ketones with biphenyls and terphenyls.

Some of the new compounds showed a well-defined activity on apoptosis or differentiation, clearly different from those of the previously studied terphenyl. Moreover, they were found to decrease the level of Bcl-2 expression, which is overexpressed in many types of cancer (Figure 35) in Bcr-Abl-expressing K562 cells.

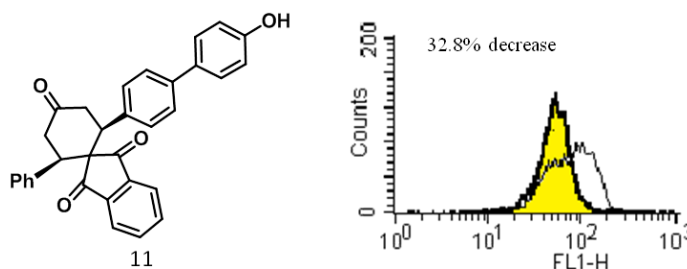


Figure 35. Effect of a representative compound **11** (30 μ M) on Bcl-2 expression in K562 cells after 24 h.

As a follow-up of these projects described above, in view of the multifactorial mechanistic nature of cancer, during the first part of PhD, my research activity has been focused on the design and synthesis of chimeric compounds able to interfere with different molecular pathways. According to this approach, the aim of my work was to synthesize new chimeric molecules (Figure 36) by linking via amide

bond fragments as suberoylanilide hydroxamic acid (SAHA **8**, Figure 27, an HDACs inhibitor approved for the treatment of cancer cutaneous T-cell lymphoma) analogues, targeting epigenetic mechanisms, together with fragments such as substituted bi/terphenyl or stilbenes derivatives able to interact with cell cycle progression, previously synthesized in our lab, and such as Sorafenib **12** (a multikinase inhibitor approved for the treatment of renal cell and hepatocellular carcinomas)^{64–67} derivatives maintaining the ureidic fragment responsible of the kinase inhibitory activity.^{68,69} Indeed it has been reported in the literature that combined treatment with vorinostat and sorafenib synergistically induces apoptosis in CML cells.⁶⁵

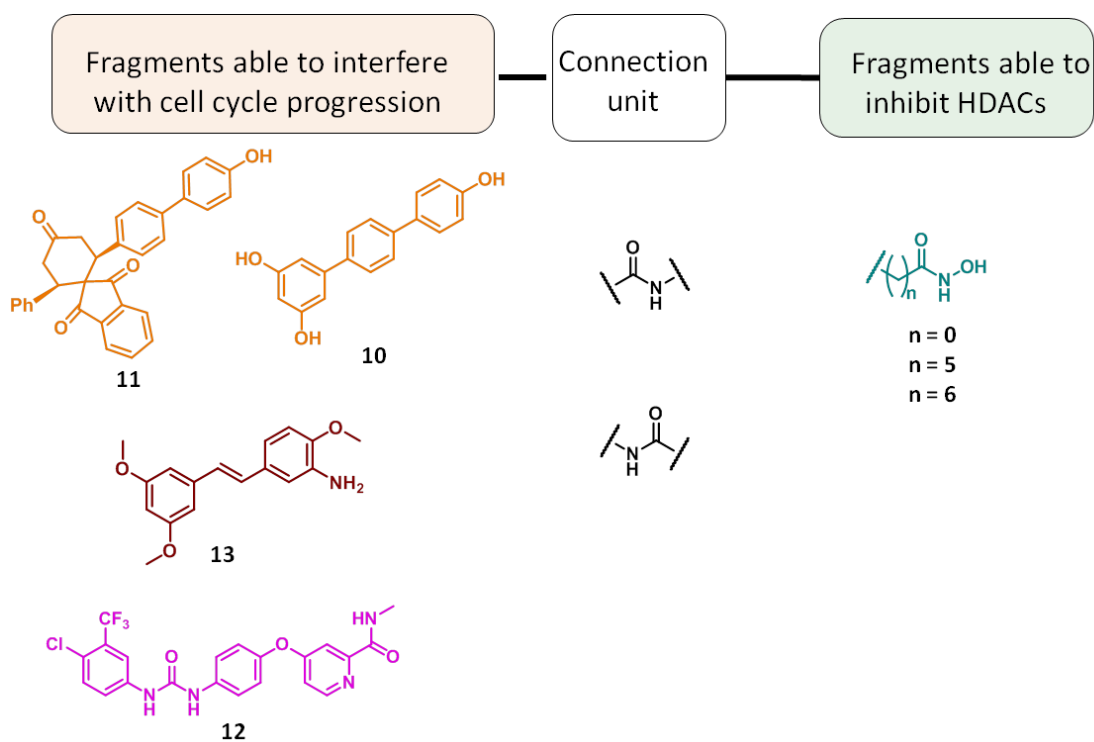


Figure 36. Design of MLs.

Retrosynthetic analysis (Figure 37) suggested that the desired chimeric compounds **14-16** could be prepared via a reverse amide bond compared with the connection unit of SAHA **8**, between bi/terphenylic acid derivatives **17** and **18** and suitable straight chains **19-20** containing an hydroxamic function previously protected. On the other hand, chimeric compounds **21** and **22** could be obtained by coupling together stilbenes derivatives **13** and diphenyl ureidic Sorafenib

fragment ⁶⁴ **23** with suberic acid monomethyl ester **24** through an amide bond similarly to SAHA; in both cases the ester function can be converted to an hydroxamic acid through reaction with hydroxylamine. In the same way, introducing the ester function in the terphenyl structure as in **26** could lead to chimeric compound **25**.

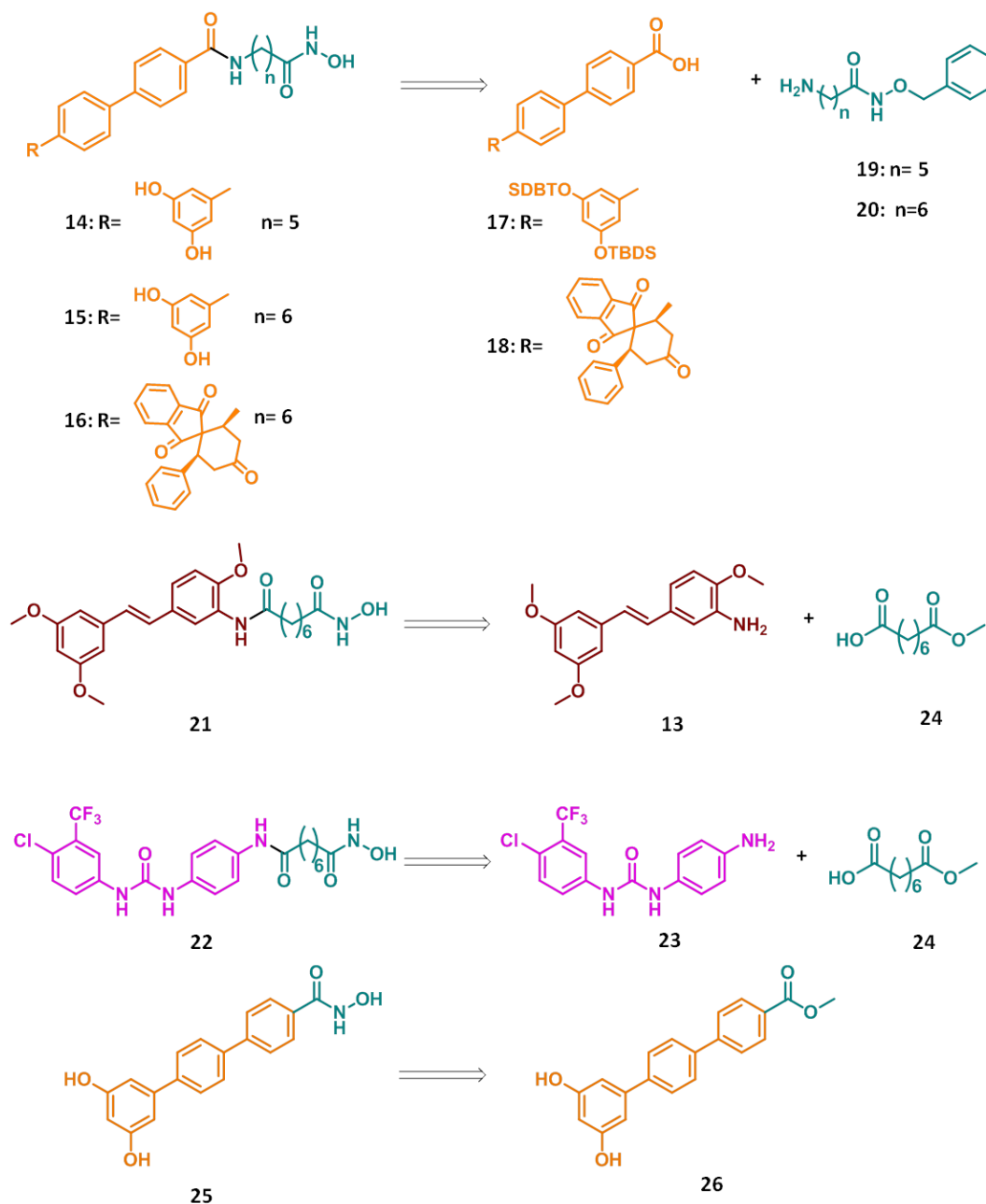
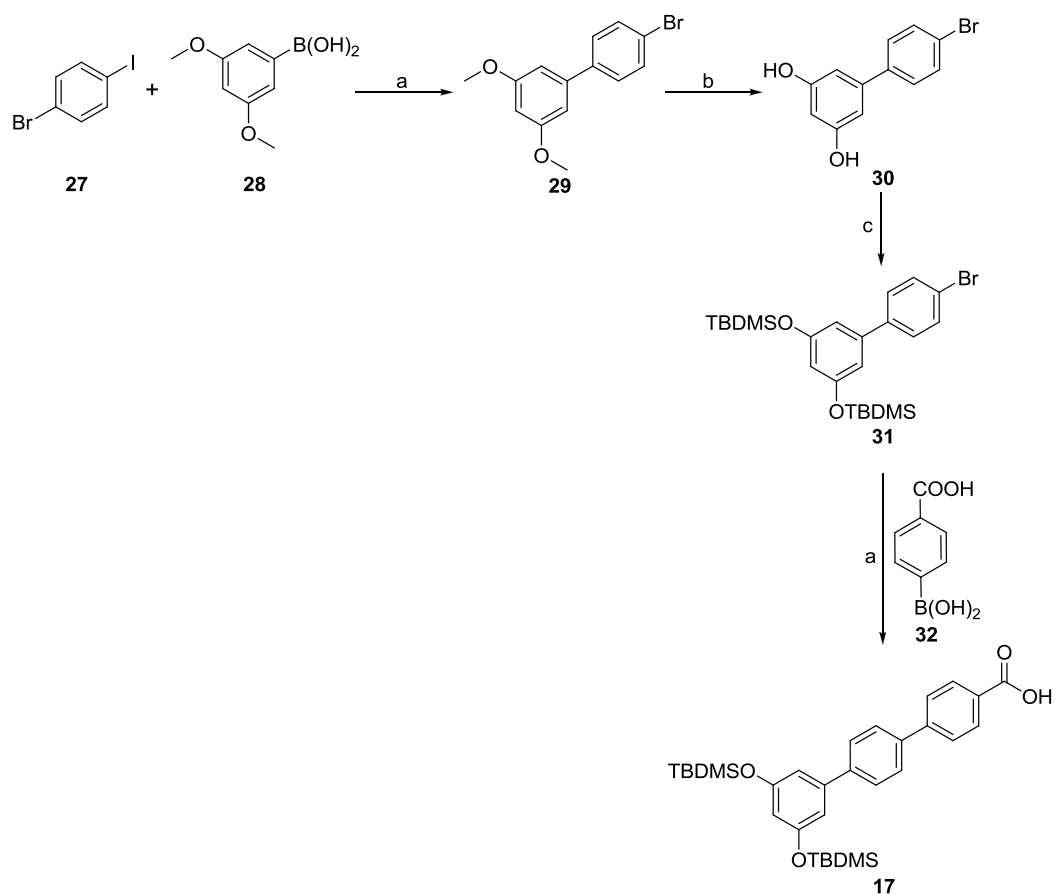


Figure 37. Retrosynthetic analysis.

All the distinct synthons were separately synthesized as described in the following.

Terphenyl acid **17** was obtained as shown in Scheme 1: a cross coupling Suzuki reaction between 1-bromo-4-iodobenzene **27** and 3,5 dimethoxy phenyl boronic acid **28** (both commercially available) gave biphenyl **29**, followed by demethylation with BBr_3 and subsequent protection of the obtained dihydroxy biphenyl **30** with TBDMS. A second Suzuki coupling between the resulting biphenyl **31** and carboxyphenyl boronic acid **32** (commercially available) afforded terphenyl acid **17**.

SCHEME 1^a

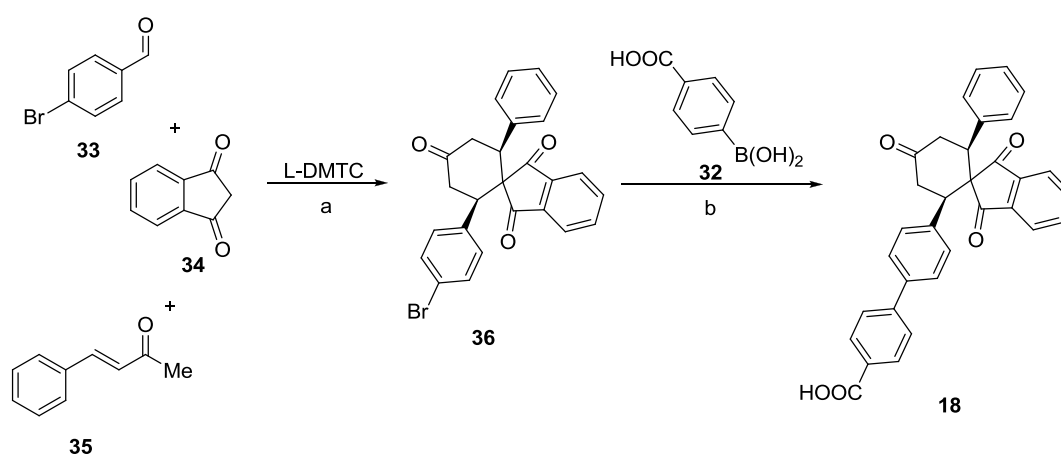


^a**Reagents and conditions:** a) $\text{Pd}(\text{PPh}_3)_4$, Na_2CO_3 2M, toluene/EtOH 3:1, 5h, reflux; b) BBr_3 1M, CH_2Cl_2 , 24h, -72° to r. t.; c) TBDMS-Cl, imidazole, DMF, 20h r. t.

Spirocyclic derivative **18** was synthesized in a highly diastereoselective way following a linear two-step synthetic route previously described by Pizzirani *et*

al.^{61,62} The first step involved a domino three-component Knoevenagel/Diels–Alder/epimerization sequence between 4-bromo-benzaldehyde **33**, 1,3-indandione **34** and *trans*-buten-2-one **35** (all of them are commercially available) in the presence of a catalytic amount of (L)-5,5-dimethyl thiazolidinium- 4-carboxylate (DMTC). The resulting spirocyclic ketone scaffold **36** presented an aryl bromide essential for the second step, that provided the desired compound **18** through a Suzuki coupling with carboxyphenyl boronic acid **32** (Scheme 2).

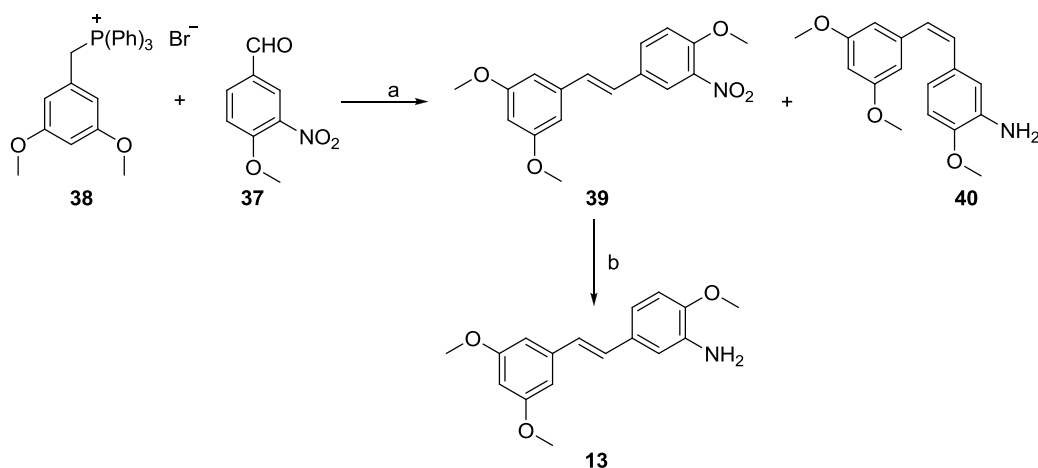
SCHEME 2^a



^a**Reagents and conditions:** a) MeOH, 72h, r.t.; b) Pd(PPh₃)₄, Na₂CO₃ 2M, THF/H₂O 3:1, 5h, reflux.

Stilbenes **13** were synthesized following synthetic protocols previously described by Roberti *et al.*⁵⁸ based on a Wittig reaction between aromatic aldehyde **37** (commercially available) and ylide **38** for the construction of the stilbenic core; the reaction produced a mixture of *trans* **39** and *cis* **40** isomers that were separated by flash chromatography. Reduction of the *trans* derivative with sodium dithionite gave the amino derivatives **13** (Scheme 3).

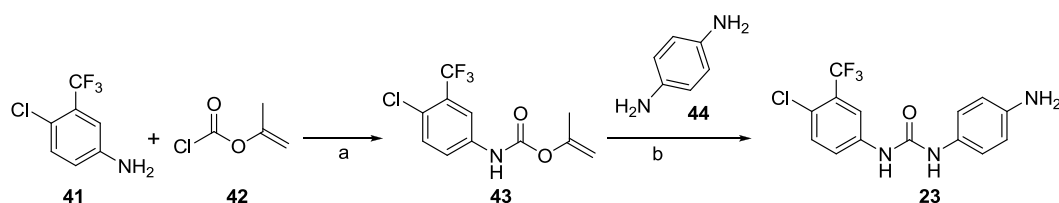
SCHEME 3^a



^a**Reagents and conditions:** a) *n*-BuLi, THF, 6 h, -78 °C to r.t.; b) Na₂S₂O₄, acetone/H₂O, 50 °C, 4h.

Diphenyl urea **23** was obtained in two steps: first coupling between 4-chloro-3-(trifluoromethyl) aniline **41** and isopropenyl chloroformate **42** (both commercially available), gave carbamic acid isopropenyl ester **43**. In the second step, a second coupling between diamine benzene **44** and derivative **43** afforded the desired urea as shown in Scheme 4.

SCHEME 4^a

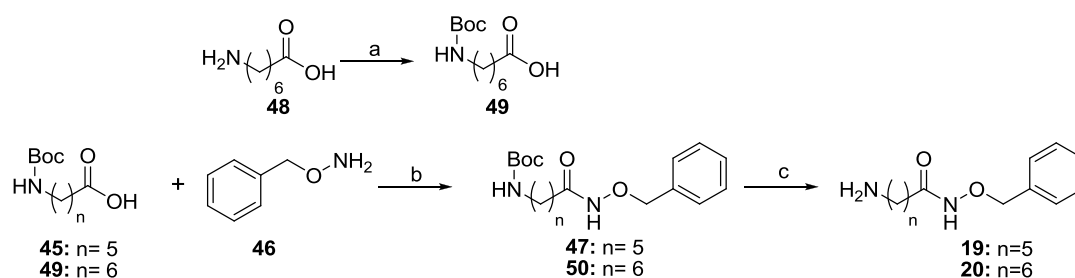


^a**Reagents and conditions:** a) NaOH, EtOAc, 1h, 5 °C to r.t.; b) toluene, 2h, reflux.

SAHA analogues containing a shorter linker of five methylenes (instead of six), are reported to maintain their HDAC inhibitory activity⁷⁰. Therefore, among the fragments able to inhibit HDACs, we thought to start with the amino chain with 5 methylenes **19**, since BOC-aminocaproic acid **45**, commercially available, is quite cheap. As shown in Scheme 5, synthon **19** is hence obtained via amide bond from the amino-protected acid **45** with hydroxybenzylamine **46**

(commercially available), and subsequent BOC removal of the resulting amide **47** with trifluoroacetic acid. Following the same procedure, amino chain **20** was synthesized starting from the BOC protection of free amino heptanoic acid **48**, which afforded amino-protected acid **49** that was coupled with hydroxybenzylamine **46**; the resulting amide **50** was deprotected in the same condition reported above to give the desired amino chain **20** (Scheme 5).

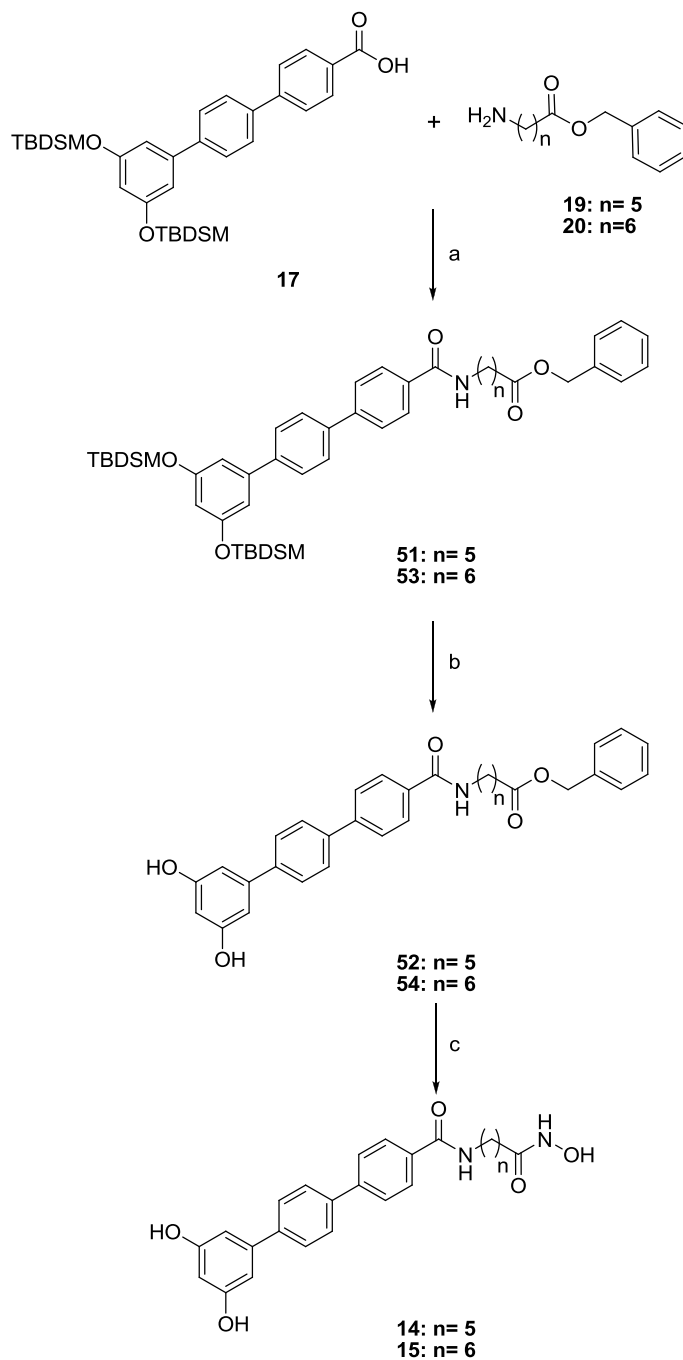
SCHEME 5^a



^a**Reagents and conditions:** a) BOC₂O, NaOH 5M, *ter*ButOH, 24h, r. t.; b) Py-BOP, DIEA, CH₂Cl₂, 48h r. t.; c) CF₃COOH/CH₂Cl₂ 1:2, 5h r. t.

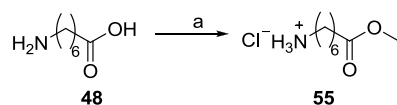
The desired hybrid hydroxamate **14** was obtained starting from EDC-OHBT coupling between the protected terphenyl derivative **17** with the amino chain **19**, giving amide **51**. Removal of the TBDMS group by TBAF gave **52** which hydrogenation of the benzyl group afforded **14** (Scheme 6). An analogue pathway was thought for synthesis of hybrid compounds **15**. After coupling of terphenyl **17** with the amino chain **20**, the resulting amide **53** was deprotected with TBAF in the same conditions reported for compound **14**, but the debenzoylation of dihydroxy derivative **54** afforded the desired compound **15** mixed with a lot of impurities and hard to purify (Scheme 6). Therefore we decide to replace the protected hydroxamic function with an ester. With this in mind, the new amino chain **55** was synthesized through an esterification with dimethoxy propane and HCl of amino heptanoic acid **48** (Scheme 7).

SCHEME 6^a



^a**Reagents and conditons:** a) HOBt, EDC, NMM, DMF, 20 h, r.t.; b) TBAF/CH₃COOH 1/1, 2h 0°C to r.t.; c) H₂, Pd/cat, THF, 4 h, r.t.

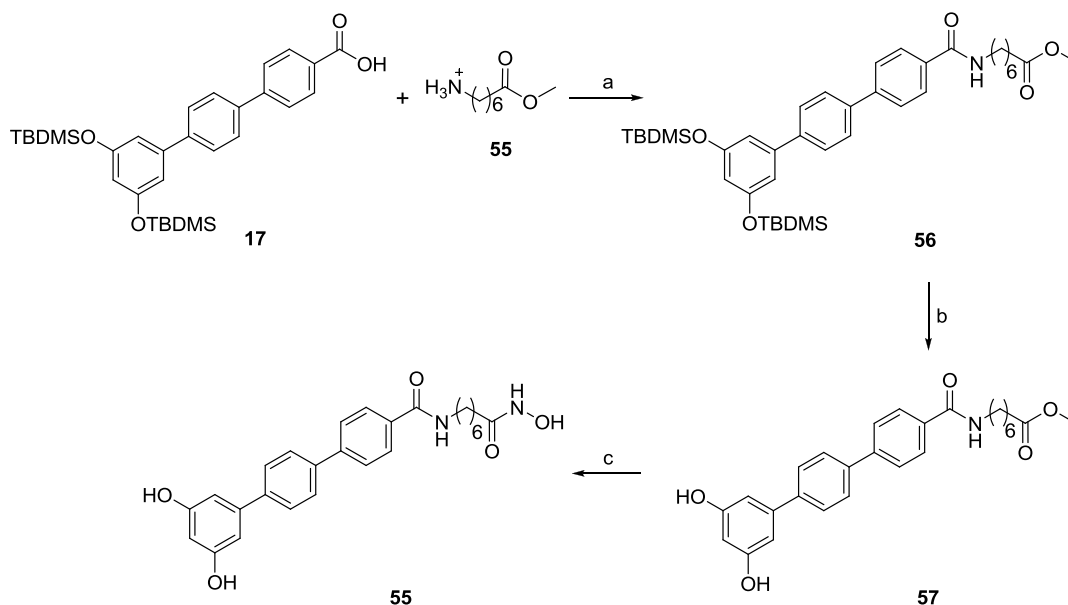
SCHEME 7^a



^a**Reagents and conditions:** a) dimethoxypropane, HCl 12N, 48h, 0 °C to r. t.

The new successful synthetic plan for compound **15** first consisted of a PyBOP coupling between terphenyl **17** and the amino methyl ester **55**. The resulting amide **56** was deprotected by TBAF giving **57** that reacted with hydroxylamine hydrochloride to obtain the hydroxamic acid function (Scheme 8).

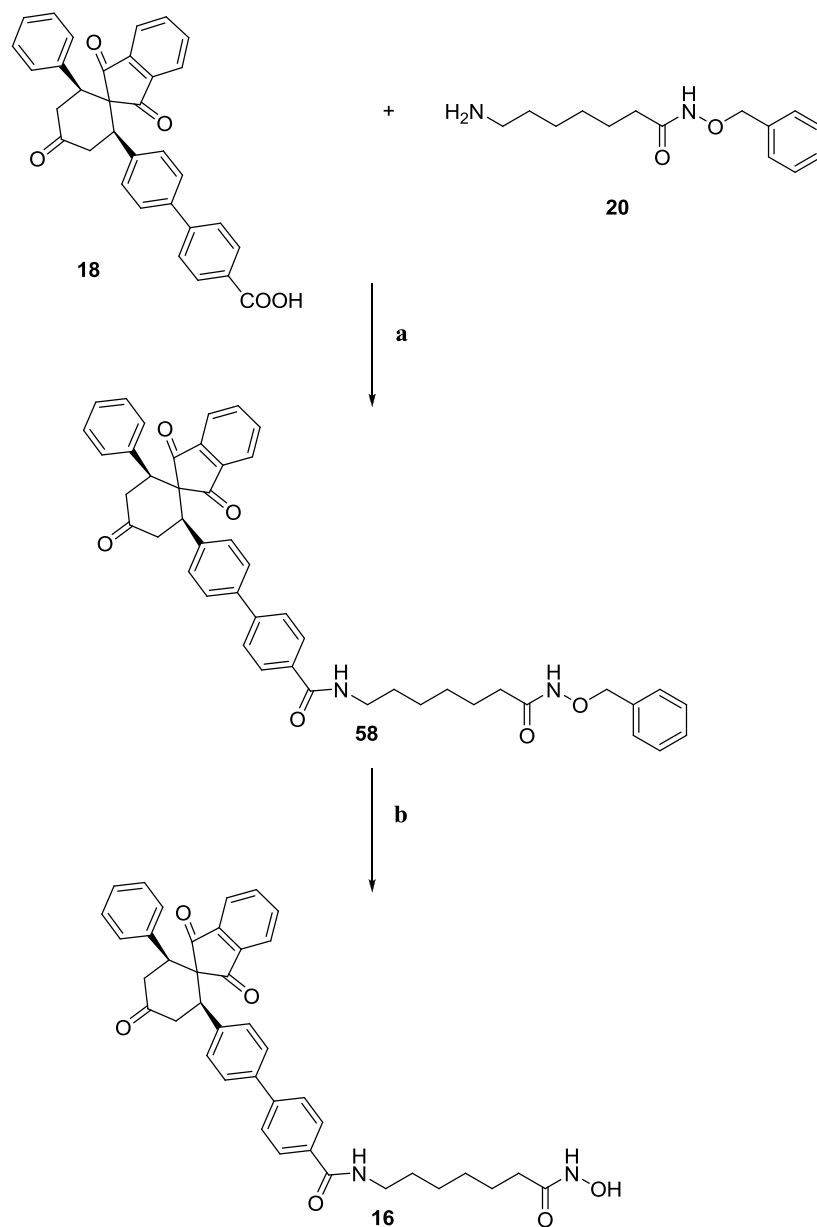
SCHEME 8^a



^a**Reagents and conditons:** a) PyBop, DIEA, CH₂Cl₂, 72h r.t.; b) TBAF/CH₃COOH 1/1, 2h 0°C to r.t.; c) NH₂OH·HCl, NaOMe, MeOH, 3h, 0°C to r. t.

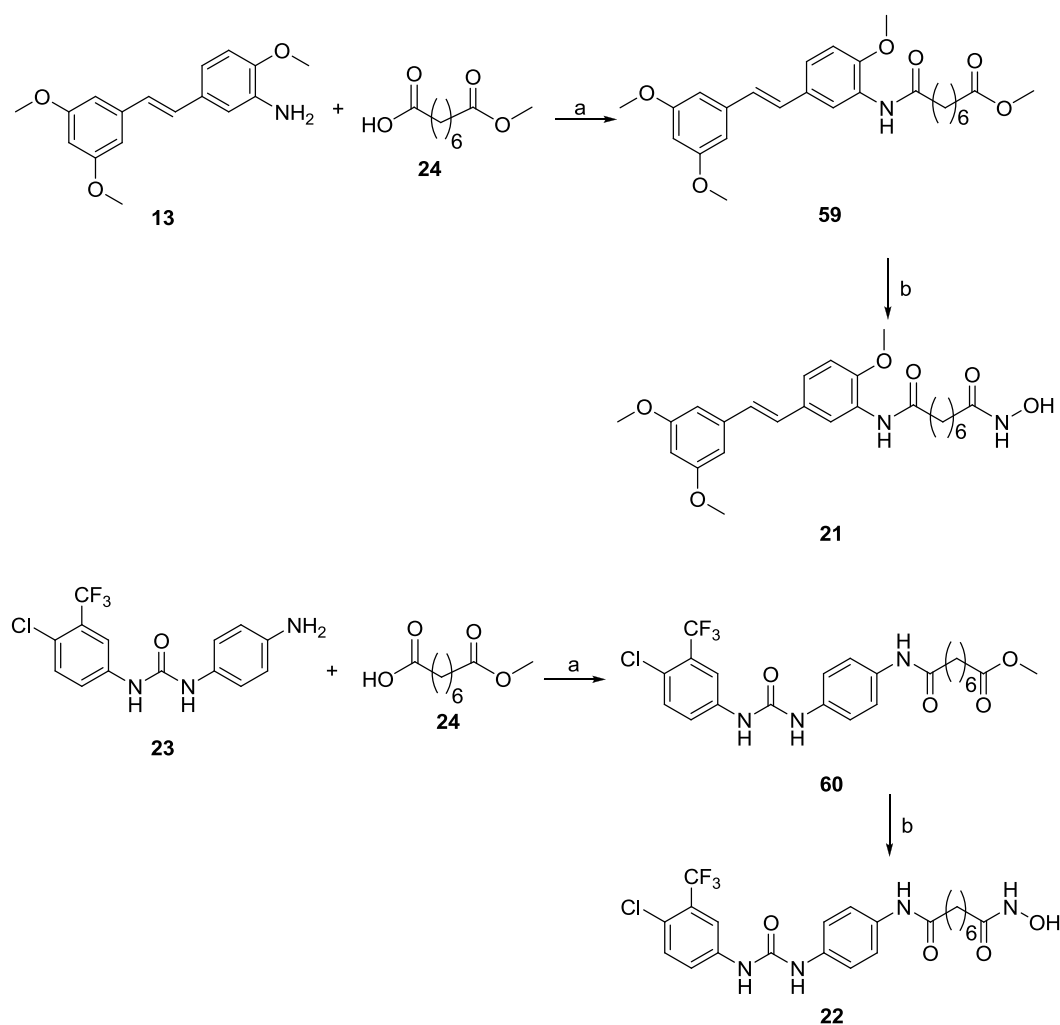
Synthetic plan for hybrid compound **16** envisaged an amide bond formation between spirocycle **18** and amino chain **20**, followed by debenzoylation of the resulting amide **58** (Scheme 9). Unfortunately this compound showed to be very unstable under all the different conditions we attempted, and it decomposed in a very short time.

SCHEME 9^a



^aReagents and conditons a) HOBt, EDC, NMM, DMF, 24h, r.t.; b) H₂, Pd/cat, THF.

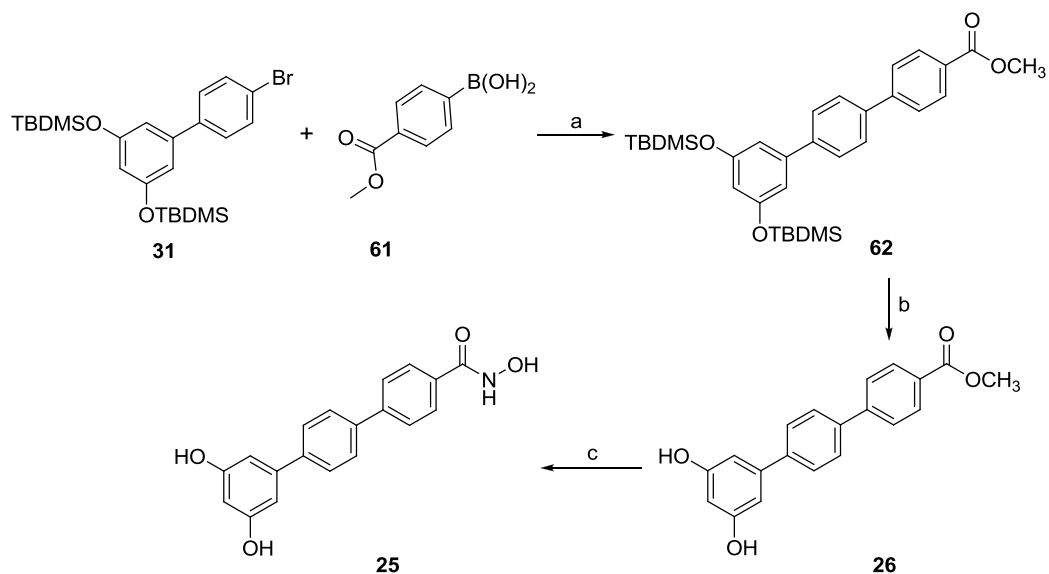
Compounds **21** and **22** were prepared via a two-step reaction: formation of an amide bond between suberic acid monomethyl ester (commercially available) **24** and the appropriate amines **13** and **23** to obtain respectively amides **59** and **60**; subsequent conversion of the methyl ester in the hydroxamic acid moiety (Scheme 10) to afford hybrid compounds **21** and **22**.

SCHEME 10^a

^a**Reagents and conditions:** a) OHBT, DCC, DMF, 48 h, r. t.; b) $\text{NH}_2\text{OH}\cdot\text{HCl}$, NaOMe, MeOH, 3h, 0 °C to r.t.

As a further development of this project, we design a new chimeric compound by merging the hydroxamic acid function in the terphenyl scaffold. The synthetic route is shown in Scheme 11: initially a Suzuki coupling between biphenyl **31** and boronic acid **61** afforded a protected terphenyl with a methyl ester moiety **62**. Removal of TBDMS provided **26**, which was treated with hydroxylamine hydrochloride to give the desired hybrid compound **25**.

SCHEME 11^a



^a**Reagents and conditons:** a) Pd(PPh₃)₄, Na₂CO₃ 2M, toluene/EtOH 3:1, reflux 5h.;b) TBAF/CH₃COOH 1/1, 2h 0 °C to r. t.; c) NH₂OH·HCl, NaOMe, MeOH, 3h, 0 °C to r. t.

The final chimeric compounds are shown in Figure 38.

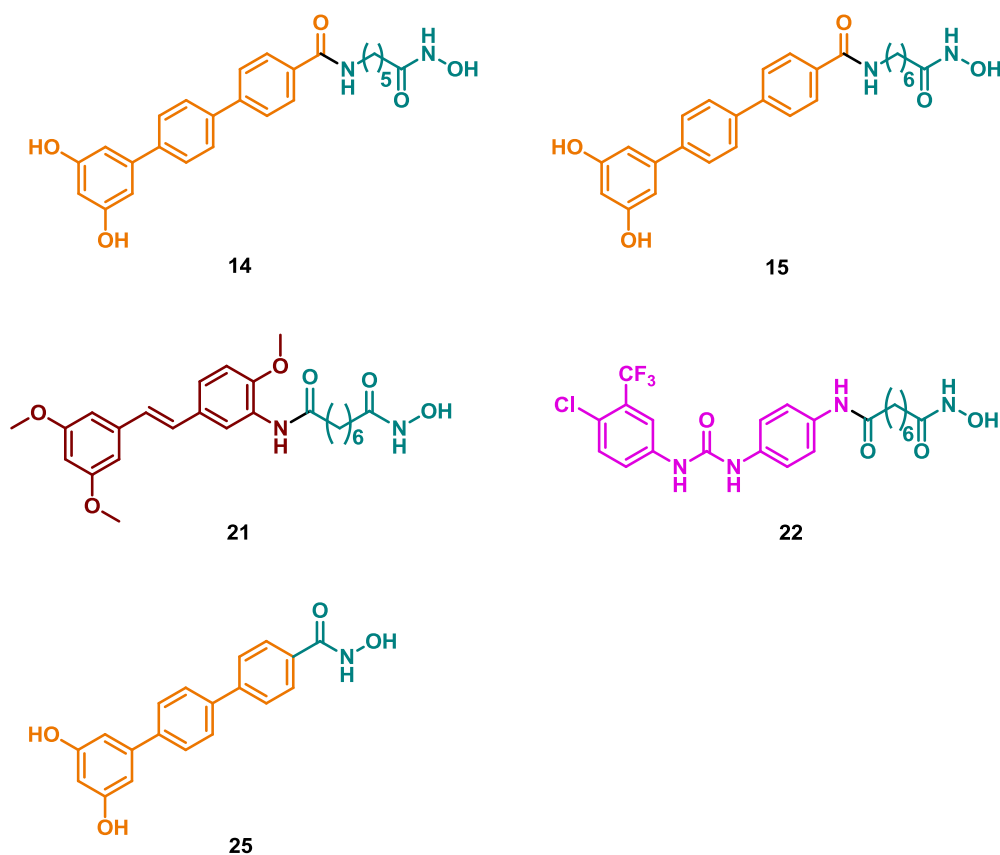


Figure 38. Final chimeric compounds.

2.2 DOS Library of Macrocyclic Peptidomimetics.

In order to acquire expertise toward new synthetic approaches for the efficient generation of libraries of potential biologically active small molecules, and especially to get experience in diversity-oriented synthesis (DOS), during the last PhD year I spent a 8 months training period in Dr Spring group at the University of Cambridge (UK). In this laboratory, one of the main research interest is directed to the development and optimization of new strategies with highly synthetic accessibility to obtain structurally diverse and complex small organic molecules, which can be used to exploit biological systems. DOS reveals to be the best way to achieve this goal.

In such a context, during my period in Spring's lab, I was involved in a project of a DOS library of small molecules based on a macrocyclic peptidomimetic framework.

Macrocycles are molecules characterized by a ring that contains at least twelve atoms. This architecture is a common structural feature observed in natural products. Although the conformation is not rigid, a macrocycle has a pre-organized ring structure that provides diverse functionality and stereochemical complexity. Therefore, key functional groups in this scaffold can address protein targets in an highly affinity and selectivity manner, and with high potency.⁷¹ Despite these unique structural properties, this class is poorly explored within drug discovery, even though over 100 macrocycle drugs derived from natural products have been developed into approved drugs. This is in part due to synthetic complexity; a DOS strategy can tackle this challenge, suggesting new efficient and flexible methods to ideally access a wide range of macrocyclic scaffolds.^{72,73}

Peptide-based molecules are also attractive therapeutic agents, considering their high specificity and low toxicity profile. However, they present critical issues such as a very short half-life, and a poor bioavailability. The use of peptidomimetics bypasses these problems associated with natural peptides. Indeed, peptidomimetics are compounds whose pharmacophores mimic a peptide or protein in 3D space retaining the ability to interact with the biological target of interest, and producing the same biological effect.⁷⁴ The modifications on the chemical structure involve changes to an existing peptide that will not occur

naturally, such as incorporation of non natural amino acids or altered backbones.⁷⁵ The latter modification can be achieved by using bioisosters of important functional groups, e.g. by introducing a triazole ring that mimics either the *cis*- or the *trans*-like configuration of the amide bond.⁷⁶

Many bioactive peptides in living systems present a macrocyclic framework, and macrocyclic peptidomimetics are found to modulate biological systems. This type of compounds consists of a chiral cyclic skeleton constrained in a certain degree of rigidity and of side chains with a well-defined orientation. Some examples of biologically active macrocyclic peptidomimetics found in nature are represented by Cyclosporin A^{77,78} **63**, a cyclic undecapeptide consisting completely of hydrophobic amino acid, which is an immunosuppressant drug to prevent graft rejection after transplant surgery and Bicyclomycin⁷⁹ **64**, that includes a diketopiperazine motif, the smallest possible cyclic peptide (Figure 39).

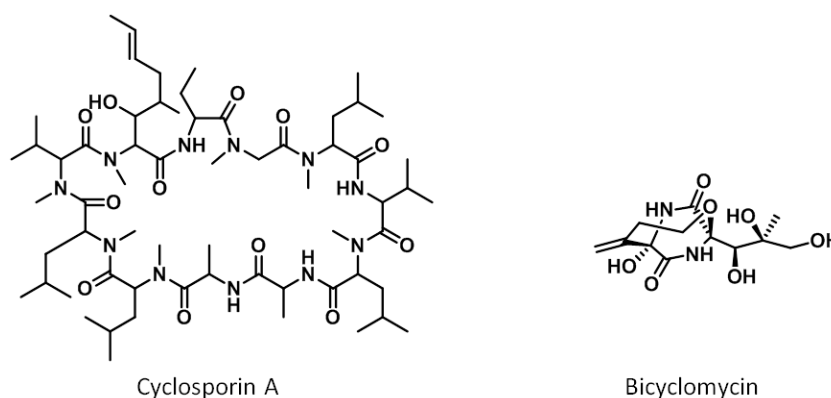


Figure 39. Example of macrocyclic peptidomimetics.

Given that, in order to find new and undescribed methodologies of broad utility for the synthesis of a diverse range of such compounds, during my stay in Spring's lab I worked on a project aimed to the construction of a DOS library of structurally diverse small molecules based on biologically relevant macrocyclic peptidomimetic frameworks.⁸⁰ This library has two main general structure types: both of them have a triazole ring as bioisoster of the amide bond, and one of them incorporates a diketopiperazine motif in the macrocycle (Figure 40). Notably, in both types there are multiple points where stereochemical and scaffold diversity can be introduced, since every molecules have at least two stereogenic centers,

and four different possible scaffolds can be obtained, such as *cis/trans*-DKPs, 1,4 and 1,5 triazole.



Figure 40. General structures of library compounds.

The synthetic strategy was based around the elegant three-phase approach called Build/Couple/Pair, pioneered by Nielsen and Schreiber⁸¹:

1) *Build phase*: asymmetric syntheses of chiral building blocks (BB) with functional groups essential for the subsequent coupling and pairing steps are performed.

In this step two kind of variously substituted amino acids were synthesized as BB: azido-amines and alkyne-acids.

2) *Couple phase*: intermolecular reactions to join BB take place. This phase, together with the previous one, provides the basis for stereochemical diversity; it is important then to have a complete control of all possible stereochemical outcomes.

Couplings via amide bond between the azido-amines and alkyne-acids were performed to obtain linear peptidomimetics.

3) *Pair phase*: intramolecular reactions that join pairwise combinations of functional groups previously incorporated in the compound are performed. This process provides the basis for skeletal diversity.

This phase comprised of two cyclization steps: first a 1,3-dipolar cycloaddition between the azide and the alkyne functionalities gave the triazol ring to generate the desired macrocyclic skeleton, then the second cyclization between the amine and carbonyl moieties introduced the diketopiperazine (DKP) motif into the framework.

In Figure 41 the outline of the B/C/P for this library is reported. Macrocycles obtained in both steps of the pair phase represent the final library compounds.

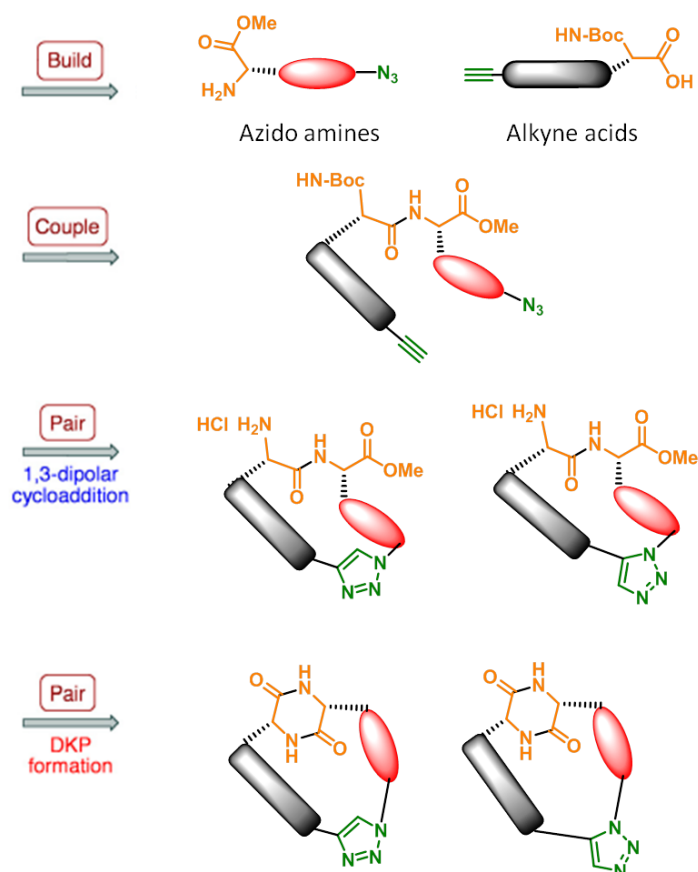


Figure 41. B/C/P strategy.

In this context, my efforts have been directed to the synthesis of rigid derivatives of library compounds. It has been reported how increasing the rigidity of a molecule can help to reduce the entropic penalty to binding and so tend to give higher affinity and more selectivity toward a particular target. Moreover, the introduction of extra-rigidity leads to additional shape diversity, thus exploring other areas of biologically relevant chemical space. A representative example is displayed by Piperazinomycin **65**,⁸² a naturally occurring macrocyclic piperazine endowed with antimicrobial and antifungal activity (Figure 42).

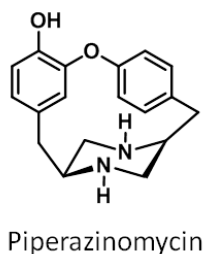
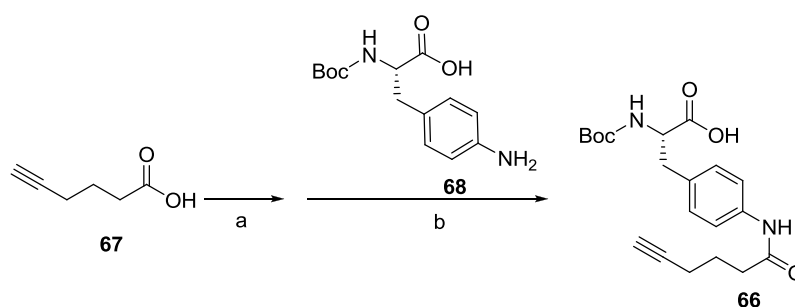


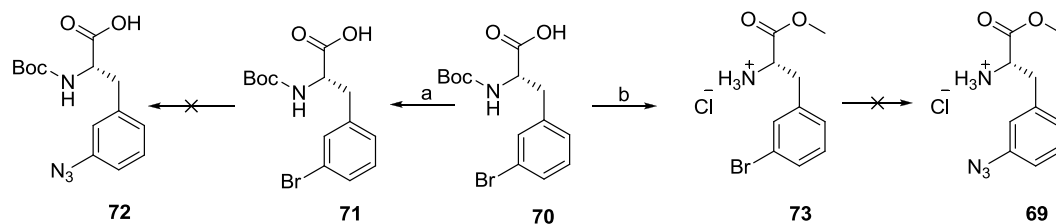
Figure 42. Piperazinomycin.

From a chemical point of view, it was envisaged to rigidify the macrocyclic scaffold by replacing an alkyl chain by an aromatic ring. For this purpose, in the *build phase* the alkyne acid **66** was synthesized starting from activation of 5-hexynoic acid **67** with DCC and Oxyma Pure, followed by coupling with Boc-phenylalanine **68**, both commercially available (Scheme 12). A first attempt for the synthesis of azide-amine **69** was made starting from commercially available 3-Br-Boc-phenylalanine **70**. First a Boc protection was performed to obtain derivative **71**, but the Ullmann-type conversion using CuI as catalyst did not lead to the aryl azide **72**. The same problem was found in a second attempt, in which the starting material was converted in ester **73** first, but did not afforded the desired compound (Scheme 13). Finally, azide amine **69** was obtained as shown in Scheme 14: 3-nitro-Boc-phenylalanine **74** (commercially available) was catalytically hydrogenated under pressure in presence of a base, to give the corresponding amino derivative **75** which was converted to azide **72** by a diazotransfer reaction. Treatment of the latter with TBAF in MeOH gave the desired building block **69**. Both syntheses of the two compounds gave high yield, an important requirement in the *build phase*, since building blocks constituted the basis for the entire library.

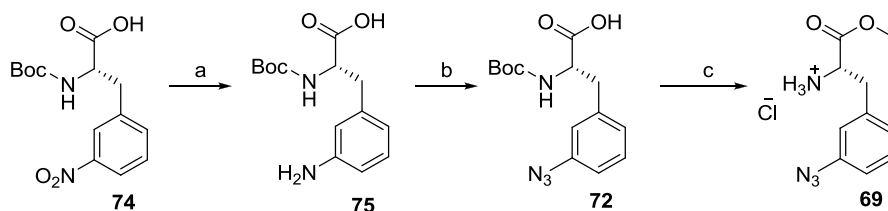
SCHEME 12^a



^aReagents and conditions: a) DCC, Oxyma Pure, DMF, 1 h, r.t.; b) DIPEA, DMF, 12 h, r.t.

SCHEME 13^a

^a**Reagents and conditions:** a) BOC₂O, NaOH 5M, *ter*ButOH, 24h, r. t.; b) TMSCl, MeOH, 12 h, 0 °C to r.t.

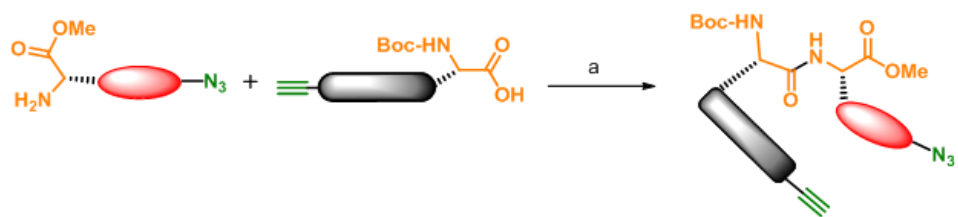
SCHEME 14^a

^a**Reagents and conditions:** a) H₂, K₂CO₃, Pd on Charcoal, MeOH, 55 psi, 3 h, r.t.; b) imidazole-sulfonyl-N₃, CuSO₄, K₂CO₃, MeOH, 18 h, r.t.; c) TMSCl, MeOH, 12 h, 0 °C to r.t.

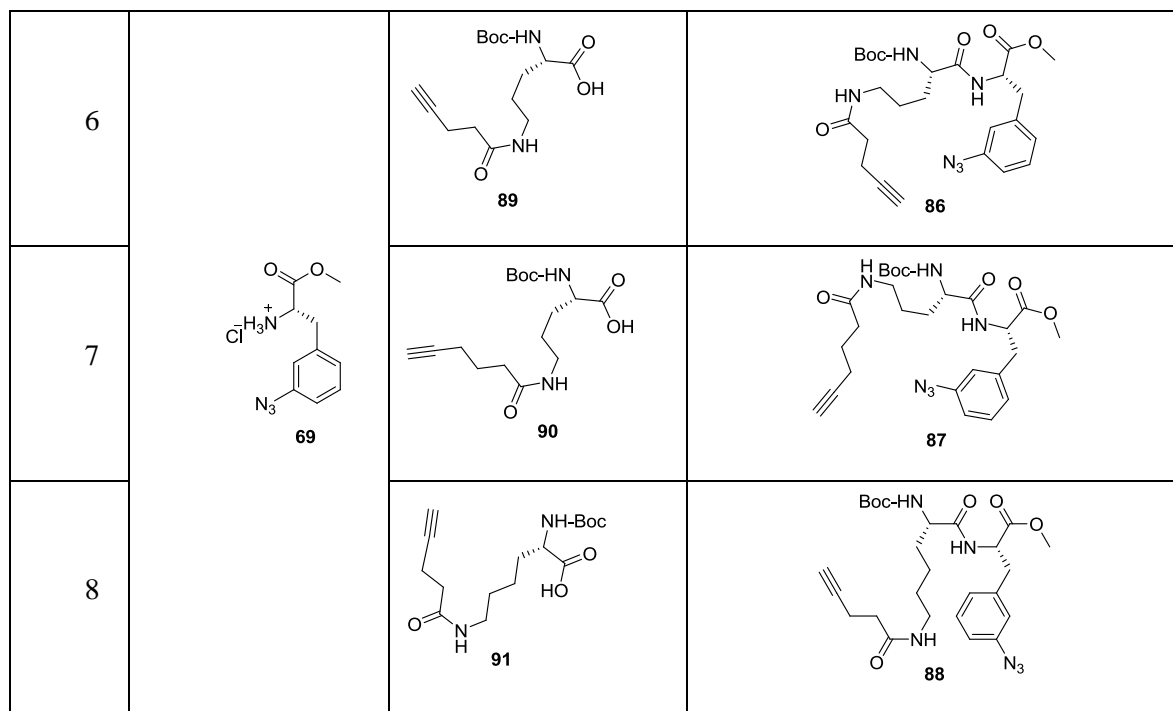
In the *couple phase*, the alkyne acid **66** was coupled via amide bond formation with the opportune azide amines **80-85** (previously synthesized in Spring's lab) to give respectively dipeptides **76-79** (Scheme 15 entry 1-5). On the other hand, azide amine **69** coupled with suitable alkyne acids **89-91** (previously synthesized in Spring's lab) under the same conditions afforded respectively dipeptides **86-88** (Scheme 15 entry 6-8).

All linear peptides were obtained as single stereoisomers.

SCHEME 15^a

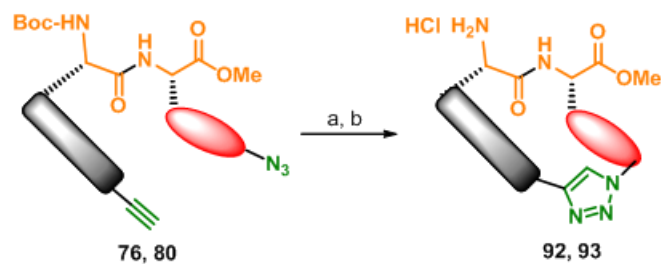


Entry	Azino amines	Alkyne acid	Linear peptides
1	<p>81</p>		<p>76</p>
2	<p>82</p>		<p>77</p>
3	<p>83</p>	<p>66</p>	<p>78</p>
4	<p>84</p>		<p>79</p>
5	<p>85</p>		<p>80</p>



^a**Reagents and conditions:** EDC·HCl, HOBt, TEA, CH₂Cl₂, 12 h, r.t.

The first step of the *pair phase* consisted of a “click” type 1,3-dipolar cycloaddition to generate 1,4 and 1,5 triazole and thus to construct the macrocyclic architecture. The regioselectivity of the reactions was under catalytic control and was confirmed by NMR and HPLC analysis: copper catalyst provided 1,4 triazole macrocycles, while ruthenium catalyst afforded the 1,5 triazole derivatives. Therefore, the linear peptides described above containing an alkyne and an azide underwent to click reactions to give macrocyclic peptidomimetics with an high degree of skeletal diversity. The conditions of these reactions were optimized by Isidro-Llobet *et al.*:⁸⁰ linear dipeptides **76** and **80** were refluxed overnight in the presence of CuI and DIPEA (“Copper route”) to give 1,4 triazole macrocycles; the subsequent Boc removal (except for **86** which deprotection led to unstable macrocycle) with HCl 4M gave the final desired compounds respectively **92** and **93**, as shown in Scheme 16.

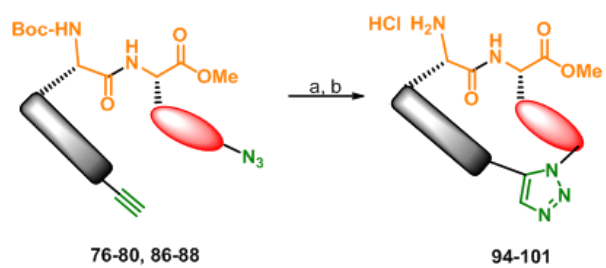
SCHEME 16^a

Entry	Linear peptides	1,4 Triazole macrocycles
1	76	<p style="text-align: center;">92</p>
2	80	<p style="text-align: center;">93</p>

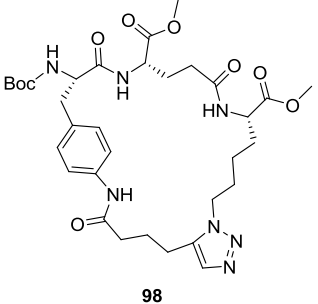
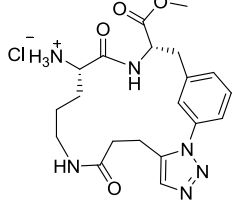
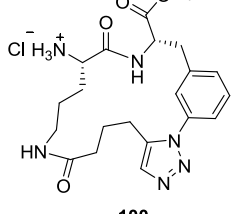
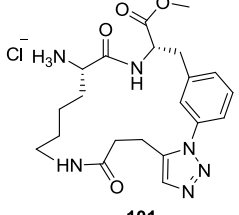
^a**Reagents and conditions:** a) CuI, DIPEA, THF, 12 h, reflux; b) HCl 4M in dioxane, 12 h, r.t.

Linear peptides **76-80**, and **86-88** were refluxed in the presence of $[\text{Cp}^*\text{RuCl}]_4$ to give 1,5 triazole regioisomers, that after BOC removal (except for **98**, which deprotection led to unstable macrocycle) in the same conditions just described, afforded macrocycles **94-101** (Scheme 17).

SCHEME 17^a



Entry	Linear peptides	1,5 Triazole macrocycles
1	76	<p style="text-align: center;">94</p>
2	77	<p style="text-align: center;">95</p>
3	78	<p style="text-align: center;">96</p>
4	79	<p style="text-align: center;">97</p>

5	80	 <p style="text-align: center;">98</p>
6	86	 <p style="text-align: center;">99</p>
7	87	 <p style="text-align: center;">100</p>
8	88	 <p style="text-align: center;">101</p>

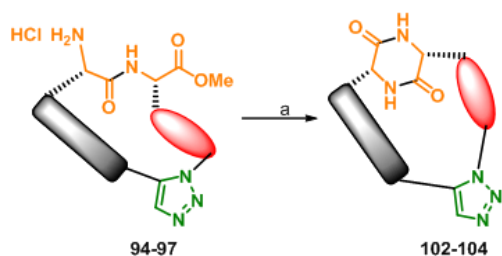
^a**Reagents and conditions:** a) [Cp*RuCl]₄, Toluene, 12 h, reflux; b) HCl 4M in dioxane, 12 h, r.t.

Ultimately, in the second step of the *pair phase*, the DKP motif was introduced in the macrocyclic scaffold by a second intramolecular cyclization between the amine and the carbonyl moieties. The synthetic methodology, described for the first time by Isidro-Llobet *et al.*,⁸⁰ looked to a synthesis microwave-assisted using solid supported NMM (morpholinomethyl polystyrene).

Because of the higher rigidity due to this additional ring closure, not all the previously synthesized macrocycles underwent to this reaction, even though longer reaction times were attempted. However, under these conditions,

macrocycles **94**, **96** and **97** were converted in the desired final compounds **102**, **103** and **104** respectively, as shown in Scheme 18.

SCHEME 18^a



Entry	Macrocycles	DKP derivatives
1	94	 102
2	96	 103
3	97	 104

^a**Reagents and conditions:** a) NMM-AcOH (1:1.5), 2-Butanol, 9 h, mw 150°C.

As a further extension of the library, new macrocycles were obtained in which one or two amino acids were introduced between the alkyne acids and the azido amines with one or two more *couple steps*. This new concept of

Build/Couple/[Couple]_n/Pair (B/C/[C]_n/P) is shown in Figure 43. In this case, DKP units cannot be obtained, since the amine is now too far from the carbonyl group.

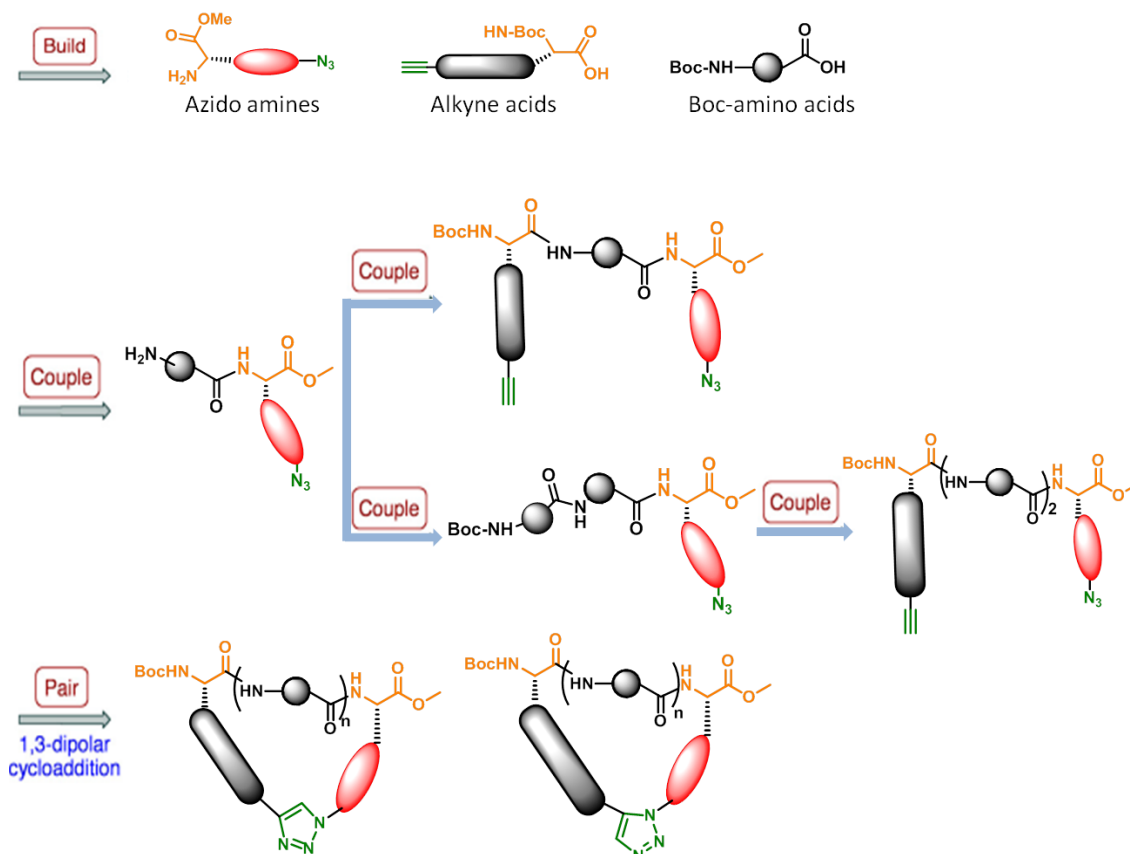
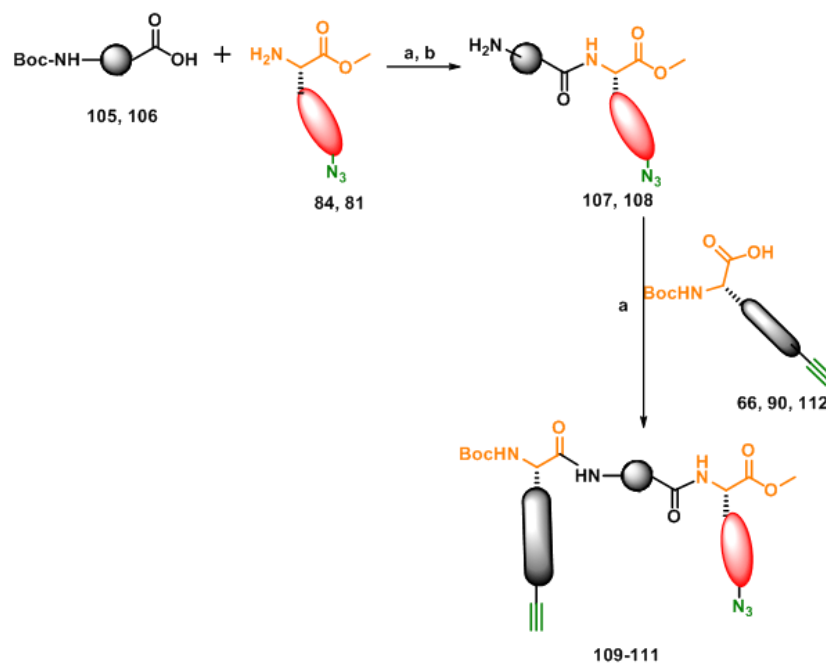


Figure 43. (B/C/[C]_n/P).

Combining commercially available Boc-alanine **105** and Boc- β -alanine **106** with suitable azide amines **84** and **81**, following by Boc removal, afforded respectively dipeptides **107**, which underwent to a second amide bond formation with alkyne acids **66** to give linear tripeptides **109**, and dipeptides **108** that after coupling with **90** and **112** (previously synthesized in Spring's lab), gave linear tripeptides **110-111** (Scheme 19).

SCHEME 19^a

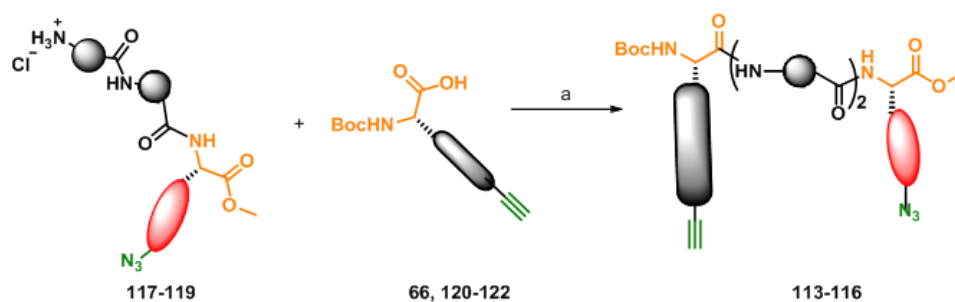


Entry	AA	Azide amines	Dipeptides	Alkyne acids	tripeptides
1	105	84	<p>107</p>	66	<p>109</p>
2	106	81	<p>108</p>	90	<p>110</p>
3			<p>108</p>	112	<p>111</p>

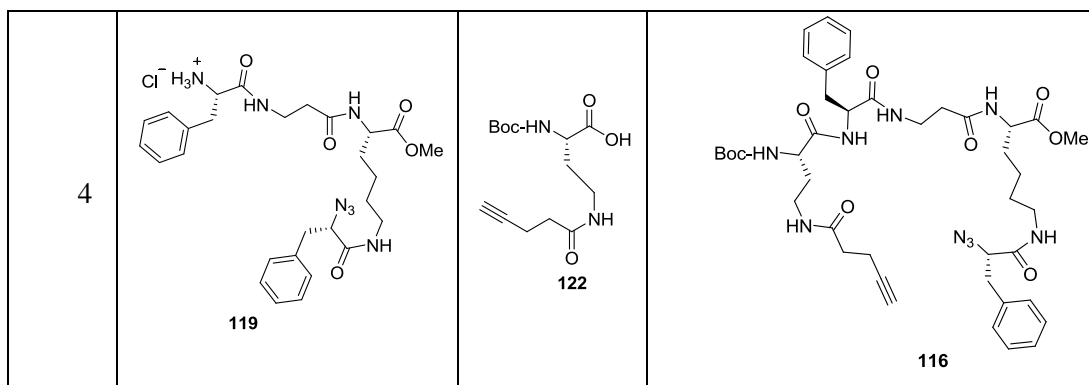
^aReagents and conditions: a) EDC·HCl, HOBt, TEA, CH₂Cl₂, 12 h, r.t.; b) TMSCl, MeOH, 12 h, 0 °C to r.t.

Taking advantage of the same appropriate coupling conditions, additional tetrapeptides **113-116** were obtained starting from precursors **117-119** previously synthesized by me (see experimental part) and alkyne acids **66**, **120-122** already synthesized in Spring's lab (Scheme 20).

SCHEME 20^a



Entry	tripeptides	Alkyne acids	tetrapeptides
1	 117	 121	 113
2	 117	 120	 114
3	 118	66	 115



^a**Reagents and conditions:** a) EDC·HCl, HOBt, TEA, CH₂Cl₂, 12 h, r.t.

All of the linear tripeptides **109-111** and tetrapeptides **113-116** obtained in the *couple phase*, reacted in the appropriate reaction conditions used for *pair phase* to afford new final macrocycles **123-130** (Figure 44).

So far more than 150 final compounds were obtained with good purity, starting from 8 different azide-amines and 14 alkyne-acids.

All the compounds are currently tested against a number of targets including different bacteria types and cancer cells.

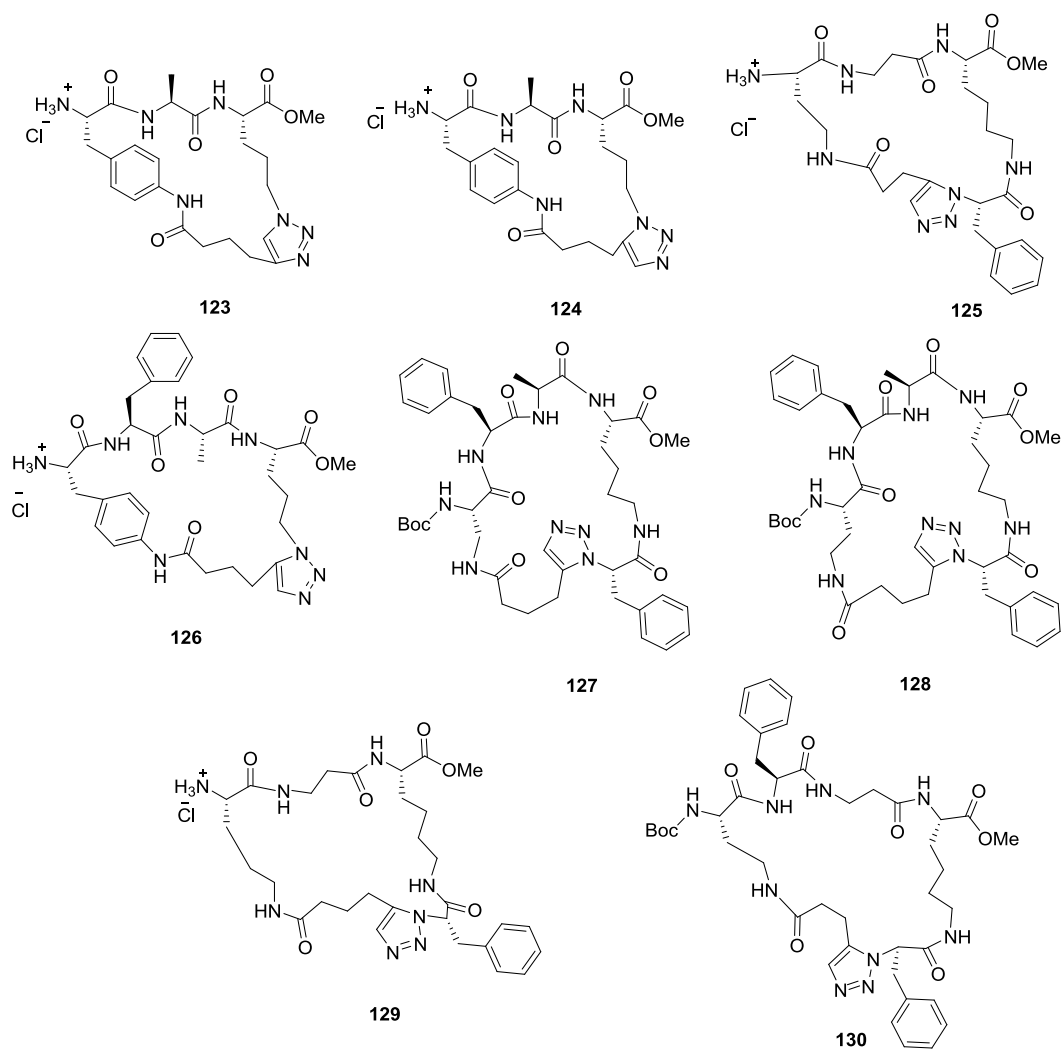


Figure 44. New macrocycles obtained with the . (B/C/[C]_n/P).

3. Biological evaluation

It has previously described the multifactorial mechanistic nature of cancer and how small molecules addressing multiple biological targets could lead to a broader activity spectrum and could represent a new key to overcome the drug resistance commonly observed in cancer chemotherapy.

To this purpose, during the first part of PhD, my research activity has been focused on the design and synthesis of chimeric compounds able to interfere with different molecular pathways involved in cancer cell, using a multitarget-directed drug design strategy. According to this approach, I synthesized new chimeric compounds (Figure 38, Table 1) by combining suberoylanilide hydroxamic acid SAHA **8** (Table 1), (approved for the treatment of cancer cutaneous T-cell lymphoma) analogues, targeting histone deacetylases, together with fragments such as terphenyl or stilbene derivatives previously synthesized in our lab, able to interact with cell cycle progression, and such as diphenyl urea fragment, responsible of the kinase inhibitory activity of Sorafenib **12** (Table 1) (a multikinase inhibitor approved for the treatment of renal cell and hepatocellular carcinomas).

The multitarget profile of the new synthesized chimeric compounds **14-15**, **21-22** and **25** was investigated in comparison with their parent compounds SAHA **8**, terphenyl **10**, *trans*-stilbene **13** and Sorafenib **12** with respect to their cytotoxic activity and their effects on cell cycle progression on leukemia Bcr-Abl-expressing K562 cell line, as well as their HDACs inhibition.

Cytotoxicity was evaluated after 48 h of exposure of tested compounds in K562 cells and then the IC₅₀ (concentration able to inhibit 50% of cell growth) was determined. The effects of each compound on cell cycle were studied by flow cytometry after 24 hours of exposure of tested compounds at the concentration able to completely block cell growth. These studies were conducted in the laboratory of Dr Tolomeo, at the Interdepartmental Center of Research in Clinical Oncology (CIROC), University of Palermo.

HDAC inhibitory activity and selectivity was evaluated after treatment of human recombinant hrHDAC1 (class I HDACs) and hrHDAC4 (class IIa HDACs) with tested compounds. Acetylation of histones and not histone substrates was determined through western blot. These studies were performed in the laboratory of Professor Altucci, University of Napoli.

In this chapter, preliminary available biological data are shown and discussed. A detailed description of analysis procedures used for testing the compounds is reported at the end of the experimental section.

3.1. Preliminary biological results of the antiproliferative activity of chimeric compounds on Bcr-Abl expressing K562 cells.

The antiproliferative activities expressed as IC_{50} of the chimeric compounds **14-15**, **21-22** and **25**, compared with corresponding parent compounds **8**, **10**, **12** and **13**, are shown in Table 1. Analysis of these data allowed some preliminary considerations about the biological profile of tested molecules as cytotoxic agents.

Hybrid compound **21**, whose structure combines the *trans*-stilbene motif with the suberoyl hydroxamic fragment of SAHA, showed the best result, displaying a remarkable cytotoxic activity ($IC_{50} = 1 \mu M$) higher than the stilbene parent compound **13** and comparable to SAHA **8**.

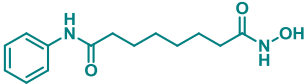
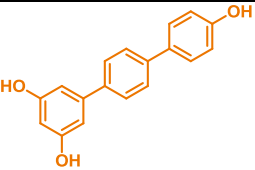
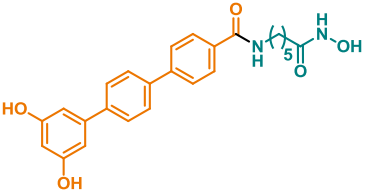
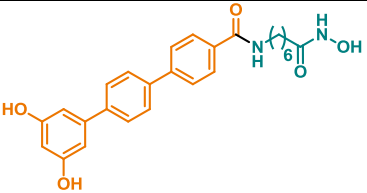
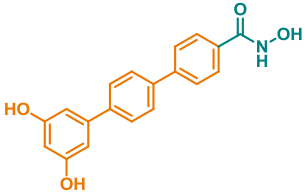
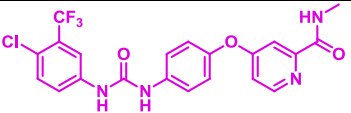
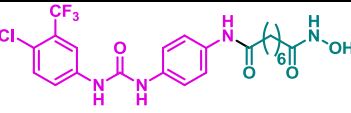
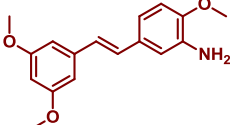
Among the chimeric hydroxamates **14-15** and **25** bearing a terphenyl fragment, the best results was obtained with compound **15** containing a six methylenes chain (like SAHA **8**), with an almost ten-fold enhanced activity ($IC_{50} = 2.5 \mu M$) than the parent terphenyl **10** but lower if compared to **8**. When the alkylic chain is reduced to five methylenes as in compound **14**, a decrease of cytotoxicity was observed, even though it is still higher if compared to the parent compound terphenyl **10**. Removal of the chain as in compound **25** resulted in a sensible decrease of activity, and this compound was found to be the less potent in term of antiproliferative activity, even though its IC_{50} was comparable to terphenyl **10**. These results suggested us that for these chimeric molecules possessing a terphenyl fragment, an alkylic chain of six methylenes (as in SAHA) could confer a better cytotoxic activity on K562 rather than a shorter chain or than no chain at all.

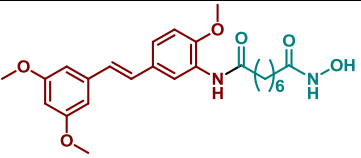
Ultimately, hybrid compound **22** bearing a diphenyl urea fragment, did not improve the cytotoxicity of the two corresponding parent compounds Sorafenib **12** and SAHA **8**.

Given the above results, all the chimeric compounds except **22** were found to have a cytotoxic profile better or at least comparable to that of parent compounds, with derivatives **21** and **15** showing to be the most potent. Both of them enhance

the cytotoxicity of their corresponding parent compound and notably hybrid compound **21** exhibits a remarkable activity comparable to SAHA.

Table 1. IC₅₀ (μM) of multiligands **14-15**, **21-22** and **25** and relatively parent compounds **8**, **10**, **12** and **13** in K562 cell line.

Compounds	Structure	IC ₅₀ (μM)
SAHA 8		1
Terphenyl 10		20
14		6
15		2.5
25		20
Sorafenib 12^a		4
22		10
Stilbene 13		2.5

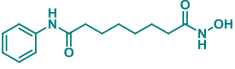
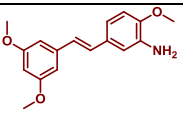
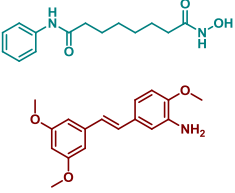
21		1
----	---	---

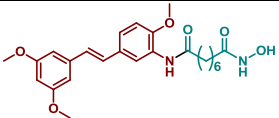
^areported in literature.⁶⁴

The effects of the selected chimeric compounds **14-15**, **25** and **21** on cell cycle were evaluated in K562 cells by flow cytometry and were compared to those of their parent compounds **8**, **10** and **13**. Analysis of G0–G1, S, G2–M and apoptotic peaks revealed that the compounds studied elicit various effects on cell cycle.

Once again the most interesting result was obtained with hybrid compound **21** that showed to have a profile comparable to the combination of the two parent compounds **8** and **13**: in both cases a recruitment of cells in G0-G1 phase and a decrease of cells in S phase were observed similarly to SAHA **8**, while the *trans*-stilbene parent compound **13** induced a remarkable recruitment of cells in S phase. (Table 2 and corresponding Figure 45).

Table 2. Comparison of the effects of parent compounds **8** and **13** alone or in association and multiligand **21** on cell cycle distribution in K562 cells.^a

Treatment	G0-G1 (%)	S (%)	G2-M (%)	A (%)
 8^b	64	8	28	8
 13^c	20	80	0	10
 8^b+13^c	65	16	20	11

 21^c	56	14	29	6
--	----	----	----	---

^aCorrelate with Figure 48. ^b40 μ M. ^c10 μ M

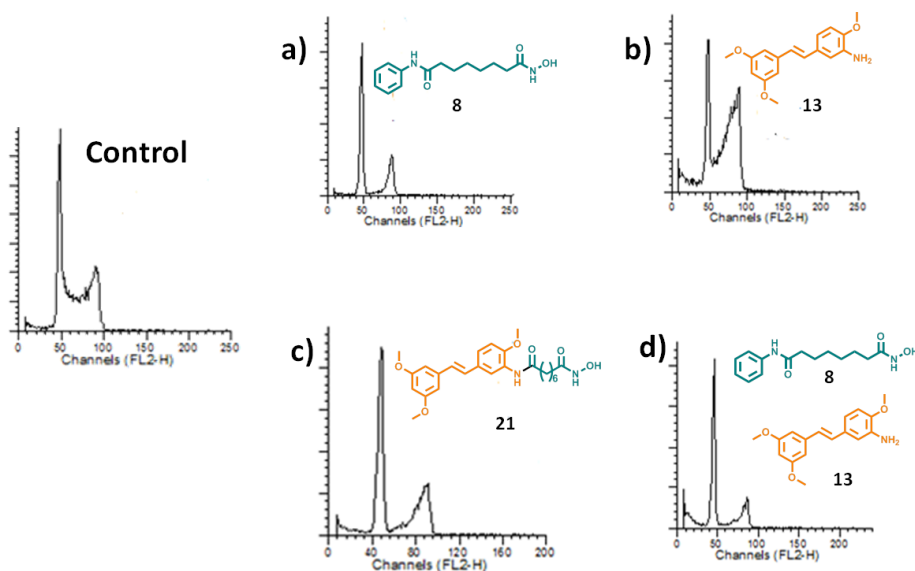
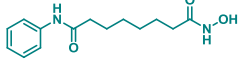
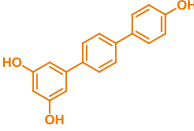
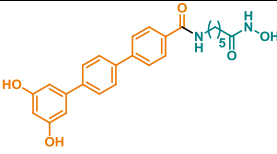
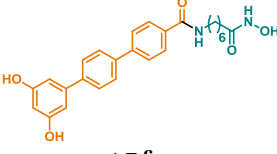
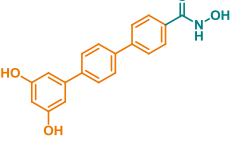


Figure 45. Cell cycle distribution of K562 cell exposed for 24 h to a) **8** (40 μ M), b) **13** (10 μ M), c) **21** (10 μ M), d) **8** (40 μ M) + **13** (10 μ M).

A totally different trend was observed within the series of chimeric compounds **14-15** and **25** all bearing the same substituted terphenyl fragment as reported in Table 3. In this case, only hybrid compound **14** maintained a block in G0-G1 as the parent compounds **8** and **10** even though a recruitment of cells in G2-M phase was also observed. Hybrid compound **15** was found to block cells in G2-M phase without affecting the G0-G1 phase. Finally hybrid compound **25** caused a recruitment of cells in the G2-M phase with a remarkable decrease of cells in the G0-G1 phase.

These preliminary results showed that all of the chimeric compounds possessing a terphenyl fragment **14-15** and **25**, differently from parent compounds **8** and **10**, increase the number of cells in G2-M phase, therefore suggesting dissimilar mechanisms of action. In this case, the alkylic chain does not seem to have an important role.

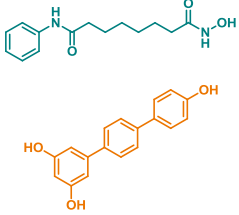
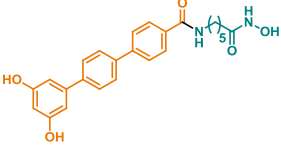
Table 3. Effects of multiligand **14-15** and **25** and parent compounds **8**, **10** on cell cycle distribution in K562 cells.

treatment	G0-G1 (%)	S (%)	G2-M (%)	A (%)
none	41	50	8	10
 8^a	54	27	19	16
 10^b	48	40	12	14
 14^c	49	32	20	11
 15^c	41	45	14	11
 25^c	16	59	25	15

^a40 μ M ^b60 μ M. ^c50 μ M.

To better investigate the cell cycle effect of compound **14**, which among the terpenyl derivatives was the only one able to block cells in G0-G1 as the parent compounds, further cell cycle analyses were performed. At higher concentration **14** showed an increased block of cells in G2-M phase; on the contrary, increasing concentrations of a combination of parent compounds **8** and **10** maintains the block of cells in G0-G1 phases as shown in Table 4 and corresponding Figure 46.

Table 4: Comparison of the effects of parent compounds **8** and **10** in association and multiligand **14** on cell cycle distribution in K562 cells.^a

treatment	G0-G1 (%)	S (%)	G2-M	A (%)
none	35	47	18	5
 8^b + 10^b	57	43	0	36
 14^c	35	25	40	7

^aCorrelate with Figure 46. ^b50 μ M. ^c100 μ M

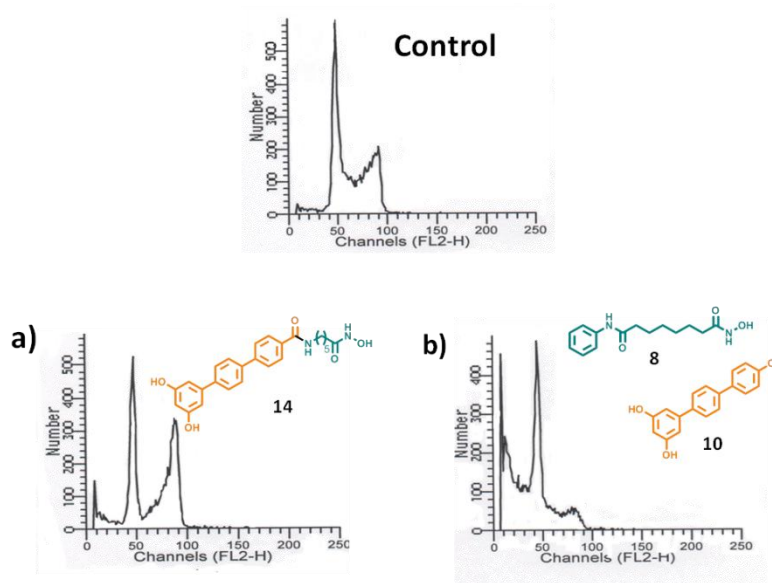


Figure 46. Cell cycle distribution of K562 cell exposed for 24 h to a) **13** (100 μ M), b) **8** (50 μ M)+ **10** (50 μ M).

So far, these preliminary biological assays on K562 cells showed that among the others, chimeric compounds **21**, bearing the *trans*-stilbene motif linked to the fragment of SAHA, is the most promising. It showed a higher cytotoxic activity even better than that of parent compound **13**. Regarding the effects on the cell

cycle it showed a behaviour similar to the combination of its parent compounds suggesting to be the only one acting as a chimeric compound.

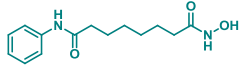
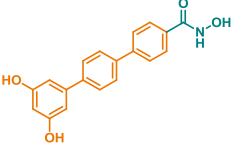
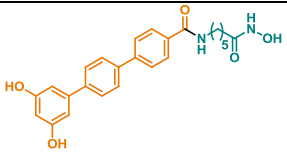
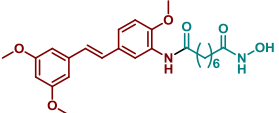
All of the hybrid molecules are currently under investigation to evaluate their ability to induce cell differentiation.

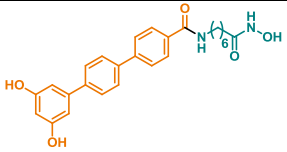
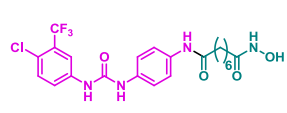
3.2 Preliminary biological results of chimeric compounds as HDAC inhibitors

In order to explore the HDACs inhibition effects, chimeric compounds **14-15**, **21-22**, and **25** were evaluated in comparison with SAHA **8** for their inhibitory activity and selectivity against hrHDAC1 (class I HDACs) (Table 5 and corresponding Figure 47) and hrHDAC4 (class IIa HDACs) (Figure 48) enzymes. All the tested compounds displayed null inhibitory activity against hrHDAC4, while the reduced acetylation in hrHDAC1 revealed interesting results. Notably, once again stilbene hydroxamate **21** showed the best profile, displaying a strong inhibitory activity (87%), higher than SAHA (60%). Similarly, hydroxamate **22** bearing the diphenyl urea fragment, showed to strongly inhibit these enzymes (85%).

Concerning the chimeric compounds **14-15** and **25**, bearing a terphenyl motif in their scaffold, the different alkylic chain seemed to not interfere so much with the inhibitory activity on HDAC1, which remains quite low.

Table 5. Human recombinant HDAC1 inhibitory activity of chimeric compounds **14-15**, **21-22**, and **25** in comparison with SAHA **8**

Compounds	Inhibition [%] at 5 μ M	Compounds	Inhibition [%] at 5 μ M
 <p>8</p>	60	 <p>25</p>	31
 <p>14</p>	62	 <p>21</p>	87

 15	49	 22	85
--	----	---	----

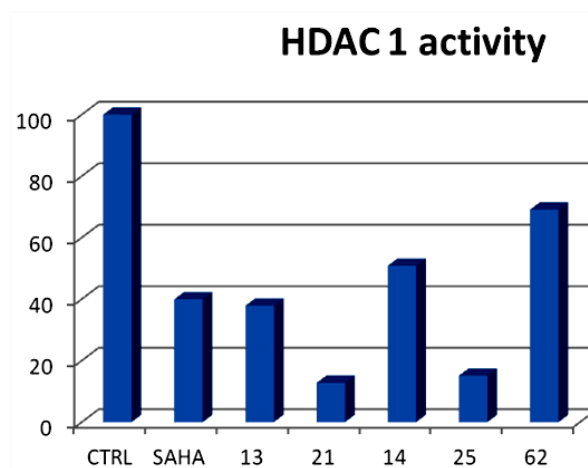


Figure 47. HDAC1 inhibitory activity of chimeric compounds.

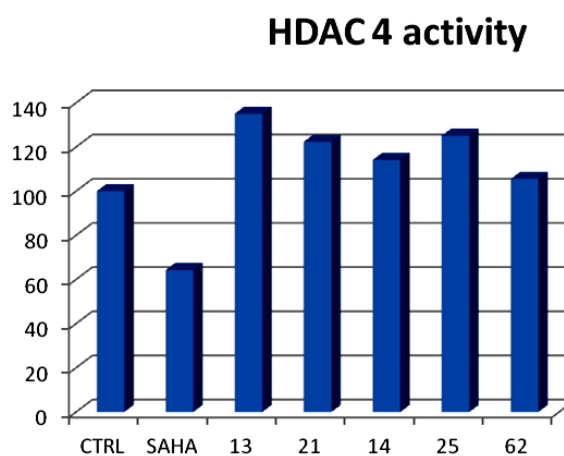


Figure 48. Human recombinant HDAC4 inhibitory activity of chimeric compounds **14-15**, **21-22**, and **25** in comparison with SAHA **8**.

In order to better investigate the activity of compounds **21** and **22** as acetylating agents further analysis wer carried out, thus a western blot analyses using human leukemia U937 cells was performed to determine the effects on the acetylation levels of histone H3 and α -tubulin (a non-histone substrate) (Figure 49).

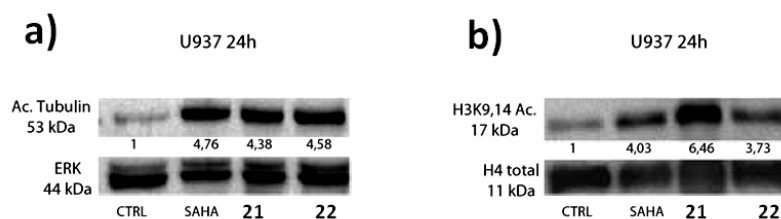


Figure 49. effects of compounds **21** and **22** on acetylation level of a) histone H3 and b) α -tubulin after 24 h of exposure at 5 μ M.

In these conditions, both of the hybrid compounds were able to increase the acetylation levels of α -tubulin (Figure 47 a) and histone H3 (Figure 47 b), having a fair correlation with their HDAC1 inhibition activities; compound **21** showed to induce an high level of acetylation particularly in H3, while hydroxamate **22** had a worse profile if compared to SAHA.

Encouraged from this results, we decide to focus our attention on hybrid stilbene hydroxamate **21**. Further western blot analyses conducted on breast cancer cells MCF7, revealed that this compound is able to increase the level of acetylation of a non-histone target such as p53 better than SAHA, as shown in Figure 50.

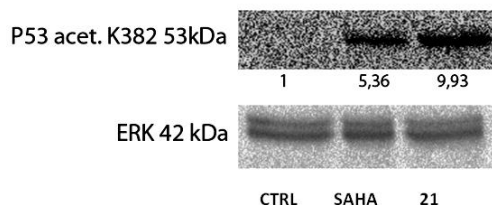


Figure 50. effects of compounds **21** on acetylation level of p53.

Although the data herein presented are only partial, chimeric compound **21** is extremely interesting because it showed to be able to interfere with cell cycle, and to be a selective and strong HDAC inhibitor.

4. Conclusions

During my PhD, I was involved in distinct research projects having as a common platform the identification of novel biologically active small molecules, which can be either lead candidates in drug discovery, or valuable chemical tools to probe molecular pathways in the field of chemical genetics. From a synthetic point of view, different approaches were used in order to achieve these goals.

Regarding the first part of my project, in view of the multifactorial mechanistic nature of cancer, the work has been focused on the design and synthesis of chimeric compounds able to interfere with different molecular pathways involved in cancer cells. Taking advantage of a multitarget-directed strategy, the new hybrid molecules were obtained by linking together suberoylanilide hydroxamic acid (SAHA) analogues, targeting histone deacetylases (HDACs), with privileged fragments able to block cell cycle, and to induce cell differentiation.^{58,59,61} A synthetic strategy for the generation of the desired chimeric compounds has been developed, providing suitable protocols for amide formations between the appropriate synthons and for the introductions of the terminal hydroxamic acid function. The multitarget profile of the synthesized compounds was investigated by evaluation of their antiproliferative activity on Bcr-abl expressing K562 cells as well as their inhibitory effects on HDACs. From preliminary biological results, hybrid compound **21**, whose structure combines a *trans*-3,5 dimethoxy-2-methoxy amino stilbene **13**⁵⁸ with the suberoyl hydroxamic fragment of SAHA, showed the most interesting profile. Notably, bioassays on K52 cell line revealed that compound **21** improved the cytotoxic activity of the parent stilbene **13**, and most importantly its effect on cell cycle was comparable to the combination of the two parent moieties **13** and SAHA **8**, proving to have the desired chimeric profile. Moreover, it exhibited also a strong and selective inhibitory activity against HDAC1, even higher than SAHA **8**. Although these are only preliminary results, compound **21** seems so far to be the only one to act as a chimeric molecule, confirming the effectiveness of our design.

With the aim of increase my knowledge on new strategies with highly synthetic accessibility for the efficient generation of structurally diverse and complex small organic molecules, I spent the last year of PhD in the laboratory of

Dr Spring, at the University of Cambridge, where I was involved in a project of a huge DOS library of macrocyclic peptidomimetics categorized in two main general structures and containing structural motifs present in many naturally occurring bioactive compounds. The synthetic strategy based around the three-phase approach called *Build/Couple/Pair*,⁸¹ together with the synthetic methodology previously developed,⁸⁰ allowed the rapid and efficient synthesis of these compounds, starting from simple amino acids as starting materials. Moreover, further bigger macrocycles were obtained by increasing the number of the *Couple* steps. All the compounds are currently tested against a number of targets including different bacteria types and cancer cells.

5. Experimental procedures

5.1 Experimental procedures of chimeric compounds

General Chemical Methods.

Reaction progress was monitored by TLC on pre-coated silica gel plates (Kieselgel 60 F₂₅₄, Merck) and visualized by UV₂₅₄ light. Flash column chromatography was performed on silica gel (particle size 40-63 μM , Merck). When needed, silica was demetallated by suspending and standing overnight in concentrated HCl, filtered and washed several times with Et₂O until free of chloride ions, and dried for 48 h at 120 °C. All solvents were distilled prior to use, except those used for Suzuki coupling reactions. All reagents were obtained from commercial sources and used without further purification. Unless otherwise stated, all reactions were carried out under an inert atmosphere. Compounds were named relying on the naming algorithm developed by CambridgeSoft Corporation and used in Chem-BioDraw Ultra 11.0. ¹H-NMR e ¹³C-NMR spectra were recorded on Varian Gemini at 200-400 MHz and 75-100 MHz respectively. Chemical shifts (δ_{H}) are reported relative to TMS as internal standard. IR-FT spectrum was obtained on a Nicolet Avatar 320 E.S.P. instrument; ν max is expressed in cm^{-1} . Mass spectrum was recorded on a V.G. 7070E spectrometer or on a Waters ZQ 4000 apparatus operating in electrospray (ES) mode.

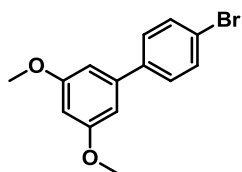
General procedure for Suzuki coupling

In distinct reactors, to a solution of the bromine derivatives **27**, **31**, **36** (1.0 equiv) in toluene (9 mL), aqueous Na₂CO₃ 2M (3.0 equiv) was added, followed by the suitable boronic acids **28**, **32** and **61** (2.0 equiv) previously dissolved in EtOH (3 mL). Each reaction mixture was deoxygenated with a stream of N₂ for 10 min and then Pd(PPh₃)₄ (0.05 equiv) was added. The mixtures were heated to reflux for 4 h, then cooled to room temperature and treated as follows. Each solution was poured into a mixture of H₂O and Et₂O, and the phases were separated. The aqueous layer was extracted with Et₂O (3 \times 15 mL) and the combined organic phases were washed with 1M NaOH and brine. The organic layer was dried over Na₂SO₄ and evaporated. Each crude product was purified by flash chromatography.

General procedure for the Silyloxy Deprotection

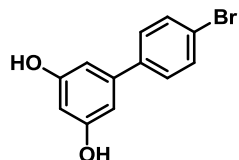
To a solution of the silyloxy-protected compound **51**, **53**, **50** and **26** (1 equiv) in THF (3 mL), a mixture of tetrabutylammonium fluoride (1M in THF)/Acetic acid 1/1 (2.1 equiv) was added at 0 °C. The solution was stirred for 2 h, then poured into sat aq NH₄Cl (5 mL), and extracted with EtOAc (2 × 5 mL). The combined organic extracts were washed with brine, dried over Na₂SO₄ and evaporated *in vacuo*. Each crude product was purified by flash chromatography.

4'-Bromo-3,5-dimethoxybiphenyl **29**⁵⁹



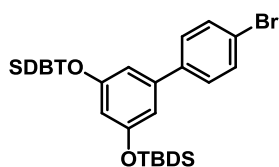
p-Iodobromobenzene **27** (0.90 g, 3.21 mmol) and 3,5-dimethoxyphenylboronic acid **28** (1.14 g, 6.36 mmol) were allowed to react according to the described general procedure for Suzuki coupling, and the crude product was purified by flash chromatography (petroleum ether/EtOAc 99.5/0.5) to give **29** (0.79 g, yield 84%) as yellow solid. ¹H-NMR (400 MHz, CDCl₃): δ= 3.83 (s, 6H), 6.47 (m, 1H), 6.67 (d, J= 2.4 Hz, 2H), 7.42 (d, J= 8 Hz, 2H), 7.53 (d, J= 8 Hz, 2H) ppm.

4'-Bromobiphenyl-3,5-diol **30**⁵⁹



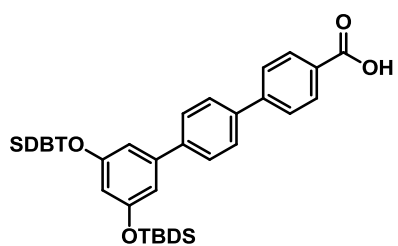
4'-Bromo-3,5-dimethoxy-biphenyl **29** (0.650 g, 2.22 mmol, 1 equiv) was dissolved in 10 mL of anhydrous CH₂Cl₂. After the mixture was cooled to -78 °C, BBr₃ (4.43 mL of 1M in CH₂Cl₂ solution, 4.43 mmol, 2 equiv) was added. The resulting reaction mixture was allowed to warm up to room temperature for 20 h, then cooled at 0 °C and treated as follows. The solution was poured into H₂O, and the two phases were separated. The aqueous layer was washed twice with CH₂Cl₂ (2 × 15 mL), and the combined organic phases were dried over Na₂SO₄ and evaporated to dryness. Purification of the crude product by flash chromatography (petroleum ether/EtOAc 90:10) yielded **30** (0.58, yield 99%) as yellow powder. ¹H-NMR (400 MHz, (CD₃OD): δ= 6.25 (m, 1H), 6.49 (d, J= 2, 2H), 7.42-7.44 (m, 2H), 7.51-7.53 (m, 2H) ppm.

(4'-Bromobiphenyl-3,5-diyl)bis(oxy) bis (*tert*-butyldimethylsilane) **31**



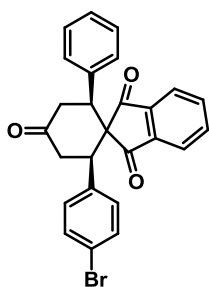
To a solution of 0.52 g (1.96 mmol, 1.0 eq) of **30** in 7 mL of dry DMF, were added *tert*-butyldimethylsilyl chloride (1.18 g, 7.85 mmol, 4.0 eq), and imidazole (0.47 g, 6.86 mmol, 3.5 equiv). The reaction mixture was stirred at room temperature for 24 h, then poured into water and extracted with CH₂Cl₂ (2 × 15 mL). The organic phase was dried over Na₂SO₄ and concentrated *in vacuo*. Purification of the crude product by flash chromatography (petroleum ether) gave **31** (0.85 g, yield 88%) as white solid. ¹H-NMR (400 MHz, CDCl₃): δ= 0.20 (s, 12H), 0.98 (s, 18 H), 6.32 (m, 1H), 6.62 (d, J= 2 Hz, 2H), 7.37 (d, J= 8 Hz, 2H), 7.51 (d, J=8 Hz, 2H) ppm; ¹³C-NMR (75 MHz, CDCl₃) δ= 18.2, 25.7, 111.3, 112.2, 112.3, 113.4, 121.6, 128.6, 129.5, 131.8, 139.9, 141.8, 156.9 ppm; IR ν_{\max} (nujol) cm⁻¹ 1588, 1461, 1258, 1171, 1031, 830.

(4''-Carboxy *p*-terphenyl-3,5-diyl)bis(oxy)bis(*tert*-butyldimethylsilane) **17**



Biphenyl **31** (0.40 g, 0.81 mmol), and 4-carboxyphenylboronic acid **32** (0.27 g, 1.62 mmol) were allowed to react according to the described general procedure for Suzuki coupling, and the crude product was purified by flash chromatography (CH₂Cl₂/CD₃OD 98.5/1.5), to give **17** (0.22 g, yield 50%) as white powder. ¹H-NMR (400 MHz, CDCl₃): δ 0.25 (s, 12H), 1.02 (t, J= 3.2 Hz, 18 H), 6.37 (s, 1H), 6.75 (d, J= 2 Hz, 2H), 7.65 (d, J= 8.4 Hz, 2H), 7.70-7.76 (m, 4H), 8.22 (d, J= 8.8 Hz, 2H) ppm; ¹³C-NMR (75 MHz, CDCl₃) δ 18.2, 25.7, 111.3, 112.4, 127.0, 127.2, 127.6, 128.1, 130.8, 138.8, 140.9, 142.2, 146.0, 156.9, 171.6 ppm.

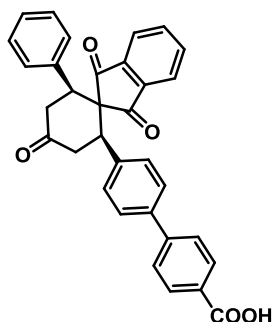
(2 β ,6 β)-2-(4-Bromophenyl)-6-phenylspiro[cyclohexane-1,2'-indene]-1',3',4-trione **36**⁶²



4-Bromobenzaldehyde **33** (0.19 g, 1 mmol, 1 equiv) and 1,3-indandione **34** (0.15 g, 1 mmol, 1 equiv) were suspended in 2 mL of MeOH, and the catalyst (*L*)-5,5-dimethyl thiazolidinium-

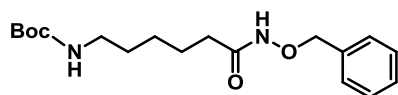
4-carboxylate (*L*-DMTC) (0.03g, 0.2 mmol, 0.02 equiv) was added. The reaction mixture was stirred for 1 h at room temperature, then (*E*)-4-phenyl-3-buten-2-one **35** was added. The suspension was allowed to stir at room temperature for 72 h then diluted with CH₂Cl₂ and treated with saturated aqueous NH₄Cl solution. The layers were separated and the aqueous phase was further extracted with dichloromethane (3 × 15 mL). The combined organic layers were dried over Na₂SO₄ and evaporated under reduced pressure. Crude product was purified by flash chromatography (petroleum ether/EtOAc 93:7) to give **36** (0.19 g, yield 42%) as a white crystalline solid. ¹H-NMR (CDCl₃) δ 2.64 (m, 2H), 3.76-3.80 (m, 4H), 6.90-6.93 (m, 3H), 6.96-6.99 (m, 4H), 7.14-7.16 (m, 2H), 7.44-7.47 (m, 2H), 7.51-7.53 (m, 1H), 7.64-7.66 (m, 1H) ppm.

4'-((2β,6β)-1',3',4-Trioxo-2-phenyl-1',3'-dihydrospiro[cyclohexane-1,2'-indene]-6-yl)biphenyl-4-carboxylic acid **18**⁶²



36 (0.2 g, 0.43 mmol) was coupled to 4-carboxyphenyl boronic acid **32** according to the above procedure for Suzuki coupling, but using THF: water (2: 1) as solvent system. The crude derivative was purified by flash chromatography (CHCl₃/MeOH 9.9: 0.1) affording **18** (0.29 g, yield 66%) as a yellow powder. ¹H-NMR ((CD₃)₂CO) δ= 2.52-2.60 (m, 2H), δ 3.76-3.96 (m, 4H), 6.98-7.08 (m, 5H), 7.19 (d, J = 8 Hz, 2H), 7.45-7.47 (m, 3H), 7.53- 7.65 (m, 4H), 7.72-7.74 (m, 1H), 8.00-8.02 (m, 2H) ppm.

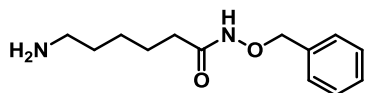
***tert*-Butyl 6-(benzyloxyamino)-6-oxohexylcarbamate **47**.**



To a solution of BOC amino caproic acid **45** (1.20 g, 5.10 mmol, 1.0 eq) in CH₂Cl₂ (15 mL) were added PyBOP (2.66 g, 5.1 mmol, 1.0 eq), DIPEA (3.5 mL, 20.4 mmol, 4.0 eq) and benzyloxyamine **46** (0.65 mL, 5.7 mmol, 1.1 eq). The mixture was stirred for 48 h at room temperature, then the crude product was purified by flash chromatography (petroleum ether/EtOAc 45/55) to give **47** (1.06 g, yield 65%) as white solid. ¹H-NMR (200 MHz, CDCl₃) δ 1.23-1.31 (m, 2H), 1.43-1.47 (m, 9 H), 1.54-1.63 (m, 4H), 2.02-2.09 (m, 2H), 3.04-3.06 (m, 2H), 4.55 (br, 1H), 4.88 (s,

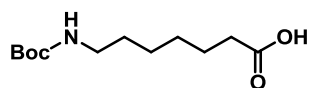
2H), 7.35 (m, 5H) ppm; ^{13}C -NMR (75 MHz, $(\text{CD}_3)_2\text{CO}$) δ 24.9, 26.2, 27.8, 29.8, 30.15, 32.5, 40.1, 77.5, 95.7, 128.3, 128.9, 136.4, 155.9, 170.0 ppm.

6-Amino-N-(benzyloxy)hexanamide (**19**).



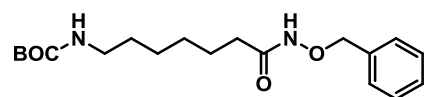
The BOC-amine **47** (0.5 g, 1.5 mmol, 1.0 equiv) dissolved in CH_2Cl_2 (1 mL) was deprotected with trifluoroacetic acid in CH_2Cl_2 1:2 (3.4 mL); after stirring 4 h at room temperature, the mixture was basificated with NH_4OH 10% to pH=7-8, then concentrated *in vacuo*. The crude product was purified by flash chromatography ($\text{CH}_2\text{Cl}_2/\text{CD}_3\text{OD}$ 90/10) to give **19** (0.32 g, yield 89%) as light yellow oil. ^1H -NMR (200 MHz, $(\text{CD}_3)_2\text{CO}$) δ 1.38-1.49 (m, 2H), 1.62-1.69 (m, 2H), 1.74-1.85 (m, 2H), 3.05-3.12 (m, 2H), 3.74-3.80 (m, 2H), 4.91 (s, 2H), 7.36-7.45 (m, 5H) ppm; IR ν_{max} (nujol) cm^{-1} 3399, 1678, 1461, 1376, 1204, 1138, 723.

7-(*tert*-Butoxycarbonylamino) heptanoic acid (**49**)⁸³



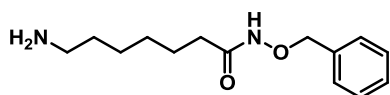
Amino heptanoic acid (**48**) (0,50 g, 3,5 mmol, 1 equiv) was suspended in 1.5 mL of *ter*ButOH and then NaOH 5M (0,7 mL, 1 equiv) was added. After stirring at room temperature for 10 minutes, Boc_2O previously dissolved in 1.2 mL of *ter*ButOH was added, and the reaction mixture was stirred for 24 h at 29°C. Then the solvent was removed, the slurry was suspended in 15 mL of water and H_2SO_4 2M was added dropwise to pH 2. The water phase was extracted with EtOAc (3×15 mL) and the collected organic phases were washed with H_2O (3×15 mL), dried over Na_2SO_4 and evaporated under reduced pressure. Crude product was purified by flash chromatography (EtOAc) to give **49** (0.15 g, yield 88%) as a white crystalline solid. IR ν_{max} (nujol) cm^{-1} 3340, 2922, 1704, 1681, 1529, 1462, 1376, 1365, 1264, 1252, 1162; ^1H -NMR (CDCl_3) δ 1.34-1.37 (m, 4H), 1.46 (s, 9H), 1.49-1.52 (m, 2H), 1.61-1.65 (m, 2H), 2.35 (t, $J = 6.6$ Hz, 2H), 3.11 (t, $J = 6.8$ Hz, 2H), 4.79 (s br, 1H) ppm.

tert*-Butyl 7-(benzyloxyamino)-7-oxoheptylcarbamate **46*



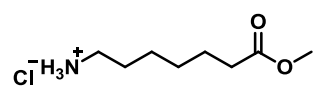
Boc-amino heptanoic acid **49** (0.30 g, 1.22 mmol, 1 equiv), PyBOP (0.70 g, 1.34 mmol, 1.1 equiv), DIPEA (0.99 mL, 4.89 mmol, 4.0 equiv), and benzylhydroxylamine **46** (0.17 mL, 1.46 mmol, 1.2 equiv) were allowed to react following the same procedure provided for compound **47**. Purification of the crude product by flash chromatography (petroleum ether/EtOAc 50/50) afforded **46** (0.35 g, yield: 88%) as a white solid. ¹H-NMR (200 MHz (CD₃)₂CO) δ 1.33-1.36 (m, 4H), 1.42 (s, 9H), 1.52-1.60 (m, 4H), 2.06-2.09 (m, 2H), 2.89-3.11 (m, 2H), 4.81 (s, 2H), 5.94 (s br, 1H), δ 7.35-7.42 (m, 5H), 10.08 (s br, 1H).

7-Amino-N-(benzyloxy)heptanamide **20**



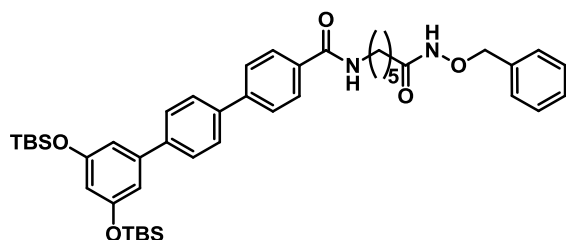
The Boc-amine **46** (0.25 g, 0.75 mmol, 1 equiv). was deprotected following the same procedure applied for **18**. Crude product was purified by flash chromatography (CH₂Cl₂/MeOH 92.5/7.5) to give **20** (0.17 g, yield 92%) as an oil. IR ν_{max} (nujol) cm⁻¹ 3581, 3374, 3202, 2919, 1673, 1461, 1376, 1204, 1137, 842; ¹H-NMR (400 MHz, (CD₃)₂CO) δ 1.30-1.36 (m, 2H), 1.38-1.41 (m, 2H), δ 1.57-1.60 (m, 2H), 1.73-1.84 (m, 2H), δ 3.05 (m, 2H), 3.70-3.74 (m, 2H), δ 4.85 (s, 2H), 7.31-7.35 (m, 3H), 7.36-7.41 (m, 2H).

7-Methoxy-7-oxoheptan-1-aminium chloride **55⁸⁴**



Amino heptanoic acid (**48**) (0.50 g, 3.5 mmol, 1 equiv) was suspended in 13 mL of 2,2 dimethoxypropane then 1.14 mL of concentrate HCl was added. The reaction mixture was stirred at room temperature for 24 h, then treated as follow. The solvent was evaporated, and the slurry was suspended in Et₂O. The resulting precipitate was washed with additional Et₂O and crystallized in EtOH/ EtOAc to afford **55** (0.5 g, yield 77%) as white crystals. ¹H-NMR (200 MHz, CDCl₃) δ 1.42 (m, 4H), 1.61-1.68 (m, 2H), 1.80 (m, 2H), 2.29-2.36 (m, 2H) 3.02 (m, 2H), 3.68 (s, 3H), 8.23 (s, br, 3H) ppm.

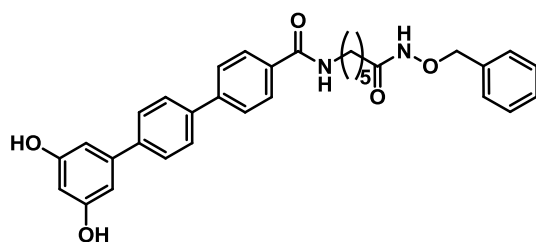
N-(6-(Benzyloxyamino)-6-oxohexyl)-3'',5''-bis-(tert-butyl dimethylsilyloxy)-p-terphenyl-4-carboxamide 51



To a cooled solution of **19** (0.08 g, 0.31 mmol, 1.0 equiv), **17** (0.2 g, 0.37 mmol, 1.2 equiv), OHBt (0.04 g, 0.34 mmol, 1.1 equiv), and EDC (0.06 g, 0.34 mmol, 1.1 equiv), in

DMF (6 mL), was added N-methyl-morpholine (0.12 mL, 1.1 mmol, 3.6 equiv). The reaction mixture was stirred for 20 h at room temperature, then EtOAc was added, and the organic phase was washed with NaHCO₃ 1M and brine, dried over Na₂SO₄ and concentrated *in vacuo*. The crude product was purified by flash chromatography (petroleum ether/EtOAc 30/70) to give **51** (0.1 g, yield 42%) as white powder. ¹H-NMR (200 MHz, CDCl₃) δ 0.26 (s, 12H), 1.03 (s, 18 H), 1.34-1.38 (m, 2H), 1.64-1.68 (m, 4H), 2.13-2.19 (m, 2H), 3.48 (m, 2H), 4.91 (s, 2H), 6.37 (s, 1H), 6.75 (d, J = 2 Hz, 2H), 7.28-7.37 (m, 5H), 7.54-7.68 (m, 6H), 7.90 (d, J = 7.6 Hz, 2H) ppm; ¹³C-NMR (75 MHz, CDCl₃) δ 1.5, 18.8, 26.2, 26.4, 29.3, 40.1, 78.6, 111.8, 112.9, 127.6, 128.0, 128.1, 129.1, 129.7, 139.5, 141.2, 142.8, 144.3, 157.4 ppm.

N-(6-(Benzyloxyamino)-6-oxohexyl)-3'',5''-dihydroxy p-terphenyl-4-carboxamide 52

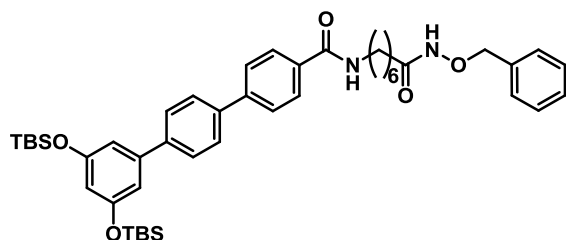


Compound **51** (0.26 g, 0.35 mmol) was deprotected following the general procedure for the silyloxy deprotection; purification of crude product by flash chromatography

(CH₂Cl₂/MeOH 98/2) afforded **52** (0.11 g, yield 60%) as white powder. ¹H-NMR (400 MHz, (CD₃)₂CO) δ 1.39-1.43 (m, 2H), 1.62-1.65 (m, 4H), 2.07-2.10 (m, 2H), 3.40-3.48 (m, 2H), 4.89 (s, 2H), 6.43 (t, J = 2 Hz, 1H), 6.69 (d, J = 2 Hz, 2H), 7.31-7.33 (m, 3 H), 7.40 (d, J = 2.4 Hz, 2H), 7.66-7.68 (m, 2H), 7.72-7.76 (m, 4H), 8.01 (d, J = 8 Hz, 2H), 8.52 (br, 1H) ppm; ¹³C-NMR (75 MHz, CD₃OD) δ 21.2, 25.1, 26.6, 30.4, 31.0, 41.1, 79.3, 103.2, 106.8, 107.1, 128.2, 128.7, 129.2, 129.9, 130.2,

130.4, 130.6, 133.3, 134.8, 137.2, 140.4, 142.6, 144.1, 145.3, 160.3, 170.2, 173.1 ppm.

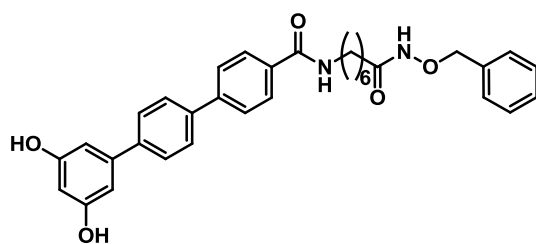
N-(7-(benzyloxyamino)-7-oxoheptyl)-3'',5''-bis-(*tert*-butyl-dimethylsilanoxy)-*p*-terphenyl-4-carboxamide **53**



20 (0.05 g, 0.22 mmol, 1 equiv), **17** (0.14 g, 0.26 mmol, 1.2 equiv), OHBt (0.03 g, 0.24 mmol, 1.1 equiv), EDC (0.05 g, 0.24 mmol, 1.1 eq.) and N-methyl-

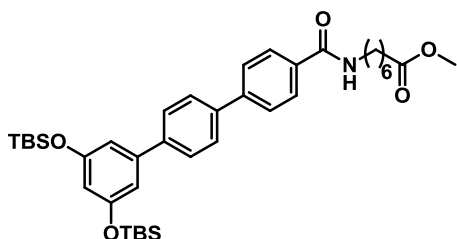
morpholine (86 μ L, 0.78 mmol, 3.6 equiv) were allowed to react following the same procedure provided for compound **51**. Purification of the crude product by flash chromatography (petroleum ether/EtOAc 40/60) afforded **53** (0.09 g, yield: 54%) as a white solid. $^1\text{H-NMR}$ (200 MHz CDCl_3) δ 0.26 (s, 12H), 1.03 (s, 12H), 1.41 (m, 4H), 1.56 (m, 4H), 2.07 (m, 2H), 3.47-3.50 (m, 2H), 4.94(s, 2H), 6.37 (m, 1H), 6.76 (d, $J=2$ Hz, 2H), 7.41 (m, 2H), 7.66-7.73 (m, 5H), 7.85-7.89 (m, 2H) ppm; $^{13}\text{C-NMR}$ (75 MHz, CDCl_3) δ 14.1, 18.2, 22.7, 25.7, 26.2, 28.4, 29.4, 29.7, 31.9, 39.7, 127.1, 127.4, 127.5, 128.4, 128.6, 129.2, 132.0, 132.2, 133.3, 139.0, 140.6, 142.2, 143.7, 156.9, 167.3 ppm.

N-(7-(Benzyloxyamino)-7-oxoheptyl)-3'',5''-dihydroxy *p*-terphenyl-4-carboxamide **54**



Compound **53** (0.16 g, 0.21 mmol) was deprotected following the general procedure for the silyloxy deprotection; purification of crude product by flash chromatography ($\text{CH}_2\text{Cl}_2/\text{MeOH}$ 90/10) afforded **54** (0.10 g) mixed with TBAF.

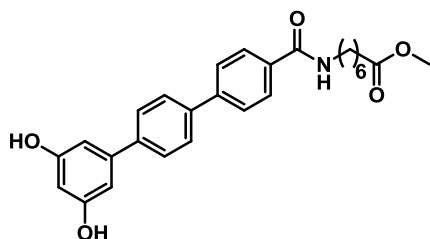
7-Methoxy-7-oxoheptyl-3'',5''-bis-(*tert*-butyl-dimethylsilanoxy)-*p*-terphenyl-4-carboxamide **56**



Terphenyl **17** (0.25 g, 0.47 mmol, 1 equiv), amine **55** (0.11 g, 0.56 mmol, 1.2

equiv), pyBOP (0.27 g, 0.51 mmol, 1.1 equiv), DIPEA, (0.40 mL, 2.33 mmol, 5equiv) were allowed to react as described for compound **47**. The residue was purified by flash chromatography (petroleum ether/EtOAc 84/18) to afford **56** (0.18, yield 57%) as white powder. ¹H-NMR (400 MHz, CDCl₃) δ 0.22 (s, 12H), 1.00 (t, J= 3.2 Hz, 18 H), 1.38-1.40 (m, 4H), 1.62-1.65 (m, 4H), 2.30 (t, J= 7.6 Hz, 2H), 3.45-3.47 (m, 2H), 3.65 (s, 3H), 6.34 (s, 1H), 6.72 (d, J=2 Hz, 2H), 7.60-7.66 (m, 6H), 7.84 (d, J= 8.4 Hz, 2H) ppm.

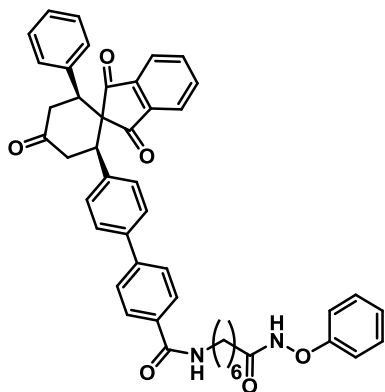
7-Methoxy-7-oxoheptyl-3'',5''-dihydroxy *p*-terphenyl-4-carboxamide **57**



Compound **56** (0.36 g, 0.53mmol) was deprotected following the general procedure for the silyloxy deprotection; purification of crude product by flash chromatography (CH₂Cl₂/MeOH 97/3) afforded **57** (0.17, 71%)

as white powder. ¹H-NMR (400 MHz, CD₃OD) δ 1.39-1.40 (m, 4H), 1.60-1.63 (m, 4H), 2.30-2.34 (m, 2H), 3.36-3.38 (m, 2H), 3.63 (s, 3H), 6.26 (s, 1H), 6.57 (d, J= 2.4 Hz, 2H), 7.62-7.65 (m, 2H), 7.70-7.72 (m, 2H), 7.74-7.76 (m, 2H), 7.87-7.89 (m, 2H) ppm.

N-(7-oxo-7-(phenoxyamino)heptyl)-4'-((2*S*,6*R*)-1',3',4-trioxo-2-phenyl-1',3'-dihydrospiro[cyclohexane-1,2'-indene]-6-yl)biphenyl-4-carboxamide **58**

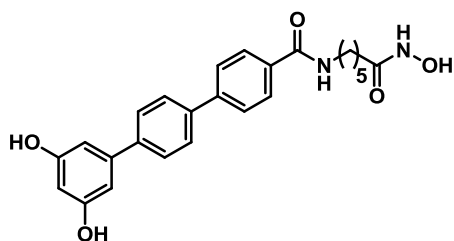


20 (0.05 g, 0.22 mmol, 1 equiv), **18** (0.12 g, 0.26 mmol, 1.2 equiv), OHBt (0.03 g, 0.22 mmol, 1.1 equiv), EDC (0.04 g, 0.24 mmol, 1.1 eq.) and N-methyl-morpholine (86 μL, 0.78 mmol, 3.6 equiv) were allowed to react following the same procedure provided for compound **51**. Purification of the crude product by flash chromatography (petroleum

ether/EtOAc 30/70) afforded **58** (0.08 g, yield: 55%) as a yellow solid. ¹H-NMR (400 MHz, CDCl₃) δ 1.27-1.37 (m, 4H), δ 1.61-1.65 (m, 4H), 2.04 (m, 2H), 2.67-2.69 (m, 2H), 3.40-3.342 (m, 2H), 3.81-3.88 (m, 4H), 4.90 (s, 2H), 6.15 (s, 1H), 6.95-7.01 (m, 5H), 7.12-7.13 (m, 2H), 7.26-7.28 (m, 3H), 7.35-7.50 (m,

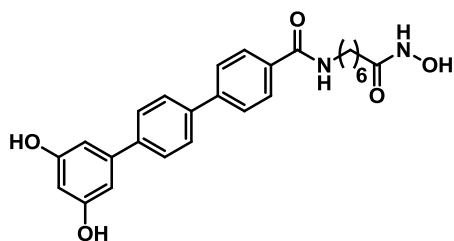
8H), 7.65-7.68 (m, 1H), 7.71-7.31 (m, 2H), 8.38 (s br, 1H) ppm; $^{13}\text{C-NMR}$ (75 MHz, CDCl_3) δ 14.6, 15.2, 17.2, 17.5, 20.8, 23.8, 24.9, 26.2, 28.3, 29.3, 29.6, 30.3, 30.9, 32.8, 39.7, 40.8, 43.3, 43.4, 48.2, 48.9, 62.0, 65.8, 122.1, 122.5, 126.7, 126.8, 127.0, 127.3, 127.7, 127.8, 128.0, 128.3, 128.5, 128.7, 129.1, 133.3, 135.4, 137.2, 137.4, 139.0, 141.9, 142.7, 142.9, 167.1, 197.9, 198.0, 201.8, 203.4, 208.2 ppm.

N-(6-(hydroxyamino)-6-oxohexyl)-3'',5''-dihydroxy *p*-terphenyl-4-carboxamide 14



Compound **48** (0.11 g, 0.21 mmol, 1 equiv) was dissolved in a mixture of THF/MeOH 90/10 (10 mL) and debenzylated by hydrogenation with H_2 over Pd/C at room temperature. After 4 h, the catalyst was filtered off, and the crude product was concentrated *in vacuo*, then triturated with CHCl_3 to give **14** (0.05 g, yield 55%) as white powder. $^1\text{H-NMR}$ (400 MHz, $(\text{CD}_3)_2\text{SO}$) δ 1.23-1.28 (m, 2H), 1.48-1.53 (m, 4H), 1.93 (t, $J=7.6$ Hz, 2H), 3.22-3.26 (m, 2H), 6.21-6.22 (m, 1H), 6.50 (d, $J=2$ Hz, 2H), 7.61 (d, $J=8.4$ Hz, 2H), 7.75-7.92 (m, 4H), 8.46 (s, 1H), 8.62 (s, 1H), 9.35 (s, 2H), 10.30 (s, 1H) ppm; $^{13}\text{C-NMR}$ (100 MHz, $(\text{CD}_3)_2\text{SO}$) δ 23.1, 24.9, 26.2, 28.9, 32.3, 101.9, 104.8, 126.3, 127.1, 127.3, 127.9, 133.5, 138.1, 140.1, 141.5, 142.0, 158.9, 165.8, 169.2 ppm; MS (ES): m/z 433 $[\text{M-H}]^-$.

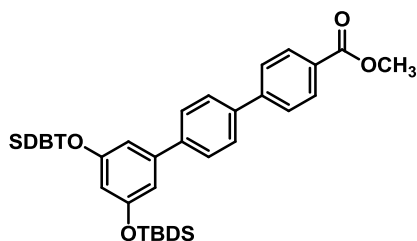
N-(7-(hydroxyamino)-7-oxoheptyl)-3'',5''-dihydroxy *p*-terphenyl-4-carboxamide 15.



To a cooled solution of methyl ester **57** (0.17 g, 0.38 mmol, 1 equiv) in MeOH/THF 2/1 (5 mL), hydroxylamine hydrochloride (0.27 g, 3.80 mmol, 10 equiv) and sodium methylate solution 30% in MeOH (0.90 mL, 4.71 mmol, 12.4 equiv) were added. The reaction mixture was stirred for 24 h at room temperature then cooled in ice-bath and acidified with HCl 6N to pH 4. Water was added to dissolve the salt, and the mixture was concentrated *in vacuo*

to remove MeOH/THF. The precipitated product was filtered, washed with diethyl ether and purified by flash chromatography on demetallated silica gel (CH₂Cl₂/MeOH 93/7), to give **15** (0.02 g, yield 11%) as red solid. ¹H-NMR (400 MHz, CD₃OD) δ 1.39-1.40 (m, 4H), 1.61-1.65 (m, 4H), 2.08 (t, J= 7.2 Hz, 2H), 3.37-3.39 (m, 2H), 6.26-6.27 (m, 1H), 6.58 (d, J= 2 Hz, 2H), 7.62-7.69 (m, 2H), 7.71-7.75 (m, 4H), 7.87-7.89 (m, 2H) ppm; ¹³C-NMR (100 MHz, CD₃OD) δ 26.6, 27.7, 29.8, 30.3, 33.7, 40.9, 102.8, 106.5, 127.8, 128.3, 128.4, 128.9, 134.5, 140.1, 142.3, 143.8, 145.0, 160.0, 170.0, 173.0 ppm; MS (ES): m/z 471 [M+Na]⁺, 447 [M-H]⁻, 483 [M-Cl]⁻.

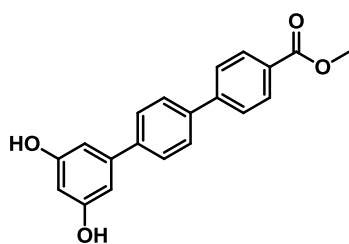
Methyl 3'',5''-bis(*tert*-butyldimethylsilyloxy) *p*-terphenyl-4-carboxylate **62**



Biphenyl **31** (0.25 g, 0.50 mmol), and 4-methoxycarbonyl-phenylboronic acid **61** (0.18 g, 1.00 mmol) were allowed to react according to the described general procedure for Suzuki coupling, and the crude product was purified by

flash chromatography (CH₂Cl₂/MeOH 98.5/1.5), to give **62** (0.26 g, yield 95%) as white powder. ¹H-NMR (200 MHz, CDCl₃) δ 0.26 (s, 12H), 1.03 (s, 18 H), 3.97 (s, 3H), 6.38 (s, 3H), 6.76 (d, J= 2.2 Hz, 2H), 7.68-7.74 (m, 6H), 8.15 (d, J=8 Hz, 2H) ppm.

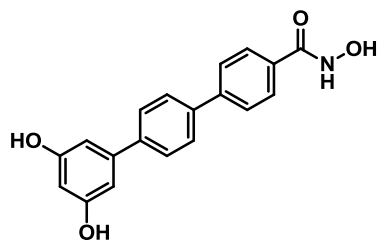
Methyl 3'',5''-dihydroxy-*p*-terphenyl-4-carboxylate **26**



Compound **62** (0.25 g, 0.45 mmol) was deprotected following the general procedure for the silyloxy deprotection; purification of crude product by flash chromatography (CH₂Cl₂/MeOH 98/2) afforded **26** (0.13, yield 89%) as white powder. ¹H-

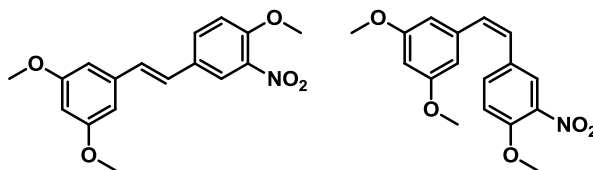
NMR (400 MHz, CD₃OD) δ 3.91 (s, 1H), 6.40 (s, 1H), 6.69 (d, J= 2 Hz, 2H), 7.70-7.72 (m, 2H), 7.81, (d, J=8.8 Hz, 2H), 7.85-7.87 (m, 2H), 8.24 (d, J= 8.8 Hz, 2H), 8.37 (br, 2H) ppm.

N-hydroxy-3'',5''-dihydroxy-*p*-terphenyl-4-carboxamide **25**



Starting from methyl ester **26** (0.14 g, 0.44 mmol, 1 equiv), compound **25** was prepared as described above for **15**, but using a strong excess of hydroxylamine hydrochloride (0.61 g, 8.74 mmol, 20 equiv) and sodium methylate solution 30% in MeOH (2.07 mL, 10.8 mmol, 24.8 equiv). The reaction mixture was stirred for 24 h at room temperature then cooled in ice-bath and acidified with HCl 6N to pH 4. Water was added to dissolve the salt, and the mixture was concentrated *in vacuo* to remove MeOH/THF. The aqueous phase was washed with CH₂Cl₂ (2 × 15 mL), then extracted with EtOAc (3 × 15 mL). The collected organic phases were dried over Na₂SO₄ and concentrated *in vacuo*. The crude product was purified by flash chromatography on demetallated silica gel (CH₂Cl₂/MeOH 90/10), to give **25** (0.05 g, 36 %) as red solid. ¹H-NMR (400 MHz, CD₃OD) δ 6.29-6.30 (m, 1H), 6.60-6.61 (m, 2H), 7.64-7.67 (m, 2H), 7.71-7.79 (m, 4H), 7.85 (d, J= 8.8 Hz, 1H), 8.11 (d, J= 8.4 Hz, 1H) ppm; ¹³C-NMR (100 MHz, CD₃OD) δ 102.9, 106.5, 127.8, 128.0, 128.3, 128.4, 128.5, 128.7, 134.4, 139.9, 140.0, 142.3, 142.4, 143.8, 145.3, 146.4, 160.0 ppm; MS (ES): m/z 322 [M+H]⁺, 344 [M+Na]⁺.

(*Z*)- and (*E*)-4-(3,5-dimethoxystyryl)-1-methoxy-2-nitrobenzene **39**, **40**⁵⁸



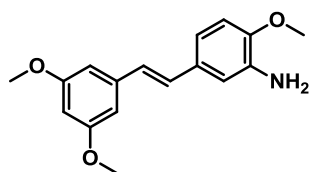
To a suspension of phosphonium salt **38** (2.67 g, 5.4 mmol, 1.4 equiv) in 60 mL of anhydrous THF at -78 °C, n-BuLi 2.5 M in hexanes (2.16 mL, 5.4 mmol, 1.0 equiv) was added and the resulting reddish solution was stirred under nitrogen for 2 h. A solution of 3-nitro-4-methoxybenzaldehyde **37** (0.70 g, 3.86 mmol, 1 equiv) in THF was added dropwise over 30 min and the mixture stirred for 4 h at room temperature then treated as follow. The reaction mixture was dilute with water and extracted with CH₂Cl₂. The combined extracts were washed with brine, dried over Na₂SO₄ and removal of the solvent under *vacuum* afforded a mixture of

trans-stilbene **40** and its *cis* isomer **39**. The two isomers were separated by flash chromatography (petroleum ether/EtOAc 97/3); *cis*-stilbene **39** (0.55 g, yield 45%) eluted first, followed by the *trans*- stilbene **40** (0.56g, yield 45%).

39: yellow oil; ¹H-NMR (400 MHz, CDCl₃) δ 3.68 (s, 6H), 3.91 (s, 3H), 6.35 (t, J= 2.4 Hz, 1H), 6.38 (m, 2H), 6.46 (d, J= 12 Hz, 1H), 6.60 (d, J= 12.4 Hz, 1H), 6.92 (d, J= 8.4 Hz, 1H), 7.41 (m, 1H), 7.76 (d, J= 2.4 Hz, 1H) ppm.

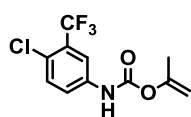
40: yellow crystals; ¹H-NMR (400 MHz, CDCl₃) δ 3.83 (s, 6H), 3.98 (s, 3H), 6.42 (m, 1H), 6.65 (d, J= 2.4 Hz, 2 H), 6.99 (m, 2H), 7.08 (m, 1H), 7.64-7.66 (m, 1 H), 8.00 (m, 1H) ppm.

(E)-5-(3,5-dimethoxystyryl)-2-methoxybenzenamine **13**⁵⁸



Nitro-derivative **40** (0.8 g, 2.5 mmol, 1 equiv) was dissolved in acetone/water (10/5 mL) and heated to 50 °C. After 30 minutes; sodium dithionite (6.06 g, 34.8 mmol, 20 equiv) was slowly added, and the mixture was refluxed for 2 h (1-4h) and then cooled at room temperature. Water was added and the product was extracted with EtOAc. The organic phases were collected, washed with brine, dried over Na₂SO₄ and solvent was removed *in vacuum*. Crude product was purified by flash chromatography on silica saturated for the 50 % with NH₃ (petroleum ether/EtOAc 87.5/12.5) to give **13** (0.45 g, yield 64%) as yellow oil. ¹H-NMR (200 MHz, CDCl₃) δ 3.85 (s, 6H), 3.89 (s, 3H), 6.40 (t, J= 2.2 Hz, 1H), 6.67 (d, J= 2.2 Hz, 2H), 6.78-6.82 (m, 2H), 6.91-7.01 (m, 3H) ppm.

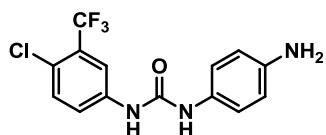
(4-Chloro-3-Trifluoromethyl-phenyl)-carbamic acid isopropenyl ester **43**



Sodium hydroxide (2.50 g, 62.5 mmol 2.5 equiv) pellets were dissolved in water (25 mL) and the mixture was cooled to 5 °C under stirring. 4-chloro-3-(trifluoromethyl) aniline **41** (5.00 g, 25.5 mmol, 1 equiv) solubilized was added in EtOAc (50 mL) keeping the temperature at 5 °C. To the obtained solution isopropenyl chloroformate **42** (3.30 mL, 30.7 mmol 1.2 equiv) was added dropwise and the reaction mixture was then stirred for 1 h at room temperature. The organic phase was washed with brine, dried over Na₂SO₄ and evaporated to obtain the desired carbamate **43** as white

crystals (6.10 g, yield 85%). The crude product was recrystallized in petroleum ether. ¹H-NMR (400 MHz, CDCl₃) δ 1.98 (s, 3H), 4.74 (m, 1H), 4.79 (d, J= 1.6Hz, 1H), 6.84 (br s, 1H), 7.42 (d, J= 8.8 Hz, 1H), 7.55 (dd, J= 2.4, 8.4 Hz, 1H), 7.74 (d, J = 2.4 Hz, 1H) ppm.

1-(4-aminophenyl)-3-(4-chloro-3-(trifluoromethyl)phenyl)urea **23**



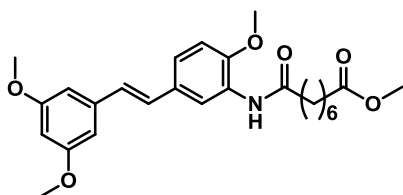
A solution of **43** (0.30 g, 1.07 mmol, 1 equiv) and benzene-1,4-diamine **44** (0.12 g, 1.07 mmol, 1 equiv) in toluene (10 mL), was heated to reflux, then methylpyrrolidine (0.11 g, 1.07 mmol, 1 equiv) was added. The resulting reaction mixture was stirred and heated to reflux for 2 h, then cooled to room temperature. The precipitate was filtered and washed with toluene and petroleum ether to give **23** as pink solid (0.31 g, yield 87%). ¹H-NMR (400 MHz, (CD₃)₂SO) δ 5.02 (br, 2H), 6.48-6.52 (m, 2H), 7.03-7.07 (m, 2H), 7.52-7.58 (m, 2H), 8.06 (d, J= 2.4 Hz, 1H), 8.29 (br, 1H), 8.97 (br, 1H).

General Procedure for amide **59-60**.

In distinct reactors, to a solution of suberic acid monomethyl ester **24** (1 equiv) in 3 mL of DMF dry were dissolved the appropriate amines **13** and **23** (1.2 equiv) and OHBt (1.2 equiv). Then DCC (1.2 equiv) was added, and the mixture was stirred at room temperature for 48 h. Afterwards, the observed precipitate of dicyclohexylurea was filtered off, while the filtrate was poured in 10 mL of cold water, and extracted with CH₂Cl₂ (2 × 15 mL), and EtOAc (2 × 15 mL). The collected organic phases were dried over Na₂SO₄ and evaporated *in vacuo*. Each crude product was purified by flash chromatography.

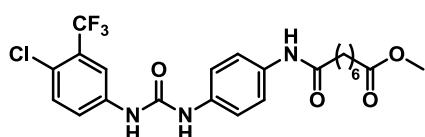
(E)-methyl-8-(5-(3,5-dimethoxystyryl)-2-methoxyphenylamino)-8-oxooctanoate **59**

Aminostilbene **13** (0.19 g, 0.67 mmol), acid **24** (0.10 g, 0.55 mmol), were allowed to react following the general procedure described above. The residue was purified by flash chromatography (petroleum ether/EtOAc 75/25) to



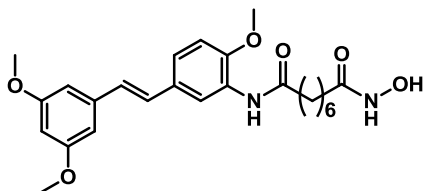
afford **59** (0.18 g, yield 71%) as white powder. $^1\text{H-NMR}$ (400 MHz, CDCl_3) δ 1.36-1.41 (m, 4H), 1.64 (t, $J=7.2\text{Hz}$, 2H), 1.73-1.76 (m, 2H), 2.30 (t, $J=7.6\text{Hz}$, 2H), 2.38-2.42 (m, 2H), 3.65 (s, 3H), 3.81 (s, 6H), 3.89 (s, 3H), 6.35 (t, $J=2.4\text{ Hz}$, 1H), 6.64 (d, $J=2.4$, 2H), 6.83 (d, $J=8.8$, 1H), 6.93-7.05 (m, 2H), 7.13 (dd, $J=2$, 8.4 Hz, 1H), 7.74 (s, 1H), 8.67 (d, $J=2\text{Hz}$ 1H) ppm.

Methyl 8-(4-(3-(4-chloro-3-(trifluoromethyl)phenyl)ureido)phenylamino)-8-oxooctanoate 60



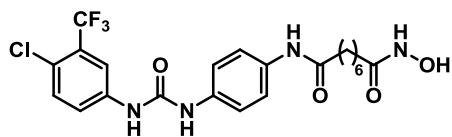
Aminourea **23** (0.32 g, 0.96 mmol), acid **24** (0.50 g, 0.80 mmol) were allowed to react following the general procedure described above. The residue was purified by flash chromatography (petroleum ether/EtOAc 70/30), and then was recrystallized in ethyl acetate/hexane to afford **60** (0.23, yield 55%) as pink solid. $^1\text{H-NMR}$ (200 MHz, $(\text{CD}_3)_2\text{CO}$) δ 1.33-1.36 (m, 4H), 1.57-1.60 (m, 2H), 1.64-1.68 (m, 2H), 2.26-2.30 (m, 2H), 2.32 (t, $J=7.6\text{ Hz}$, 2H), 7.41-7.43 (m, 2H), 7.52 (d, $J=8.8\text{ Hz}$, 1H), 8.45 (br, 1H), 8.99 (br, 1H) ppm.

(E)-N1-(5-(3,5-dimethoxystyryl)-2-methoxyphenyl)-N8 hydroxyoctanediamide 21



A procedure analogous to the one described for the synthesis of **15** was applied using **59** (0.17 g, 0.37 mmol) as starting material. The reaction mixture was stirred for 3 h at room temperature then after acidification and removal of the solvent *in vacuo*, the crude product was filtered and washed with Et_2O to yield **21** (0.11 g, yield 64%) as white powder. $^1\text{H-NMR}$ (400 MHz, CD_3OD) δ 1.38-1.39 (m, 4H), 1.60-1.64 (m, 2H), 1.70 (t, $J=7.2$, 2H), 2.06-2.10 (m, 2H), 2.41-2.44 (m, 2H), 3.78 (s, 6H), 3.87 (s, 3H), 6.34-6.35 (m, 1H), 6.65 (d, $J=2.4\text{Hz}$, 2H), 6.94-6.98 (m, 2H), 7.02-7.06 (m, 1H), 7.24-7.25 (m, 1H), 8.18 (d, $J=1.6\text{Hz}$, 1H) ppm; $^{13}\text{C-NMR}$ (100 MHz, CD_3OD) δ 26.6, 26.7, 29.8, 33.7, 37.7, 55.7, 56.4, 100.6, 105.3, 111.9, 121.1, 124.9, 128.2, 128.4, 129.7, 131.3, 140.9, 141.0, 151.3, 162.5, 174.7 ppm; MS (ES): m/z 479 $[\text{M}+\text{Na}]^+$.

N1-(4-(3-(4-chloro-3-(trifluoromethyl) phenyl) ureido) phenyl) -N8-hydroxyoctanediamide **22**



A procedure analogous to the one described for the synthesis of **15** was applied using **60** (0.20 g, 0.40 mmol) as starting material but using a strong excess of hydroxylamine hydrochloride (0.56 g, 8.00 mmol, 20 equiv) and sodium methylate solution 30% in MeOH (1.90 mL, 9.92 mmol, 24.8 equiv). The reaction mixture was stirred for 24 h at room temperature then cooled in ice-bath and acidified with HCl 6N to pH 4. Water was added to dissolve the salt, and the mixture was concentrated *in vacuo* to remove MeOH/THF. The aqueous phase was washed with CH₂Cl₂, then extracted with EtOAc(2 × 15 mL). The collected organic phases were dried over Na₂SO₄, the *solvent* was *evaporated* and the crude product was triturated with diethyl ether to give **25** (0.13 g, 72%) as brown powder. ¹H-NMR (400 MHz, CD₃OD) δ 1.35-1.38 (m, 4H), 1.60- 1.63 (m, 2H), 1.68 (t, J= 7.2Hz, 2H), 2.06-2.09 (m, 2H), 2.31-2.35 (m, 2H), 7.35 (d, J= 8.8 Hz, 2H), 7.46-7.48 (m, 3H), 7.58 (d, J= 2.4Hz, 1H), 7.96 (d, J=2.4 Hz 1H) ppm; ¹³C-NMR (100 MHz, CD₃OD) δ 26.6, 26.8, 29.8, 29.9, 33.7, 37.8, 118.6, 118.7, 118.8, 121.1, 121.5, 121.9, 122.9, 124.2, 125.4, 125.6, 128.4, 129.3 (q, J= 31Hz, CF₃), 133.0, 135.3, 136.2, 140.3, 154.9, 173.0, 174.4 ppm; MS (ES): m/z 523 [M+Na]⁺.

5.2 Experimental procedures of DOS library

General Chemical Methods.

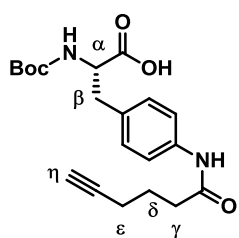
Reactions were monitored by thin layer chromatography (TLC) using commercially prepared glass plates pre-coated with Merck silica gel 60 F254. Adsorbed compounds were either viewed by the quenching of UV fluorescence ($\lambda_{max} = 254$ nm) or by staining with potassium permanganate solution. Purification of compounds by column chromatography was achieved using slurry-packed Merck 9385 Kieselgel 60 silica gel (230-400 mesh) under a positive pressure of nitrogen. Solvents used for reactions were dried over an appropriate drying agent and then distilled under nitrogen gas. The solvents used for chromatographic purposes were distilled prior to use by means of conventional distillation procedures. All reagents were obtained from commercial sources and used without further purification. Unless otherwise stated, non-aqueous reactions were performed using oven-dried glassware under an atmosphere of nitrogen. Temperatures at 0 °C were maintained using an ice-water bath. Compounds were named relying on the naming algorithm developed by CambridgeSoft Corporation and used in Chem-BioDraw Ultra 11.0. Reactions involving microwave irradiation were performed using a CEM Discover[®] microwave apparatus in 10 mL microwave tubes with clip lids. ¹H-NMR spectra were recorded using an internal deuterium lock at ambient probe temperatures on the following instruments: Avance III 400 QNP (400 MHz) and Bruker Avance 500 Cryo Ultrashield (500 MHz). Chemical shifts (δ_H) are quoted in ppm to the nearest 0.01 ppm and are referenced to the deuterated solvent peak. ¹³C-NMR spectra were recorded using an internal 191 deuterium lock on the following instruments: Bruker Avance III 400 QNP (100 MHz) and Bruker Avance 500 Cryo Ultrashield (125 MHz). Chemical shifts (δ) are quoted in ppm to the nearest 0.1 ppm and are referenced to the deuterated solvent peak. Infrared spectra were recorded neat on a Perkin Elmer Spectrum One spectrometer with internal referencing. Selected absorption maxima (ν_{max}) are reported on the wavenumber scale (cm^{-1}). Melting points were obtained using a Büchi Melting Point B-545 apparatus and are uncorrected. Specific rotations were measured using a Perkin Elmer 343 Polarimeter at the D-line of sodium (589 nm). $[\alpha]_D$ values are reported in $10^{-1} \text{ deg.cm}^2.\text{g}^{-1}$ and concentration (c) is given in g/100 mL.

Analytical high pressure liquid chromatography (HPLC) was performed on an Agilent 1260 Infinity using a SUPELCOTM ABZ⁺PLUS HPLC column (150 mm × 4.6 mm, 3 μm) with a gradient of 5-100% acetonitrile (with 0.05% TFA) in water (with 0.05% TFA) over 15 min at a flow rate of 1 ml.min⁻¹ and UV detection (λ_{max} = 220 nm and 254 nm). Retention times are reported to the nearest 0.01 min. Peak area percentages are calculated for UV absorbance at 220 nm or 254 nm, as indicated.

Liquid chromatography mass spectrometry (LC-MS) was conducted on an Agilent 1100 series LC with an ESCi Multi-Mode Ionisation Waters ZQ spectrometer. LC system: solvent A: 10 mM NH₄OAc + 0.1% HCOOH in water; solvent B: 95% acetonitrile + 5% H₂O + 0.05% HCOOH; column: SupelcosilTM ABZ⁺PLUS column (33 mm × 4.6 mm, 3 μm); gradient: 0.0-0.7 min: 0% B, 0.7-4.2 min: 0-100% B, 4.2-7.7 min: 100% B, 7.7-8.5 min: 100-0% B; DAD spectrum: 190 nm - 600 nm, interval 2.0 nm, peak width 0.200 min). Only molecular ions are reported. ESI refers to the electrospray ionisation technique.

High resolution mass spectra were recorded in either the EI⁺ or EI⁻ mode on a Micromass Q-TOF mass spectrometer or a Waters LCT Premier Time of Flight mass spectrometer. Reported mass values are recorded within the error limits of ±5 ppm mass units. Only molecular ions are reported. ESI refers to the electrospray ionisation technique.

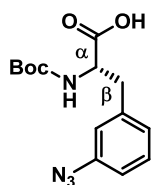
Boc-L-4-amino-phenylalanine(N-4-hexynoyl)-OH **66**



To a solution of 5-hexynoic acid **67** (0.528 mL, 4.67 mmol, 1 equiv) and Oxyma pure (634 mg, 4.67 mmol, 1 equiv) in dry DMF, was added DCC (964 mg, 4.67 mmol, 1 equiv). After 1 h of stirring at room temperature, a solution of Boc-L-4-amino-phenylalanine-OH **68** (1.31 g, 4.67 mmol, 1 equiv) and DIPEA (1.70 mL, 10.3 mmol, 2.2 equiv) in dry DMF was added, and the reaction mixture was stirred overnight. The precipitated dicyclohexylurea was filtered off, and the solvent evaporated under reduced pressure. The slurry was dissolved in 15 mL of EtOAc, and the organic phase was washed with 5% citric acid (2 x 10 mL), dried over MgSO₄ and evaporated to dryness. Purification by flash chromatography of the crude product (CH₂Cl₂/ MeOH/ AcOH 98.5/1.5/1)

afforded Boc-L-4-amino-phenylalanine(N-4-hexynoyl)-OH **66** (1.13 g, yield 64%) as a white solid. HPLC: t_r : 9.90 min (98%). $[\alpha]_{D=26.2}^{26.2} = +15$ (c 0.001, MeOH). mp= 138-140. IR: ν_{max} : 3549, 3351, 2975, 2162, 2008, 1727, 1706, 1661, 1597, 1523, 1411, 1367, 1308, 1248, 1161, 1057, 1027, 939, 897, 829, 779 cm^{-1} . 1H NMR (400 MHz, DMSO): δ = 1.30 (s, 9H, t Bu), 1.75-1.70 (m, 2H, δ CH₂), 2.18 (td, 2H, ϵ CH₂, J= 7, 2.6Hz), 2.36 (t, 2H, γ CH₂ J= 7.6Hz), 2.76-2.70 (m, 1H, β CH₂), 2.79 (t, 1H, alkyne, J=2.5 Hz), 2.90 (dd, 1H, β CH₂, J= 20, 4 Hz), 4.00 (m, 1H, α CH), 7.02 (d, 1H, NH carbamate, J= 8.4 Hz), 7.15 (d, 2H, CH aniline, J= 7.6Hz), 7.45 (d, 2H, CH aniline, J= 8.4 Hz), 9.83 (s, 1H, NH aniline), 12.4 (br, 1H, COOH) ppm. ^{13}C NMR (100 MHz, DMSO): δ = 17.8 (δ CH₂), 24.4 (ϵ CH₂), 28.6 (CH₃ t Bu), 35.5 (γ CH₂), 36.3 (β CH₂), 55.8 (α CH), 72.1 (CH alkyne), 78.5 (C), 84.5 (C), 119.3 (CH aniline), 129.7 (CH aniline), 133.0 (C), 138.1 (C), 155.9 (C), 170.9 (C), 174.0 (C), ppm. HRMS (ESI): m/z calcd for C₂₀H₂₇N₂O₅ [M+ H]⁺ 375.1920, found 375.1927.

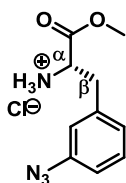
N-Boc-3-azide-L-phenylalanine **72**



N-Boc-3-nitro-L-phenylalanine **74** (610 mg, 1.95 mmol, 1equiv) was dissolved in 25 mL of MeOH, following by addition of K₂CO₃ (323 mg, 2.34 mmol, 1.2 equiv) and 10% Pd on charcoal. The reaction mixture was hydrogenated at room temperature under 55 psi. After 4 h the reaction is stopped, filtered over Celite and evaporated to dryness to give of N-Boc-3-amine-L-phenylalanine as potassium salt **75** (white solid), which was used in the next reaction without further purification. N-Boc-3-amine-L-phenylalanine potassium salt (0.672 g, 1.95 mmol, 1 equiv), imidazol sulfonyl azide bisulfate (635 mg, 2.34 mmol, 1.2 equiv), CuSO₄ pentahydrate (5 mg, 0.0195 mmol, 0.01 equiv), were dissolved in 12 mL of MeOH, and the reaction mixture was stirred at room temperature for 18 hours. The solvent was evaporated, and 6 mL of water was added to the slurry. The aqueous phase was acidified with HCl 1M until pH 3, and extracted with EtOAc (3 x 15mL); the organic phase was dried over MgSO₄ and purified by flash chromatography (CH₂Cl₂/MeOH/AcOH 95/5/0.6) to give N-Boc-3-azide-L-phenylalanine **72** as a pink solid (0.33 g, yield 55%). HPLC: t_r : 11.28 min (97%). 1H NMR (400 MHz, CDCl₃): δ = 1.43 (s, 9H, CH₃ t Bu), 3.12–2.98 (m, 1H, β CH₂), 3.21 (dd, J = 7.7, 5.9

Hz, 1H, β CH₂), 4.60 (d, J = 5.5 Hz, 1H, α CH), 4.96 (d, J = 7.5 Hz, 1H, NH), 6.84 (s, 1H, CH arom.), 6.94 (dd, J = 8.0, 2.2 Hz, 1H, CH arom.), 6.97 (d, J = 7.6 Hz, 1H, CH arom.), 7.29 (t, J = 7.8 Hz, 1H, CH arom.) ppm. ¹³C NMR (100 MHz, CDCl₃): δ = 28.4 (CH₃ ^tBu), 37.7 (β CH₂), 53.4 (α CH), 77.5 (C), 117.9 (CH arom.), 120.1 (CH arom.), 126.1 (CH arom), 130.3 (CH arom.), 138.1 (C), 140.4 (C), 155.5 (C=O), 175.3 (C=O) ppm. HRMS (ESI): *m/z* calcd for C₁₄H₁₈N₄O₄Na [M+ Na]⁺ 329.1220, found 329.1209.

3-Azide-L-phenylalanine methyl ester hydrochloride **69**



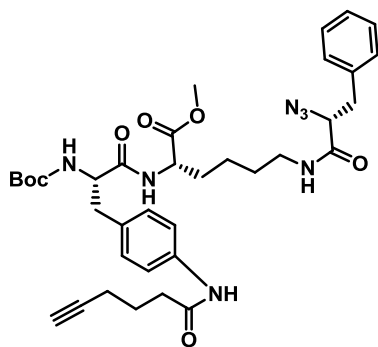
TMSCl (0.684 mL, 5.40 mmol, 5 equiv) was added to 3 mL of ice-cooled MeOH. After stirring 10 minutes, N-Boc-3-azide-L-phenylalanine **72** (330 mg, 1.08 mmol, 1 equiv) was added and the reaction was stirred at room temperature overnight. The solvent was removed under reduced pressure, co-evaporations with CH₂Cl₂ (x3) were performed, and the product was dried at high vacuum to give **69** as a violet solid (0.26 g, yield 94%). HPLC: *t_r*: 7.02 min (98%). [α]^{26.2}_D = +9 (c 0.000867, MeOH). mp = 160-162. IR: ν_{max} : 2825, 2628, 2106, 1735, 1593, 1578, 1492, 1479, 1441, 1390, 1290, 1242, 1211, 1140, 1082 cm⁻¹. ¹H NMR (500 MHz, DMSO): δ = 3.13 (d, J = 6.7 Hz, 2H, β CH₂), 3.69 (s, 3H, OCH₃), 4.34 (t, J = 6.6 Hz, 1H, α CH), 7.06 – 6.97 (m, 3H, CH arom.), 7.37 (t, J = 7.9 Hz, 1H, CH arom.), 8.52 (br, 3H, NH₃⁺) ppm. ¹³C NMR (125 MHz, DMSO): δ = 35.6 (β CH₂), 52.9 (OCH₃), 53.1 (α CH), 118.3 (CH), 120.2 (CH), 126.4 (CH), 130.4 (CH), 136.8 (C), 139.7 (C), 169.4 (C=O) ppm. HRMS (ESI): *m/z* calcd for C₁₀H₁₃N₄O₂ [M+ H]⁺ 221.1039, found 221.1047.

General procedures for linear peptidomimetics **76-80**, **86-88** synthesis.

Azido-amines hydrochloride salt (1 equiv), alkyne-carboxylic acids (1 equiv) and HOBt·H₂O (1.1 equiv) were dissolved in 7 mL of dry CH₂Cl₂. TEA (2.2 equiv) was added, and just after that EDC·HCl (1.1 equiv) suspended in 2 mL of CH₂Cl₂ was added. The reaction mixture was stirred overnight at room temperature, then the solvent removed under reduced pressure; the slurry was suspended in EtOAc (15 mL) and washed with H₂O (2 x 6 mL), saturated aqueous NaHCO₃ (2 x 6 mL), 5% citric acid (2x 6 mL), and again H₂O (2 x 6 mL). The

organic phase was dried over MgSO_4 , evaporated to dryness and used in the next step without any further purification unless otherwise stated.

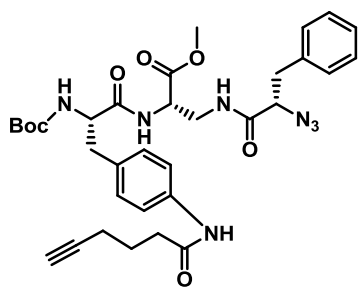
Methyl 6-(2-azido-3-phenylpropanamido)-2-((S)-2-(tert-butoxy-carbonylamino)-3-(4-hex-5-ynamidophenyl) propanamido) hexanoate **76**



Alkyne acid **66** (112 mg, 0.30 mmol), azido-amine **81** (111 mg, 0.30 mmol), HOBT· H_2O (50.5 mg, 0.33 mmol), TEA (0.92 mL, 0.67 mmol), EDC·HCl (63.3 mg, 0.33 mmol), were allowed to react according to the described general procedure for linear peptidomimetics, yielding **76** as white powder (178 mg, yield 86%). HPLC: t_r : 11.9 min

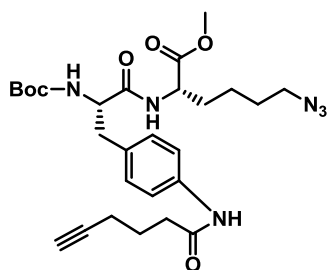
(87%), LCMS: t_r : 4.4 min, 690.2 (MH^+).

Methyl 3-(2-azido-3-phenylpropanamido)-2-((S)-2-(tert-butoxy-carbonylamino)-3-(4-hex-5-ynamidophenyl)propanamido)propanoate **77**



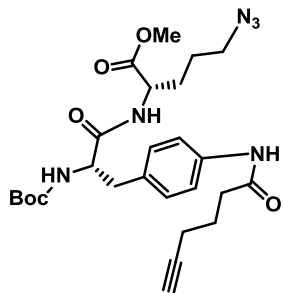
A procedure analogous to the one used for **76** but with **82** (98 mg, 0.30 mmol) as azido amine yielded **77** (168 mg, yield 86%) as white solid. HPLC: t_r : 11.7 min (87%), LCMS: t_r : 4.5 min, 648.26 (MH^+).

Methyl 6-azido-2-((S)-2-(tert-butoxycarbonylamino)-3-(4-hex-5-ynamidophenyl) propanamido) hexanoate **78**



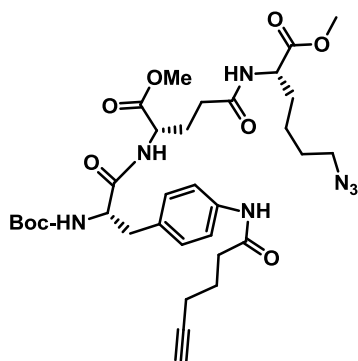
A procedure analogous to the one used for **76** but with **83** (66.8 mg, 0.30 mmol) azido amine yielded **78** (143 mg, yield 88%) as white solid. HPLC: t_r : 11.6 min (97%), LCMS: t_r : 4.4 min, 543 (MH^+).

(S)-Methyl 5-azido-2-((S)-2-(tert-butoxycarbonylamino)-3-(4-hex-5-ynamidophenyl)propanamido)pentanoate **79**



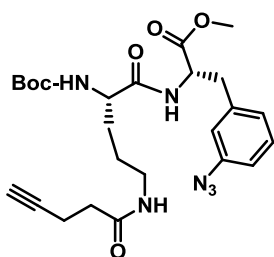
A procedure analogous to the one used for **76** but with **84** (62.6 mg, 0.30 mmol) as azido amine yielded **79** (133 mg, yield 84%) as white solid. HPLC: t_r : 11.3 min (90%), LCMS: t_r : 4.4 min, 527 (M^-).

(6S,9S)-Methyl 14-(4-azidobutyl)-6-(4-hex-5-ynamidobenzyl)-9-(methoxycarbonyl)-2,2-dimethyl-4,7,12-trioxo-3-oxa-5,8,13-triazapentadecan-15-oate **80**



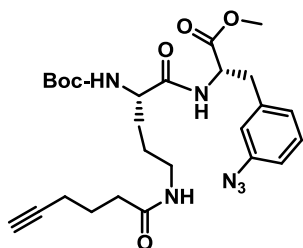
A procedure analogous to the one used for **76** but with **85** (110 mg, 0.30 mmol) as azide amine yielded **80** (158 mg, yield 77%) as pale yellow solid. HPLC: t_r : 11.2 min (84%), LCMS: t_r : 4.3 min, 686.29 (MH^+).

(S)-Methyl 3-(3-azidophenyl)-2-((S)-2-(tert-butoxycarbonylamino)-5-pent-4-ynamidopentanamido)propanoate **86**



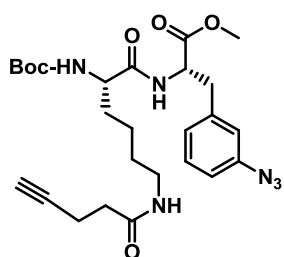
Azido amine **69** (77 mg, 0.30 mmol), alkyne acid **89** (94 mg, 0.30 mmol), HOBt·H₂O (51 mg, 0.33 mmol), TEA (0.92 mL, 0.67 mmol), EDC·HCl (63 mg, 0.33 mmol) were allowed to react according to the described general procedure for linear peptidomimetics, yielding **86** as white solid (130 mg, yield 84%). HPLC: t_r : 10.92 min (83%), LCMS: t_r : 4.3 min, 515.21 (MH^+).

(S)-Methyl-3-(3-azidophenyl)-2-((S)-2-(tert-butoxycarbonylamino)-5-hex-5-ynamidopentanamido)propanoate 87



A procedure analogous to the one used for **86** but with **90** (88 mg, 0.30 mmol) as alkyne acid, yielded **87** (122 mg, yield 77%) as white solid. HPLC: t_r : 11.18 min (77%), LCMS: t_r : 4.4 min, 529.29 (MH^+).

(S)-Methyl 3-(3-azidophenyl)-2-((S)-2-(tert-butoxycarbonylamino)-6-pent-4-ynamido)hexanamido)propanoate 88

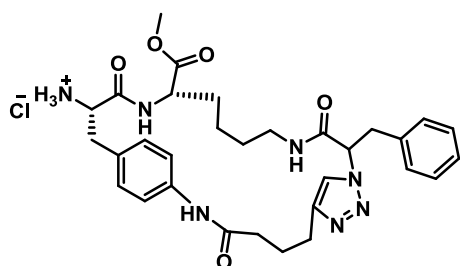


A procedure analogous to the one used for **86** but with **91** (88 mg, 0.30 mmol) as alkyne acid yielded **88** (117 mg, yield 77%) as yellow solid. HPLC: t_r : 11.08 min (77%), LCMS: t_r : 4.3 min, 529.29 (MH^+).

General procedures for synthesis of macrocycles 92-93 1,4-triazole.

Linear peptides (1 equiv) were suspended under N_2 in 25 mL of dry THF or dry toluene (specified on each compound), then DIPEA (3 equiv) was added. The reaction mixture was bubbled under Ar for 10 minutes; at this point CuI (2 equiv) was added and the reaction refluxed under N_2 for 15 h. Then it was cooled to room temperature and the solvent was evaporated under reduced pressure. The resulting BOC-protected compound was stirred overnight at room temperature with HCl 4M in dioxane, the co-evaporated with CH_2Cl_2 to afford the desired macrocycle, unless otherwise stated.

Macrocyclic peptidomimetic (1,4-triazole) 92

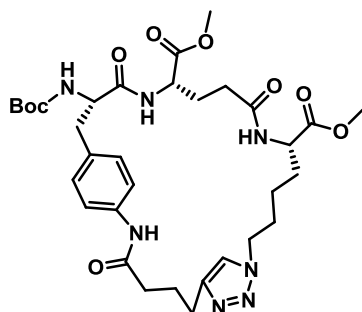


Linear peptide **76** (24 mg, 0.035 mmol), DIPEA (0.17 mL, 0.105 mmol) and CuI (13 mg, 0.07 mmol) in THF were allowed to react according to the described general procedure for macrocycles 1,4-triazole.

Crude product was purified by flash column ($CH_2Cl_2/MeOH$ 95/5), then treated

with 1.5 mL of HCl 4M in dioxane yielding **92** as a pale yellow solid (2.4 mg, yield 11%). HPLC: t_r : 7.59 min (79%), LCMS: t_r : 3.2 min, 590.21 (MH⁺).

Macrocyclic peptidomimetic (1,4-triazole) **93**

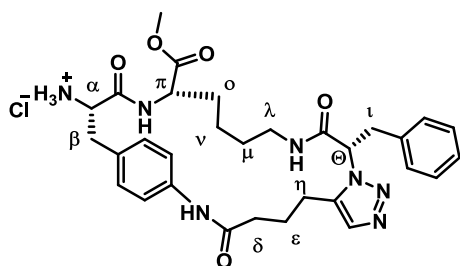


Linear peptide **80** (24 mg, 0.035 mmol) DIPEA (0.17 mL, 0.105 mmol) and CuI (13 mg, 0.07 mmol) in THF were allowed to react according to the described general procedure for macrocycles 1,4-triazole. Crude product was purified by flash column (CH₂Cl₂/MeOH 95/5) yielding **93** as a pale yellow solid (3 mg, yield 12%). HPLC: t_r : 8.46 min (93%), LCMS: t_r : 3.7 min, 686.29 (MH⁺).

General procedures for synthesis of macrocycles **94-101** 1,5-triazole.

Linear peptides (1 equiv) were suspended in 25 mL of dry toluene under N₂. The reaction mixture was heated to 80 °C and bubbled with Ar for 10 minutes. [Cp**Ru*Cl]₄ (0.1 equiv) was added, and the reaction was refluxed for 20 h under N₂. Then it was cooled to room temperature and the solvent was evaporated under reduced pressure. The crude product was purified by flash chromatography. The resulting BOC-protected compound was stirred overnight at room temperature with HCl 4M in dioxane, the co-evaporated with CH₂Cl₂ to afford the desired macrocycle, unless otherwise stated.

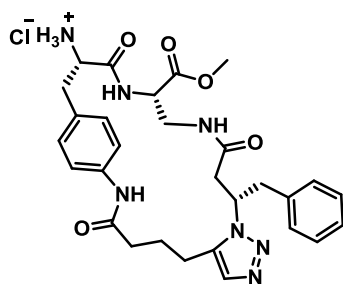
Macrocyclic peptidomimetic (1,5-triazole) **94**



Linear peptide **76** (24 mg, 0.035 mmol) and [Cp**Ru*Cl]₄ (3 mg, 0.0035 mmol) were allowed to react according to the described general procedure for macrocycles 1,5-triazole. Crude product was purified by flash column (CH₂Cl₂/MeOH 95/5), then treated with 1.5 mL of HCl 4M in dioxane yielding **94** as a pale yellow solid (11 mg, 50% yield). HPLC: t_r : 7.40 min (89%), LCMS: t_r : 3.2 min. IR: ν_{max} : 3311, 2922, 2852, 2161, 2029, 1726, 1661, 1601, 1537, 1456, 1416, 1253, 1119, 828, 749, 700 cm⁻¹. ¹H NMR (400 MHz, DMSO):

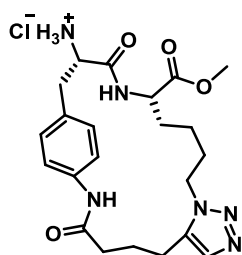
δ = 0.92-0.76 (vCH₂), 1.12-1.03(m, 2H, ϵ CH₂), 1.32-1.14 (4H, oCH₂, μ CH₂), 1.45 (t, 2H, λ CH₂, J = 14.5 Hz), 2.85-2.74 (m, 1H β CH₂, 2H δ CH₂, 2H η CH₂), 3.16 (s, 1H, β CH₂), 3.47-3.44 (m, 2H, ι CH₂), 3.58 (s, OCH₃), 3.66 (d, 1H, π CH, J = 1.5 Hz), 4.02 (m, 1H α CH), 5.36-5.32 (m, 1H, θ CH), 7.19 (s, 1H, CH triazole), 7.23-7.14 (m, 6H, 2CH aniline, 4 CH arom), 7.53-7.49 (m, 3H, 2CH aniline and 1CH arom.), 8.11 (br, NH), 8.25 (br NH), 8.49 (br, NH₃), 10 (br, NH aniline), ppm. ¹³C NMR (100 MHz, DMSO): δ = 21.8 (CH₂), 22.3 (CH₂), 28.3 (CH₂), 29.0 (CH₂), 35.0(CH₂), 36.1 (CH₂), 36.3 (CH₂), 43.5 (CH₂), 51.6 (CH), 52.9 (CH), 60.2 (CH₂), 62.5 (CH), 66.3 (CH₂), 70.6 (CH₂), 71.9 (CH₂), 72.1 (CH₂), 118.9 (CH), 126.5 (CH), 128.1 (CH), 129.1 (CH), 129.9 (CH), 131.6 (CH), 136.8 (C), 137.4 (C), 138.2 (C), 166.9 (C), 167.1 (C), 170.7 (C), 170.8 (C), ppm. HRMS (ESI): m/z calc. for C₃₁H₄₀N₇O₅ [M+ H]⁺ 590.309, found 590.3080.

Macrocyclic peptidomimetic (1,5-triazole) **95**



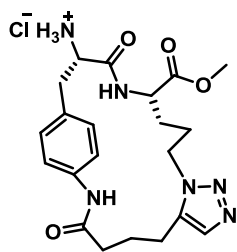
Linear peptide **77** (23 mg, 0.035 mmol) and [Cp*₂RuCl]₄ (3 mg, 0.0035 mmol) were allowed to react according to the described general procedure for macrocycles 1,5-triazole. Crude product was purified by flash column (CH₂Cl₂/MeOH 96/4), then treated with 1.5 mL of HCl 4M in dioxane yielding **95** as a white solid (3 mg, 15% yield). HPLC: t_r : 6.97 min (92%), LCMS: t_r : 3.1 min 548.13 (MH⁺).

Macrocyclic peptidomimetic (1,5-triazole) **96**



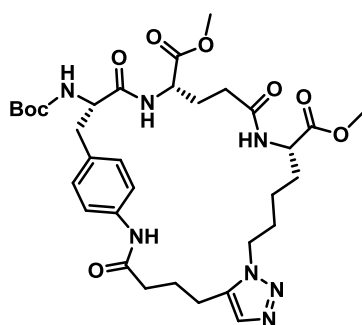
Linear peptide **78** (19 mg, 0.035 mmol) and [Cp*₂RuCl]₄ (3 mg, 0.0035 mmol) were allowed to react according to the described general procedure for macrocycles 1,5-triazole. Crude product was purified by flash column (CH₂Cl₂/MeOH 95/5), then treated with 1.5 mL of HCl 4M in dioxane yielding **96** as a yellow solid (11 mg, 66% yield). HPLC: t_r : 5.69 min (98%), LCMS: t_r : 2.8 min 443.15 (MH⁺).

Macrocyclic peptidomimetic (1,5-triazole) **97**



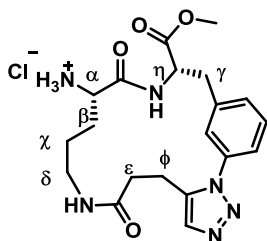
Linear peptide **79** (19 mg, 0.035 mmol) and $[\text{Cp}^*\text{RuCl}]_4$ (3 mg, 0.0035 mmol) were allowed to react according to the described general procedure for macrocycles 1,5-triazole. Crude product was purified by flash column ($\text{CH}_2\text{Cl}_2/\text{MeOH}$ 95/5), then treated with 1.5 mL of HCl 4M in dioxane yielding **97** as a yellow solid (11 mg, 68% yield). HPLC: t_r : 5.37 min (95%), LCMS: t_r : 2.8 min 429.13 (MH^+).

Macrocyclic peptidomimetic (1,5-triazole) **98**



Linear peptide **80** (24 mg, 0.035 mmol) and $[\text{Cp}^*\text{RuCl}]_4$ (3 mg, 0.0035 mmol) were allowed to react according to the described general procedure for macrocycles 1,5-triazole. Crude product was purified by flash column $\text{CH}_2\text{Cl}_2/\text{MeOH}$ 95/5 yielding **98** as a pale yellow solid (10 mg, 42% yield). HPLC: t_r : 8.69 min (90%), LCMS: t_r : 3.8 min 686.29 (MH^+).

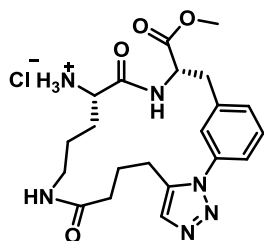
Macrocyclic peptidomimetic (1,5-triazole) **99**



Linear peptide **86** (18 mg, 0.035 mmol) and $[\text{Cp}^*\text{RuCl}]_4$ (3 mg, 0.0035 mmol) were allowed to react according to the described general procedure for macrocycles 1,5-triazole. Crude product was purified by flash column ($\text{CH}_2\text{Cl}_2/\text{MeOH}$ 95/5), then treated with 1.5 mL of HCl 4M in dioxane yielding **99** as a red powder (12 mg, 76% yield). HPLC: t_r : 5.72 min (90%), LCMS: t_r : 2.9 min 415.11 (MH^+). IR: ν_{max} : 3232, 3054, 2937, 2112, 1737, 1678, 1643, 1543, 1493, 1440, 1214, 1117, 1041, 871 cm^{-1} . ^1H NMR (500 MHz, DMSO): δ = 1.23-1.38 (m, 2H χCH), 2.40 – 2.32 (m, 2H βCH), 2.95 – 3.04 (m, 2H, ϕCH), 3.08 (dd, J = 15.0, 8.7 Hz, 1H, γCH), 3.19-3.22 (m, 1H, ϵCH), 3.31 (dd, J = 14.1, 8.8 Hz, 1H, γCH), 3.58 (s, 3H, OMe), 3.95 (m, 1H, αCH), 4.58 (m, 1H, ηCH), 7.34 (d, J = 7.3 Hz, 1H arom), 7.45 (d, J = 7.5 Hz, 1H arom), 7.53 (t, J = 7.7 Hz, 1H arom), 7.69 (s, 1H triazole), 7.75 (s, 1H), 8.13 (d, J = 12.4 Hz, NH_3), 8.85 (d, J = 5.7 Hz, NH), ppm. ^{13}C NMR (126

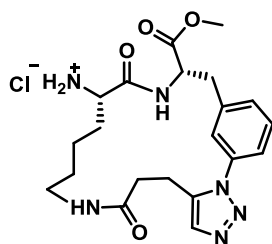
MHz, DMSO): δ = 20.7, 24.3, 28.2, 34.3, 35.2, 36.5, 51.4, 52.4, 54.1, 60.6, 66.8, 71.0, 72.6, 124.4, 126.2, 130.2, 131.1, 132.5, 136.4, 137.9, 139.9, 170.0, 170.1, 171.6 ppm. HRMS (ESI): m/z calc. for $C_{20}H_{27}N_6O_4$ $[M+H]^+$ 415.2088, found 415.2079.

Macrocyclic peptidomimetic (1,5-triazole) **100**



Linear peptide **87** (19 mg, 0.035 mmol) and $[Cp^*RuCl]_4$ (3 mg, 0.0035 mmol) were allowed to react according to the described general procedure for macrocycles 1,5-triazole. Crude product was purified by flash column ($CH_2Cl_2/MeOH$ 95/5), then treated with 1.5 mL of HCl 4M in dioxane yielding **100** as a brown solid (11 mg, 68% yield). HPLC: t_r : 5.78 min (86%), LCMS: t_r : 2.9 min 429.16 (MH^+).

Macrocyclic peptidomimetic (1,5-triazole) **101**

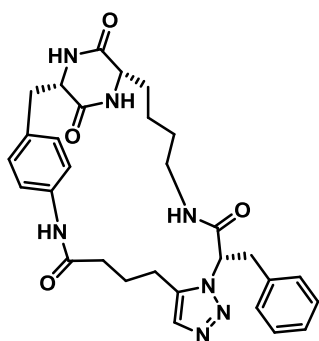


Linear peptide **88** (19 mg, 0.035 mmol) and $[Cp^*RuCl]_4$ (3 mg, 0.0035 mmol) were allowed to react according to the described general procedure for macrocycles 1,5-triazole. Crude product was purified by flash column ($CH_2Cl_2/MeOH$ 95/5), then treated with 1.5 mL of HCl 4M in dioxane yielding **101** as a light brown powder (10 mg, 61% yield). HPLC: t_r : 5.72 min (89%), LCMS: t_r : 2.9 min 429.16 (MH^+).

General procedures for DKPs **102-104** formation.

1,4-triazole or 1,5-triazole macrocycles (1 equiv) suspended in 2-Butanol and morpholinomethyl-polystyrene (NMM resin) (5.6 equiv) were placed in a microwave reactor. AcOH (7.1 equiv) was added and the reaction was heated with MW to 150 °C for 3H (unless otherwise stated). Then the resin was filtered off and washed several times with MeOH and CH_2Cl_2 . The filtrate was evaporated to dryness performing co-evaporations with CH_2Cl_2 (x3) yielding the final DKP compound.

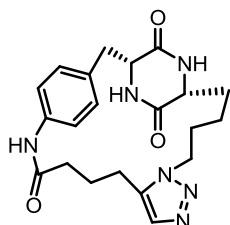
Macrocyclic Diketopiperazine (1,5-triazole) **102**



min, 558.18 (MH⁺).

94 (5 mg, 0.0081 mmol), NMM resin (13 mg, 0.046 mmol) and AcOH (3.3 μ L, 0.058 mmol) in 0.7 mL of 2-butanol were allowed to react according to the described general procedure for DKPs but extending the reaction time to 9 hours, yielding **102** as yellow powder (2.2 mg, 48% yield). HPLC: t_r : 7.27 min (95%). LCMS: t_r : 3.4

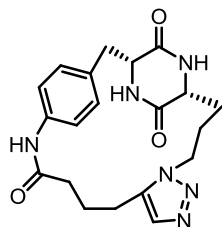
Macrocyclic Diketopiperazine (1,5-triazole) **103**



HPLC: t_r : 5.32 min (78%), LCMS: t_r : 3.0 min, 411.13 (MH⁺).

96 (6 mg, 0.0011 mmol), NMM resin (18 mg, 0.064 mmol) and AcOH (4.5 μ L, 0.078 mmol) in 0.7 mL of 2-butanol were allowed to react according to the described general procedure for DKPs but extending the reaction time to 9 hours, yielding **103** as yellow solid (0.4 mg, 9% yield).

Macrocyclic Diketopiperazine (1,5-triazole) **104**



(87%), LCMS: t_r : 2.9 min, 397.12 (MH⁺).

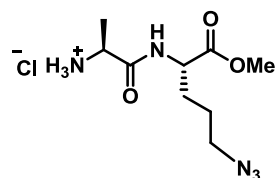
97 (5 mg, 0.0010 mmol), NMM resin (15 mg, 0.054 mmol) and AcOH (4.0 μ L, 0.069 mmol) in 0.7 mL of 2-butanol were allowed to react according to the described general procedure for DKPs but extending the reaction time to 9 hours, yielding **104** as white powder (1.6 mg, 42% yield). HPLC: t_r : 5.06 min

General procedures for B/C/C/P and B/C/C/CP linear peptidomimetics's synthesis.

Azido-amines hydrochloride salt (1 equiv) and Boc-protected amino acids (1 equiv) were coupled together following the general procedure for linear peptidomimetics described above. The resulting dipeptides were then treated with a solution of TMSCl (5 equiv) in iced-cooled MeOH overnight at room

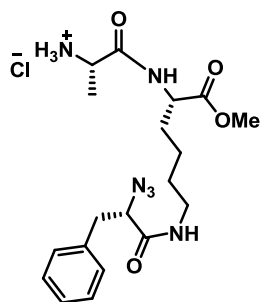
temperature in order to remove the BOC group, and again another coupling is performed with the suitable alkyne acids (1 equiv).

(S)-1-((S)-5-azido-1-methoxy-1-oxopentan-2-ylamino)-1-oxopropan-2-aminium chloride 107



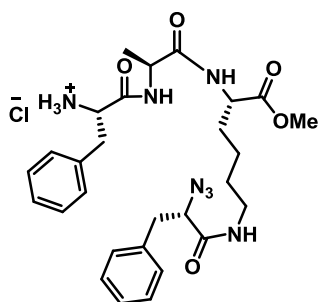
84 (188 mg, 0.90 mmol), Boc-L-Ala-OH **105** (170 mg, 0.90 mmol), HOBt·H₂O (154 mg, 0.99 mmol), TEA (0.28 mL, 1.98 mmol), EDC·HCl (190 mg, 0.99 mmol) were allowed to react according to the described general procedure for linear peptidomimetics, and the resulting dipeptides was treated with TMSCl (0.47 mL, 3.7 mmol) in 1.8 mL of MeOH. Co-evaporation with CH₂Cl₂ were performed to give **107** hydrochloride salt as a white foam (248 mg, 98% yield). HPLC: t_r: 9.66 min (83%), LCMS: t_r: 0.5 min, 244.1 (MH⁺).

(S)-1-((S)-6-((S)-2-azido-3-phenylpropanamido)-1-methoxy-1-oxohexan-2-ylamino)-1-oxopropan-2-aminium chloride 131



81 (333 mg, 0.90 mmol), Boc-LAla-OH **105** (170 mg, 0.90 mmol), HOBt·H₂O (154 mg, 0.99 mmol), TEA (0.28 mL, 1.98 mmol), EDC·HCl (190 mg, 0.99 mmol) were allowed to react according to the described general procedure for linear peptidomimetics, and the resulting dipeptides was treated with TMSCl (0.60 ml) in 2.3 mL of MeOH. Co-evaporations with CH₂Cl₂ were performed to give **131** hydrochloride salt as a white foam (372 mg, 94% yield). HPLC: t_r: 7.95 min (90%), LCMS: t_r: 3.3 min, 405.21 (MH⁺).

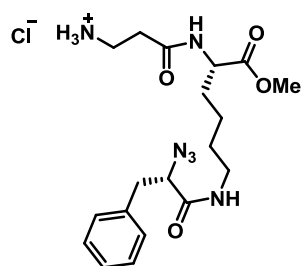
(S)-1-((S)-1-((S)-6-((S)-2-azido-3-phenylpropanamido)-1-methoxy-1-oxohexan-2-ylamino)-1-oxopropan-2-ylamino)-1-oxo-3-phenylpropan-2-aminium chloride 117



131 (372 mg, 0.84 mmol), Boc-L-Phe-OH **68** (223 mg, 0.84 mmol), HOBt·H₂O (143 mg, 0.92 mmol), TEA (0.26 mL, 1.85 mmol), EDC·HCl (176 mg, 0.92 mmol) were allowed to react according to the described general

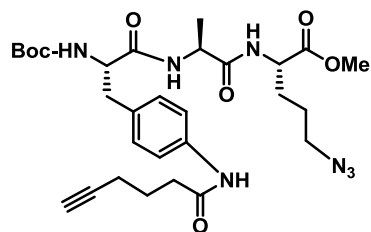
procedure for linear peptidomimetics, and the resulting tripeptides was treated with TMSCl (0.60 mL) in 2.3 mL of MeOH. Co-evaporation with CH₂Cl₂ were performed to give **117** hydrochloride salt as a white foam (440 mg, 89% yield). HPLC: t_r: 8.91 min (77%), LCMS: t_r: 3.5 min, 552.33 (MH⁺).

3-((S)-6-((S)-2-azido-3-phenylpropanamido)-1-methoxy-1-oxohexan-2-ylamino)-3-oxopropan-1-aminium chloride **108**



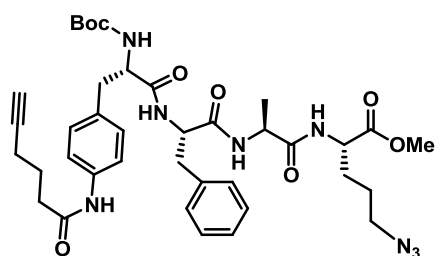
81 (333 mg, 0.90 mmol), Boc-βAla-OH **106** (170 mg, 0.90 mmol), HOBt·H₂O (154 mg, 0.99 mmol), TEA (0.28 mL, 1.98 mmol), EDC·HCl (190 mg, 0.99 mmol) were allowed to react according to the described general procedure for linear peptidomimetics, and the resulting dipeptides was treated with TMSCl (0.60 ml) in 2.3 mL of MeOH. Co-evaporations with CH₂Cl₂ were performed to give **108** hydrochloride salt as a white foam (357 mg, 90% yield). HPLC: t_r: 7.80 min (86%), LCMS: t_r: 3.3 min, 405.17 (MH⁺).

(6S,9S,12S)-methyl 12-(3-azidopropyl)-6-(4-hex-5-ynamidobenzyl)-2,2,9-trimethyl-4,7,10-trioxo-3-oxa-5,8,11-triazatridecan-13-oate **109**



107 (83 mg, 0.29 mmol), **66** (110 mg, 0.29 mmol), HOBt·H₂O (50 mg, 0.32 mmol), TEA (0.09 mL, 0.65 mmol), EDC·HCl (62 mg, 0.32 mmol) were allowed to react according to the described general procedure for linear peptidomimetics, yielding **109** as a white solid (129 mg, 73% yield). HPLC: t_r: 10.71 min (88%), LCMS: t_r: 4.22 min, 600.34 (MH⁺).

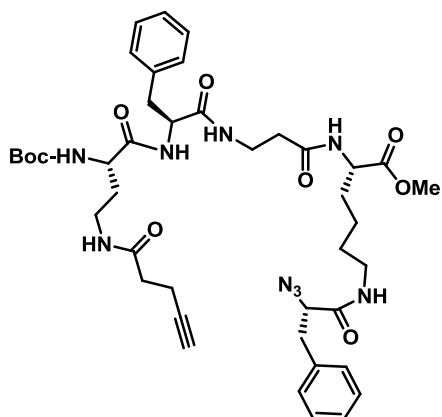
(6S,9S,12S,15S)-methyl 15-(3-azidopropyl)-9-benzyl-6-(4-hex-5-ynamidobenzyl)-2,2,12-trimethyl-4,7,10,13-tetraoxo-3-oxa-5,8,11,14-tetraazahexadecan-16-oate **115**



107 (83 mg, 0.29 mmol), Boc-L-Phe-OH **68** (78 mg, 0.29 mmol), HOBt·H₂O (50 mg, 0.32 mmol), TEA (0.09 mL, 0.65 mmol),

EDC·HCl (62 mg, 0.32 mmol) were allowed to react according to the described general procedure for linear peptidomimetics, and the resulting tripeptides was treated with TMSCl (0.14 mL, 1.1 mmol) in 0.5 mL of MeOH. Co-evaporations with CH₂Cl₂ were performed to give **118** hydrochloride salt as a white foam (91 mg, 72% yield, 81% purity by HPLC). **118** (91 mg, 0.21 mmol), underwent to another coupling following the usual procedure described above, but using **70** (79 mg, 0.21 mmol) and the right amount of HOBt·H₂O (36 mg, 0.23 mmol), TEA (0.07 mL, 0.47 mmol), EDC·HCl (45 mg, 0.23 mmol), affording **115** as a white solid (97 mg, 61% yield). HPLC: t_r: 11.67 min (82%), LCMS: t_r: 4.46 min, 747.50 (MH⁺).

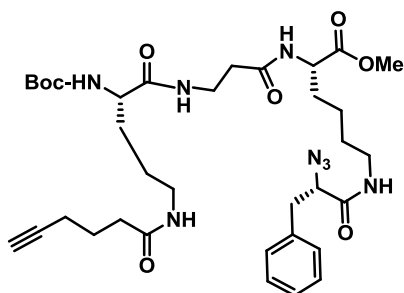
(6S,9S,16S)-methyl 16-(4-((S)-2-azido-3-phenylpropanamido)butyl)-9-benzyl-2,2-dimethyl-4,7,10,14-tetraoxo-6-(2-pent-4-ynamidoethyl)-3-oxa-5,8,11,15-tetraazaheptadecan-17-oate **116**



108 (119 mg, 0.27 mmol), Boc-L-Phe-OH **68** (72 mg, 0.27 mmol), HOBt·H₂O (43 mg, 0.28 mmol), TEA (0.08 mL, 0.59 mmol), EDC·HCl (54 mg, 0.28 mmol), were allowed to react according to the described general procedure for linear peptidomimetics, and the resulting tripeptides was treated with TMSCl (0.14 mL, 1.1 mmol) in 0.5 mL of MeOH.

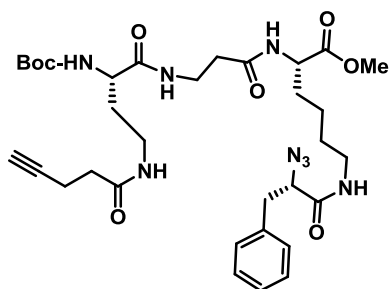
Co-evaporation with CH₂Cl₂ were performed to give **119** hydrochloride salt as a white solid (128 mg, 80% yield, 78% purity by HPLC). **119** (63 mg, 0.11 mmol), underwent to another coupling following the usual procedure described above, but using **122** (79 mg, 0.21 mmol) as the alkyne acid and the right amount of HOBt·H₂O (19 mg, 0.12 mmol), TEA (0.04 mL, 0.24 mmol), EDC·HCl (21 mg, 0.12 mmol), affording **116** as a white solid (66 mg, 72% yield). HPLC: t_r: 11.05 min (77%), LCMS: t_r: 4.3 min, 832.64 (MH⁺).

(6S,13S)-methyl 13-(4-((S)-2-azido-3-phenylpropanamido)butyl)-6-(3-hex-5-ynamidopropyl)-2,2-dimethyl-4,7,11-trioxo-3-oxa-5,8,12-triazatetradecan-14-oate **110**



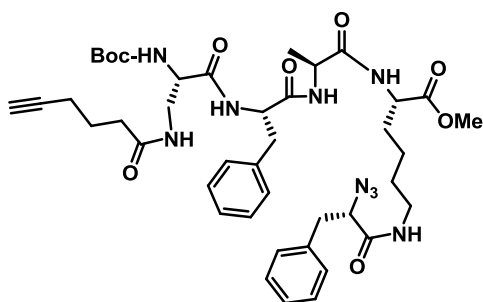
108 (119 mg, 0.27 mmol), **90** (88 mg, 0.29 mmol), HOBt·H₂O (43 mg, 0.28 mmol), TEA (0.08 mL, 0.59 mmol), EDC·HCl (54 mg, 0.28 mmol) were allowed to react according to the described general procedure for linear peptidomimetics, yielding **110** as a pale yellow solid (119 mg, 62% yield). HPLC: *t_r*: 10.35 min (80%), LCMS: *t_r*: 4.2 min, 713.52 (MH⁺).

(6S,13S)-methyl 13-(4-((S)-2-azido-3-phenylpropanamido)butyl)-2,2-dimethyl-4,7,11-trioxo-6-(2-pent-4-ynamidoethyl)-3-oxa-5,8,12-triazatetradecan-14-oate **111**



108 (119 mg, 0.27 mmol), **112** (80 mg, 0.29 mmol), HOBt·H₂O (43 mg, 0.28 mmol), TEA (0.08 mL, 0.59 mmol), EDC·HCl (54 mg, 0.28 mmol) were allowed to react according to the described general procedure for linear peptidomimetics, yielding **111** as a white solid (125 mg, 67% yield). HPLC: *t_r*: 10.09 min (82%), LCMS: *t_r*: 4.1 min, 685.47 (MH⁺).

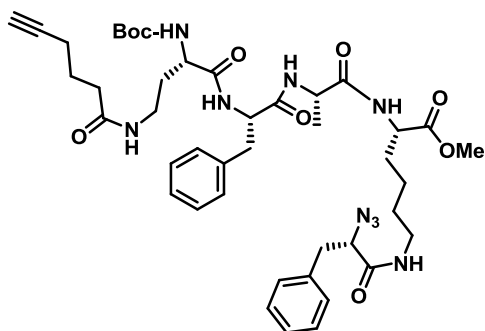
(6S,9S,12S,15S)-methyl 15-(4-((S)-2-azido-3-phenylpropanamido)butyl)-9-benzyl-6-(hex-5-ynamidomethyl)-2,2,12-trimethyl-4,7,10,13-tetraoxo-3-oxa-5,8,11,14-tetraazahexadecan-16-oate **114**



117 (147 mg, 0.25 mmol), **120** (75 mg, 0.25 mmol), HOBt·H₂O (43 mg, 0.28 mmol), TEA (0.08 mL, 0.59 mmol), EDC·HCl (54 mg, 0.28 mmol) were allowed to react according to the described general procedure for linear

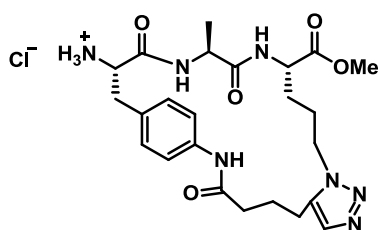
peptidomimetics; the crude product was purified by flash chromatography ($\text{CH}_2\text{Cl}_2/\text{MeOH}$ 96/4) yielding **114** as a white solid (128 mg, 62% yield). HPLC: t_r : 11.79 min (79%), LCMS: t_r : 4.5 min, 832.57 (MH^+).

(6S,9R,12S,15S)-methyl 15-(4-((S)-2-azido-3-phenylpropanamido)butyl)-9-benzyl-6-(2-hex-5-ynamidoethyl)-2,2,12-trimethyl-4,7,10,13-tetraoxo-3-oxa-5,8,11,14-tetraazahexadecan-16-oate **113**



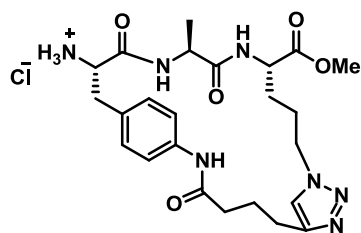
A procedure analogous to the one used for **114** but with **121** (78 mg, 0.25 mmol) as alkyne acid yielded **113** (168 mg, 79% yield) as white solid. HPLC: t_r : 11.60 min (78%), LCMS: t_r : 4.5 min, 846.67 (MH^+).

B/C/C/P macrocycle 1,5 triazole **124**



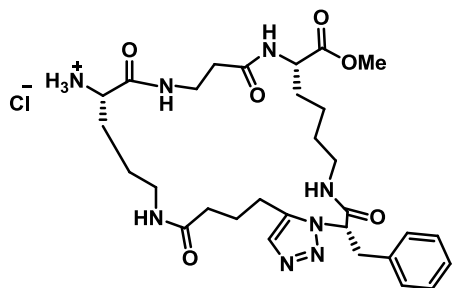
Linear peptide **109** (21 mg, 0.035 mmol) and $[\text{Cp}^*\text{RuCl}]_4$ (3 mg, 0.0035 mmol) were allowed to react according to the described general procedure for macrocycles 1,5-triazole. Crude product was purified by flash column ($\text{CH}_2\text{Cl}_2/\text{MeOH}$ 90/10), then treated with 1.5 mL of HCl 4M in dioxane yielding **124** as a brownish solid (8 mg, 45% yield). HPLC: t_r : 5.36 min (88%), LCMS: t_r : 2.8 min 500.28 (MH^+).

B/C/C/P macrocycle 1,4 triazole **123**



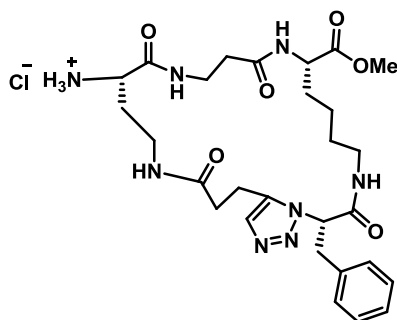
Linear peptide **109** (21 mg, 0.035 mmol), DIPEA (0.17 mL, 0.105 mmol) and CuI (13 mg, 0.07 mmol) in THF were allowed to react according to the described general procedure for macrocycles 1,4-triazole. Crude product was purified by flash column ($\text{CH}_2\text{Cl}_2/\text{MeOH}$ 95/5), then treated with 1.5 mL of HCl 4M in dioxane yielding **123** as yellow solid (4 mg, 21% yield). HPLC: t_r : 5.34 min (72%), LCMS: t_r : 2.8 min, 500.28 (MH^+).

B/C/C/P macrocycle 1,5 triazole **129**



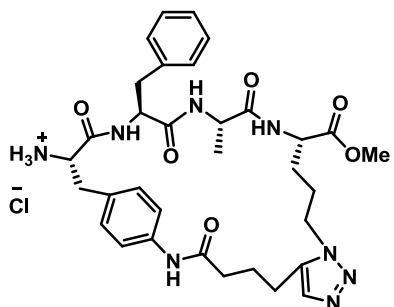
Linear peptide **110** (25 mg, 0.035 mmol) and $[\text{Cp}^*\text{RuCl}]_4$ (3 mg, 0.0035 mmol) were allowed to react according to the described general procedure for macrocycles 1,5-triazole. Crude product was purified by flash column ($\text{CH}_2\text{Cl}_2/\text{MeOH}$ 90/10), then treated with 1.5 mL of a solution of TMSCl on ice-cooled MeOH (1.1 mL in 4.4 mL) overnight at room temperature yielding **129** as a brown solid (11mg, 48% yield). HPLC: t_r : 6.89 min (83%), LCMS: t_r : 3.2 min 613.32 (MH^+).

B/C/C/P macrocycle 1,5 triazole **125**



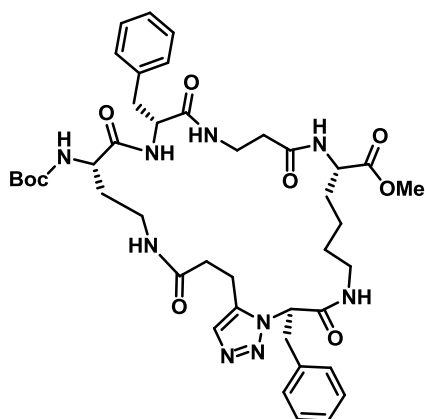
Linear peptide **111** (24 mg, 0.035 mmol) and $[\text{Cp}^*\text{RuCl}]_4$ (3 mg, 0.0035 mmol) were allowed to react according to the described general procedure for macrocycles 1,5-triazole. Crude product was purified by flash column ($\text{CH}_2\text{Cl}_2/\text{MeOH}$ 90/10), then treated with 1.5 mL of a solution of TMSCl on ice-cooled MeOH (1.1 mL in 4.4 mL) overnight at room temperature yielding **125** as a yellow solid (10 mg, 46% yield). HPLC: t_r : 6.85 min (80%), LCMS: t_r : 3.2 min 585.33 (MH^+).

B/C/C/C/P macrocycle 1,5 triazole **126**



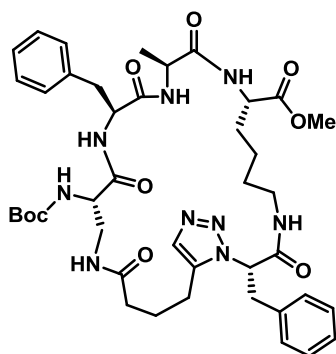
Linear peptide **115** (26 mg, 0.035 mmol) and $[\text{Cp}^*\text{RuCl}]_4$ (3 mg, 0.0035 mmol) were allowed to react according to the described general procedure for macrocycles 1,5-triazole. Crude product was purified by flash column ($\text{CH}_2\text{Cl}_2/\text{MeOH}/\text{MeOH}$ 92/8), then treated with 1.5 mL of HCl 4M in dioxane yielding **126** as white solid (5 mg, 21% yield). HPLC: t_r : 6.65 min (80%), LCMS: t_r : 3.1 min 647.36 (MH^+).

B/C/C/C/P macrocycle 1,5 triazole **130**



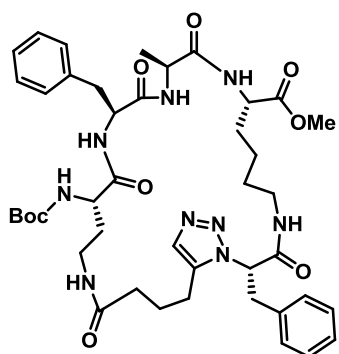
Linear peptide **116** (66 mg, 0.079 mmol) and $[\text{Cp}^*\text{RuCl}]_4$ (9 mg, 0.0079 mmol) were allowed to react according to the described general procedure for macrocycles 1,5-triazole. Crude product was purified by flash column ($\text{CH}_2\text{Cl}_2/\text{MeOH}$ 95/5) yielding **130** as yellow solid (10 mg, 15% yield). HPLC: t_r : 8.40 min (93%), LCMS: t_r : 4.1 min 832.64 (MH^+).

B/C/C/C/P macrocycle 1,5 triazole **127**



Linear peptide **114** (29 mg, 0.035 mmol) and $[\text{Cp}^*\text{RuCl}]_4$ (3 mg, 0.0035 mmol) were allowed to react according to the described general procedure for macrocycles 1,5-triazole. Crude product was purified by flash column ($\text{CH}_2\text{Cl}_2/\text{MeOH}$ 95/5) yielding **127** as yellow solid (13 mg, 43% yield). HPLC: t_r : 10.27 min (89%), LCMS: t_r : 4.2 min 832.56 (MH^+).

B/C/C/C/P macrocycle 1,5 triazole **128**



Linear peptide **117** (30 mg, 0.035 mmol) and $[\text{Cp}^*\text{RuCl}]_4$ (3 mg, 0.0035 mmol) were allowed to react according to the described general procedure for macrocycles 1,5-triazole. Crude product was purified by flash column ($\text{CH}_2\text{Cl}_2/\text{MeOH}$ 90/10) yielding **128** as yellow solid (13 mg, 43% yield). HPLC: t_r : 10.17 min (92%), LCMS: t_r : 4.1 min 846.59 (MH^+).

5.3 Detailed biological methods

Cells

K562 human myeloid cell line was used in this study. K562 is a cell line expressing the anti-apoptotic oncogene Bcr-Abl.

Cell cultures

Continuous neoplastic cells were grown in RPMI 1640 (Gibco Grand Island, NY, USA) containing 10% FCS (Gibco), 100 U/ml penicillin (Gibco), 100 µg/ml streptomycin (Gibco), and 2mM L-glutamine (Sigma Chemical Co, St Louis, MO) in a 5% CO₂ atmosphere at 37 °C.

Samples preparation

Each compound was dissolved in dimethylsulphoxide (DMSO) in a stock solution at a concentration of 20 mM, stored at -20 °C and protected from light. In each experiment DMSO never exceeded 0.2% and this percentage did not interfere with cell growth.

Cytotoxicity assays

To evaluate the number of live and dead neoplastic cells, the cells were stained with trypan blue and counted on a hemocytometer. To determine the growth inhibitory activity of the compounds tested, 2×10^5 cells were plated into 25 mm wells (Costar, Cambridge, UK) in 1 mL of complete medium and treated with different concentrations of each compound. After 48 h of incubation, the number of viable cells was determined and expressed as percent of control proliferation.

Flow cytometry analysis of cell cycle

Cells were washed once in ice-cold PBS and resuspended at 1×10^6 mL in a hypotonic fluorochrome solution containing propidium iodide (Sigma) 50 µg/ml in 0.1% sodium citrate plus 0.03% (v/v) nonidet P-40 (Sigma). After 30 minutes of incubation the fluorescence of each sample was analysed as single-parameter frequency histograms using a FACScan flow cytometer (Becton Dickinson, San Jose, CA). Distribution of cells in cell cycle was determined using the ModFit LT

program (Verity Software House, Inc). Apoptosis was determined by evaluating the percentage of hypoploid nuclei accumulated in the sub-G0-G1 peak after labeling with propidium iodide.

Histone H3, α -tubulin and p53 acetylation in U937 cells

For determination of α -tubulin and p53 acetylation, 25 μ g of total protein extracts were separated on a 10% polyacrylamide gel and blotted. Western blots were shown for acetylated α -tubulin (Sigma, dilution 1:500) and p53 (Sigma) and total ERKs and Actin (Santa Cruz, dilution 1:1000) were used to normalise for equal loading. For quantification of histone H3 acetylation, 100 μ g of total protein extracts were separated on a 15% polyacrylamide gel and blotted. Western blots were shown for acetylated histone H3 (Upstate) and total tubulin (Sigma) was used to normalise for equal loading.

Fluorimetric human recombinant HDAC1 and 4 Assays

The HDAC Fluorescent Activity Assay for HDAC1 and 4 is based on the Fluor de Lys Substrate and Developer combination (BioMol) and has been carried out according to supplier's instructions and as previously reported. First, the inhibitors and purified recombinant HDAC1 or HDAC4 enzymes have been pre-incubated at RT for 15 minutes in assay buffer before substrate addition, the Fluor de Lys Substrate, which comprises an acetylated lysine side chain. Briefly, for HDAC1 and HDAC4, 100 ng of recombinant proteins have been used per assay, respectively. Full length HDAC1 and HDAC4 with C-terminal His tag were expressed using baculovirus expression systems. Deacetylation sensitizes the substrates that, in the second step, treatment with the developer produces a fluorophore. Fluorescence has been quantified with a TECAN Infinite M200 station.

6. Galloflavin

One of the emerging new hallmarks of cancer¹² involves the capability of a tumoral cell to modify or reprogram its energy metabolism in order to most effectively support neoplastic proliferation.⁸⁵ Indeed, cancer cells produce ATP by conversion of glucose to lactate, thus causing a large amount of lactic acid, while normal cells produce ATP from glucose through oxidative phosphorylation. This phenomenon, known as Warburg effect, suggests that specifically targeting this metabolic profile can be a rational approach to apply in anti-cancer therapies.

Lactate dehydrogenase (LDH) represents one of the most interesting key enzymes of this metabolic pathway; it is involved in the final step of aerobic glycolysis, which converts pyruvate into lactate, utilizing NADH as co-factor. LDH is a very well-characterized enzyme: in mammalian cells, it is a tetrameric complex composed of two different subunit types, LDH-A (prevalent in neoplastic tissues) and LDH-B. The combination of these two isoforms can give rise to homotetrameric structure or to heterogeneous enzyme complexes. LDH isoenzymes share a very similar structure but differ in their tissue distribution, kinetic and regulatory properties.

The inhibition of LDH could represent a potential approach to anti-neoplastic chemotherapy, since it was observed that neoplastic cells with a reduction of LDH levels showed a decreased tumorigenicity, and humans with a hereditary deficiency of the A or B LDH isoforms do not have symptoms, except for muscle rigidity and myoglobinuria, which can appear in individuals with LDH-A deficiency after strenuous exercise.

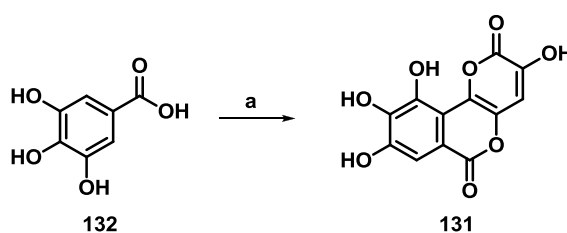
Despite these peculiarities, only a few inhibitors are reported in literature. Oxamic acid was the only well-characterized and specific inhibitor of both LDH-A and LDH-B isoforms; it displayed its mechanism of action by competing with pyruvic acid, the enzyme's natural substrate. However, this molecule had poor cellular penetration, and it was found to inhibit aerobic glycolysis and the proliferation of tumor cells cultured *in vitro* only at millimolar concentrations,⁸⁵ which cannot be expected to be reached *in vivo*.

To this purpose, during my PhD, as a side project I worked on a research program aimed at identifying novel LDH inhibitors. A structure-based virtual screening was applied to the NCI Diversity Set, and 20 molecules were selected for their affinity to LDH-A then taken from the NCI for testing. Some of the

selected compounds displayed enzyme inhibition at a micromolar level; encouraged from this results, in order to provide adequate amounts of one of these substances for further biological studies, my work was focused on the synthesis of Galloflavin **131**,⁸⁶ not available from commercial sources.

Galloflavin **131** was obtained by oxidation on air of a basic solution of gallic acid **132** (Scheme 21). Reproducible conditions for this synthesis were defined following the previously reported procedure,⁸⁷ and for the first time Galloflavin was fully characterized.

Scheme 21^a



^aReagent and conditions: KOH 5M, air, water/ethanol, 12 h, room temp

Galloflavin was found to inhibit both human A and B LDH isoforms, and to block the aerobic glycolysis and ATP synthesis in human hepatocellular carcinoma PLC/PRF/5 cells, without interfering with their mitochondrial function. These promising results prompted further ongoing investigation about Galloflavin as antitumor agent; recently studies proved its antiproliferative effect at micromolar concentration on different breast cancer cell lines.⁸⁸

Noteworthy, at present Galloflavin is sold by Toronto Research Chemicals and ABI Chem.

Experimental section

Gallic acid **132** (1.00 g, 5.87 mmol) was dissolved in H₂O/EtOH 1:1 (8.00 mL) 1/1 in a large beaker. KOH 5 M (4.70 mL, 23.5 mmol) was added dropwise and the reaction mixture was vigorously stirred in air at room temperature for 12 hours. The precipitated green potassium salt was filtered and re-dissolved in 5 ml

H₂O at 50°C, then acidified to pH 4 with HCl 2N. The precipitated galloflavin was filtered, washed with Et₂O and CH₂Cl₂ and evaporated to dryness *in vacuo* to give 165 mg (0.59 mmol) of Galloflavin **131** as green solid. Yield: 10%. ¹H-NMR (DMSO) δ 6.92 (s, 1H), 7.19 (s, 1H) ppm; ¹³C-NMR δ 107.4, 110.7, 111.2, 111.8, 132.8, 133.9, 141.0, 141.1, 141.8, 147.2, 157.5, 159.4 ppm; IR ν_{max} (Nujol) 3352, 1682, 1613, 1584, 1462, 1413, 1376, 1345, 1299, 1176, 1091 cm⁻¹. HPLC t_R = 6.1 min (acetonitrile/phosphoric acid aqueous solution 8.67 mM, 15/85 v/v). UV/vis (acetonitrile/phosphoric acid aqueous solution 8.67 mM, 15/85 v/v): λ_{max}/nm: 224, 258, 378. MS (ES): m/z 279 (M + H⁺), 301 (M + Na⁺), 317 (M + K⁺).

7. Bibliographic References

1. Fishman, M. C. & Porter, J. A. Pharmaceuticals: a new grammar for drug discovery. *Nature* **437**, 491–3 (2005).
2. Cong, F., Cheung, A. K. & Huang, S.-M. a Chemical genetics-based target identification in drug discovery. *Annu Rev Pharmacol Toxicol* **52**, 57–78 (2012).
3. Gershell, L. J. & Atkins, J. H. A brief history of novel drug discovery technologies. *Nat Rev Drug Discov* **2**, 321–7 (2003).
4. Cavalli, A. *et al.* Multi-target-directed ligands to combat neurodegenerative diseases. *J Med Chem* **51**, 347–72 (2008).
5. Strebhardt, K. & Ullrich, A. Paul Ehrlich's magic bullet concept: 100 years of progress. *Nat Rev Cancer* **8**, 473–80 (2008).
6. Drews, J. Case histories, magic bullets and the state of drug discovery. *Nat Rev Drug Discov* **5**, 635–40 (2006).
7. Capdeville, R., Buchdunger, E., Zimmermann, J. & Matter, A. Glivec (STI571, imatinib), a rationally developed, targeted anticancer drug. *Nat Rev Drug Discov* **1**, 493–502 (2002).
8. Hopkins, A. L. Network pharmacology: the next paradigm in drug discovery. *Nat Chem Biol* **4**, 682–90 (2008).
9. Morphy, R., Kay, C. & Rankovic, Z. From magic bullets to designed multiple ligands. *Drug Discov Today* **9**, 641–51 (2004).
10. Morphy, R. & Rankovic, Z. Designing multiple ligands - medicinal chemistry strategies and challenges. *Curr Pharm Des* **15**, 587–600 (2009).
11. Morphy, R. & Rankovic, Z. Fragments, network biology and designing multiple ligands. *Drug Discov Today* **12**, 156–60 (2007).
12. Hanahan, D., Weinberg, R. A. & Francisco, S. The Hallmarks of Cancer. *Cell* **100**, 57–70 (2000).
13. Petrelli, A. & Giordano, S. From single- to multi-target drugs in cancer therapy: when aspecificity becomes an advantage. *Curr Med Chem* **15**, 422–432 (2008).
14. Chen, L., Wilson, D., Jayaram, H. N. & Pankiewicz, K. W. Dual Inhibitors of Inosine Monophosphate Dehydrogenase and Histone Deacetylases for Cancer Treatment. *J Med Chem* **50**, 6685–6691 (2007).
15. Mahboobi, S. *et al.* Novel chimeric histone deacetylase inhibitors: a series of lapatinib hybrides as potent inhibitors of epidermal growth factor

- receptor (EGFR), human epidermal growth factor receptor 2 (HER2), and histone deacetylase activity. *J Med Chem* **53**, 8546–55 (2010).
16. Mahboobi, S. *et al.* Design of chimeric histone deacetylase- and tyrosine kinase-inhibitors: a series of imatinib hybrids as potent inhibitors of wild-type and mutant BCR-ABL, PDGF-Rbeta, and histone deacetylases. *J Med Chem* **52**, 2265–79 (2009).
 17. Gediya, L. K. *et al.* Design, synthesis, and evaluation of novel mutual prodrugs (hybrid drugs) of all-trans-retinoic acid and histone deacetylase inhibitors with enhanced anticancer activities in breast and prostate cancer cells in vitro. *J Med Chem* **51**, 3895–904 (2008).
 18. Roberti, M. ., Bottegoni, G. . & Recanatini, M. Multiple Ligand Strategy in anticancer drug discovery. *Multifunctional Drugs: New Chimeras in Medicinal Chemistry*, Rapposelli, S., Ed. Transworld Research Network: Kerala 217–242 (2010).
 19. Brown, J. B. & Okuno, Y. Systems biology and systems chemistry: new directions for drug discovery. *Chem Biol* **19**, 23–8 (2012).
 20. Altmann, K.-H. *et al.* The state of the art of chemical biology. *Chembiochem* **10**, 16–29 (2009).
 21. Schreiber, S. L. Small molecules: the missing link in the central dogma. *Nat Chem Biol* **1**, 64–6 (2005).
 22. Stockwell, B. R. Exploring biology with small organic molecules. *Nature* **432**, 846–854 (2011).
 23. Kugawa, F., Watanabe, M. & Tamanoi, F. Chemical Biology / Chemical Genetics / Chemical Genomics : Importance of Chemical Library. *Chem-Bio Informatics Journal* **7**, 49–68 (2007).
 24. Szymkowski, D. E., Avenue, W. L. & Ca, M. Chemical genomics versus orthodox. *Drug Discov Today* **8**, 157–159 (2003).
 25. Spring, D. R. Chemical genetics to chemical genomics: small molecules offer big insights. *Chem Soc Rev* **34**, 472 (2005).
 26. Stockwell, B. R. Chemical genetics: ligand-based discovery of gene function. *Nat Rev Genet* **1**, 116–125 (2000).
 27. Barker, A., Kettle, J. G., Nowak, T. & Pease, J. E. Expanding medicinal chemistry space. *Drug Discov Today* **00**, (2012).
 28. Koch, M. a *et al.* Charting biologically relevant chemical space: a structural classification of natural products (SCONP). *Proc Natl Acad Sci U S A* **102**, 17272–7 (2005).

29. Schreiber, S. L. Organic synthesis toward small-molecule probes and drugs. *Proc Natl Acad Sci U S A* **108**, 6699–702 (2011).
30. Lipinski, C. & Hopkins, A. Navigating chemical space for biology and medicine. *Nature* **432**, 855–861 (2004).
31. Burke, M. D. & Schreiber, S. L. A planning strategy for diversity-oriented synthesis. *Angew Chem Int Ed Engl* **43**, 46–58 (2004).
32. Schreiber, S. L. Target-Oriented and Diversity-Oriented Organic Synthesis in Drug Discovery. *Science* **287**, 1964–1969 (2000).
33. Corey, E. J. The Logic of Chemical Synthesis: Multistep Synthesis of Complex Carbogenic Molecules (Nobel Lecture). *Angew Chem Int Ed Engl* **30**, 455–465 (1991).
34. Galloway, W. R. J. D., Isidro-Llobet, A. & Spring, D. R. Diversity-oriented synthesis as a tool for the discovery of novel biologically active small molecules. *Nat Commun* **1**, 80 (2010).
35. Hann, M. M., Leach, A. R. & Harper, G. Molecular Complexity and Its Impact on the Probability of Finding Leads for Drug Discovery. *J Chem Inf Comput Sci* **41**, 856–864 (2001).
36. Pardee, a B. A restriction point for control of normal animal cell proliferation. *Proc Natl Acad Sci U S A* **71**, 1286–90 (1974).
37. Bartek, J., Bartkova, J. & Lukas, J. The retinoblastoma protein pathway and the restriction point. *Curr. Opin. Cell Biol.* **8**, 805–814 (1996).
38. Weinberg, R. a The retinoblastoma protein and cell cycle control. *Cell* **81**, 323–30 (1995).
39. Fiorini, A. *et al.* Lack of p53 Affects the Expression of Several Brain Mitochondrial Proteins: Insights from Proteomics into Important Pathways Regulated by p53. *PloS one* **7**, e49846 (2012).
40. Brown, J. M. & Attardi, L. D. The role of apoptosis in cancer development and treatment response. *Nat Rev Cancer* **5**, 231–7 (2005).
41. No Title. <http://www.caspases.org/>
42. Shi, Y. Mechanisms of Caspase Activation and Inhibition during Apoptosis. *Mol Cell* **9**, 459–470 (2002).
43. Wu, M. Apoptosis : Molecular Mechanisms. *Encyclopedia of life sciences* (2001).
44. No Title. <http://www.celldeath.de/encyclo/aporev/aporev.htm>

45. Leist, M. & Jäättelä, M. Four deaths and a funeral: from caspases to alternative mechanisms. *Nat Rev Mol Cell Biol* **2**, 589–98 (2001).
46. Shi, Y. Activation of Initiator Caspases: History, Hypotheses, and Perspectives. *J. Cancer Mol.* **1**, 9–18 (2005).
47. Cotter, T. G. Apoptosis and cancer: the genesis of a research field. *Nat Rev Cancer* **9**, 501–7 (2009).
48. Banerjee, H. N. & Verma, M. Epigenetic mechanisms in cancer. *Biomark Med* **3**, 397–410 (2009).
49. Khorasanizadeh, S. The Nucleosome: From Genomic Organization to Genomic Regulation University of Virginia Health System. *Cell* **116**, 259–272 (2004).
50. Jenuwein, T. & Allis, C. D. Translating the histone code. *Science (New York, N.Y.)* **293**, 1074–80 (2001).
51. Strahl, B. D. & Allis, C. D. The language of covalent histone modifications. *Nature* **403**, 41–45 (2000).
52. Allfrey, G., Faulkner, R. & Mirsky, A. E. Acetylation and methylation of histones and their possible role in the regulation of RNA synthesis. *Proc Natl Acad Sci U S A* **315**, 786–794 (1964).
53. Barneda-Zahonero, B. & Parra, M. Histone deacetylases and cancer. *Mol Oncol* **6**, 579–89 (2012).
54. No Titl. <http://www.hdacis.com/>
55. Kim, H.-J. & Bae, S.-C. Histone deacetylase inhibitors: molecular mechanisms of action and clinical trials as anti-cancer drugs. *Am J Transl Res* **3**, 166–79 (2011).
56. Saharan, R., Singh, R., Nagar, N. & Verma, S. HDAC inhibitors: a new armour in anti-cancer therapeutics. *Pharmacophore* **2**, 104–113 (2011).
57. Marks, P. *et al.* Histone deacetylases and cancer: causes and therapies. *Nat Rev Cancer* **1**, 194–202 (2001).
58. Roberti, M. *et al.* Synthesis and biological evaluation of resveratrol and analogues as apoptosis-inducing agents. *J Med Chem* **46**, 3546–54 (2003).
59. Pizzirani, D. *et al.* Antiproliferative agents that interfere with the cell cycle at the G1→S transition: further development and characterization of a small library of stilbene-derived compounds. *ChemMedChem* **3**, 345–55 (2008).

60. Roberti, M. *et al.* Identification of a terphenyl derivative that blocks the cell cycle in the G0-G1 phase and induces differentiation in leukemia cells. *J Med Chem* **49**, 3012–8 (2006).
61. Pizzirani, D. *et al.* Identification of biphenyl-based hybrid molecules able to decrease the intracellular level of Bcl-2 protein in Bcl-2 overexpressing leukemia cells. *J Med Chem* **52**, 6936–40 (2009).
62. Pizzirani, D., Roberti, M. & Recanatini, M. Domino Knoevenagel/Diels–Alder sequence coupled to Suzuki reaction: a valuable synthetic platform for chemical biology. *Tetrahedron Lett* **48**, 7120–7124 (2007).
63. Liu, J.-K. Natural terphenyls: developments since 1877. *Chem Rev* **106**, 2209–23 (2006).
64. Kuckertz, M. *et al.* Comparison of the effects of two kinase inhibitors, sorafenib and dasatinib, on chronic lymphocytic leukemia cells. *Onkologie* **35**, 420–6 (2012).
65. Down-regulation, C. I. P., Dasmahapatra, G., Yerram, N. & Dai, Y. Synergistic Interactions between Vorinostat and Sorafenib in Chronic Myelogenous Leukemia Cells Involve Mcl-1 and. *Clin Cancer Res* **13**, 4280–4290 (2007).
66. Plaza-Menacho, I. *et al.* Sorafenib functions to potently suppress RET tyrosine kinase activity by direct enzymatic inhibition and promoting RET lysosomal degradation independent of proteasomal targeting. *J Biol Chem* **282**, 29230–40 (2007).
67. Wilhelm, S. M. *et al.* Preclinical overview of sorafenib, a multikinase inhibitor that targets both Raf and VEGF and PDGF receptor tyrosine kinase signaling. *Molecular cancer therapeutics* **7**, 3129–40 (2008).
68. Wan, P. T. C. *et al.* Mechanism of activation of the RAF-ERK signaling pathway by oncogenic mutations of B-RAF. *Cell* **116**, 855–67 (2004).
69. Zhang, J., Yang, P. L. & Gray, N. S. Targeting cancer with small molecule kinase inhibitors. *Nat Rev Cancer* **9**, 28–39 (2009).
70. Curtin, M. L. *et al.* Succinimide hydroxamic acids as potent inhibitors of histone deacetylase (HDAC). *Bioorg Med Chem Lett* **12**, 2919–23 (2002).
71. Driggers, E. M., Hale, S. P., Lee, J. & Terrett, N. K. The exploration of macrocycles for drug discovery--an underexploited structural class. *Nat Rev Drug Discov* **7**, 608–24 (2008).
72. O’Connell, K. M. G. *et al.* A two-directional strategy for the diversity-oriented synthesis of macrocyclic scaffolds. *Org Biomol Chem* **10**, 7545–51 (2012).

73. Kopp, F., Stratton, C. F., Akella, L. B. & Tan, D. S. Diversity-Oriented Synthesis Approach to Macrocycles via Oxidative Ring Expansion. *Nature chemical biology* **8**, 358–365 (2012).
74. Vagner, J., Qu, H. & Hruby, V. J. Peptidomimetics, a synthetic tool of drug discovery. *Curr Opin Chem Biol.* **12**, 292–296 (2009).
75. Kharb, R., Rana, M., Sharma, P. C., Yar, M. S. & Delhi, N. Therapeutic importance of peptidomimetics in medicinal chemistry. *J Chem Pharm Res* **3**, 173–186 (2011).
76. Horne, W. S., Olsen, C. a, Beierle, J. M., Montero, A. & Ghadiri, M. R. Probing the bioactive conformation of an archetypal natural product HDAC inhibitor with conformationally homogeneous triazole-modified cyclic tetrapeptides. *Angew Chem Int Ed Engl* **48**, 4718–24 (2009).
77. Green, C. J. Cyclosporin A. *the lancet* **313**, 110– (1979).
78. Liskamp, R. M. J., Rijkers, D. T. S. & Bakker, S. E. *Bioactive Macrocyclic Peptides and Peptide Mimics*. 1–28 (2008).
79. Kohsaka, M. & Imanaka, H. Bicyclomycin, a new antibiotic. *J Antibiot* **XXV**, 569–575 (1972).
80. Isidro-Llobet, A. *et al.* Diversity-oriented synthesis of macrocyclic peptidomimetics. *Proc Natl Acad Sci U S A* **108**, 6793–8 (2011).
81. Nielsen, T. E. & Schreiber, S. L. Towards the optimal screening collection: a synthesis strategy. *Angew Chem Int Ed Engl* **47**, 48–56 (2008).
82. Boger, D. L. & Zhou, J. Total Synthesis of (+)-Piperazinomycin. *J. Am. Chem. Soc.* **115**, 11426–11433 (1993).
83. Jakobsen, C. M. *et al.* Design, synthesis, and pharmacological evaluation of thapsigargin analogues for targeting apoptosis to prostatic cancer cells. *J Med Chem* **44**, 4696–703 (2001).
84. Schmuck, C., Rehm, T., Geiger, L. & Schäfer, M. Synthesis and self-association properties of flexible guanidiniocarbonylpyrrole-carboxylate zwitterions in DMSO: intra- versus intermolecular ion pairing. *J Org Chem* **72**, 6162–70 (2007).
85. Fiume, L. *et al.* Galloflavin prevents the binding of lactate dehydrogenase A to single stranded DNA and inhibits RNA synthesis in cultured cells. *Biochem Biophys Res Commun* **430**, 466–9 (2013).
86. Manerba, M. *et al.* Galloflavin (CAS 568-80-9): a novel inhibitor of lactate dehydrogenase. *ChemMedChem* **7**, 311–7 (2012).

87. Grimshaw, J., Haworth, R. D. & Pindred, H. K. Galloflavin. Part II. *J Chem Soc* 833 (1955).doi:10.1039/jr9550000833
88. Farabegoli, F. *et al.* Galloflavin, a new lactate dehydrogenase inhibitor, induces the death of human breast cancer cells with different glycolytic attitude by affecting distinct signaling pathways. *European journal of pharmaceutical sciences : official journal of the European Federation for Pharmaceutical Sciences* **47**, 729–38 (2012).